Development and Characterization of a Predictive Cell-based Test Method for the Identification of Substances with Estrogenic Properties

Inaugural-Dissertation

to obtain the academic degree

Doctor rerum naturalium (Dr. rer. nat.)

submitted to the

Department of Biology, Chemistry and Pharmacy

of Freie Universität Berlin

by

Marja Kornhuber

2020

This work was conducted at the German Federal Institute for Risk Assessment and the German Center for the Protection of Laboratory Animals in the unit Strategies for Toxicological Assessment from May 2016 to February 2020 under the supervision of Prof. Dr. Gilbert Schönfelder.

1. Reviewer: Prof. Dr. Gilbert Schönfelder
2. Reviewer: Prof. Dr. Stephan Sigrist

Date of Defense:16.06.2020

Affidavit

I hereby declare that the thesis entitled “Development and characterization of a predictive cell-based test method for the identification of substances with estrogenic properties” has been carried out at the German Federal Institute of Risk Assessment in Berlin under the guidance of Prof. Dr. Gilbert Schönfelder in the time period 01.05.2016 - 20.02.2020 and is the result of my independent work.

Furthermore, I confirm that no sources have been used in the preparation of this thesis other than those indicated in the thesis itself.

Berlin, 20.02.2020

Acknowledgment

First of all, I want to sincerely thank Prof. Dr. Schönfelder and Dr. Oelgeschläger for providing the topic of my thesis and support in conducting this work.

I also want to thank Dr. Sebastian Dunst for his scientific guidance, support and the many constructive discussions.

I am grateful to all the members of the German Federal Institute for Risk Assessment unit 93 and 91 for providing a productive and enjoyable working atmosphere. Everyone was always helpful and open for questions.

I want to thank my family and friends for always being there for me.

Last but not least, I want to thank Prof. Dr. Sigrist for accepting the duty of being the second reviewer of this thesis.

Content

Summary 1

Zusammenfassung 2

1. Introduction 3

1.1. Estrogens and the endocrine system 3

1.1.1. Estrogen function and synthesis 3

1.1.2. Estrogen signaling 4

1.1.3. Breast cancer 6

1.1.4. Breast cancer at the cellular level 8

1.2. Endocrine disruption 11

1.2.1. Endocrine active/disrupting chemicals 13

1.2.2. Chemical regulations and available test methods 16

2. Purpose 20

3. Results 21

3.1. Characterization of adherens junction organization as a novel estrogen specific endpoint 21

3.1.1. Antiestrogen treatment causes adherens junction reorganization 21

3.1.2. Adherens junction reorganization is estrogen receptor α specific 26

3.1.3. Adherens junction reorganization is a relevant functional endpoint 34

3.2. Development of a high throughput compatible assay set-up 55

3.2.1. Optimization of staining method and computational analysis 55

3.2.2. Optimization of the measuring time point 60

3.2.3. Definition of a cytotoxicity read-out 63

3.2.4. Definition of a prediction model using a test set of six substances 66

3.2.5. Validation of the E-Morph Assay with eleven additional substances 71

3.2.6. The predictive capacity of the E-Morph Assay 73

4. Discussion 75

4.1. Adherens junction reorganization is ERα mediated 75

4.2. Adherens junction reorganization is a functionally relevant endpoint 77
4.3. Signaling pathways involved in adherens junction reorganization 79
4.4. Adherens junction reorganization as an endpoint in a high-throughput compatible test method for estrogenic substances – the E-Morph Assay 83
4.5. Characterization of the limitations and applicability of the E-Morph Assay ... 85
4.6. Characterization of the predictive capacity of the E-Morph Assay 87
5. Conclusion and Outlook 88
6. Materials 90
6.1. Equipment 90
6.2. Cell culture 90
6.3. Staining reagents 91
6.4. DNA and RNA constructs 92
6.5. Kits 94
6.6. General material 94
6.7. Buffers and solutions 96
7. Methods 98
7.1. Cell culture 98
7.2. Cell imaging methods 99
7.3. RNA biologic methods 100
7.4. Protein biologic methods 102
7.5. Bioinformatics 104
7.5.1. Analysis of Western blot data 104
7.5.2. Quantitative image analysis for adherens junction reorganization 104
8. References 107
9. List of Figures and Tables 113
10. List of Abbreviations 115
11. List of publications 116

Summary

The endocrine system is an integral part during development and the regulation of various physiological processes in the human body. Dysregulation of the endocrine system has frequently been linked to the development of adverse health effects including cancer. Man-made chemicals that have the capacity to interfere with the endocrine system thereby eliciting adverse health effects (termed endocrine disrupting chemicals (EDC)) are therefore of high concern. Available *in vitro* assays that allow the identification and characterization of EDCs mainly provide information on mechanisms and pathways of endocrine activity. However, these assays usually do not cover functional endpoints that are predictive for adversity such as hormone-related tumor formation and progression, necessitating the use of complex *in vivo* studies that require high numbers of test animals.

This thesis introduces the E-Morph Assay: a novel robust and predictive *in vitro* test method that allows the identification and characterization of chemicals that interfere with the estrogen signaling pathway. The development of this assay is based on the finding that estrogen signaling modulates the organization of adherens junctions (AJ) in the human MCF7 breast cancer cell line. The specificity of this effect to the estrogen receptor α (ERα) signaling pathway could be verified by inhibition and knock down studies targeting ERα, while modulation of the G-protein-coupled estrogen receptor 1 (GPER1) did not have any influence. It could further be shown that AJ reorganization is mediated by the ERα target gene Amphiregulin (AREG) involving a crosstalk with the epidermal growth factor receptor (EGFR) and the downstream RhoA and Src family kinase signaling pathways.

These cancer-related signaling pathways support the mechanistic and clinical relevance of AJ organization to be used as a novel functional endpoint in the E-Morph Assay for high-content/high-throughput phenotypic screening. The development of a 96 well plate assay set-up and a pipeline for automated image acquisition and quantitative image analysis allows the rapid testing of chemicals at multiple concentrations. Pilot screening using a test set of 17 reference chemicals with known estrogenic properties demonstrated a high predictive capacity of the E-Morph Assay.

In conclusion, the E-Morph Assay will provide a valuable *in vitro* screening method to identify and characterize chemicals with estrogenic activity using estrogen-dependent changes in AJ organization as a functional readout.

Zusammenfassung

Das endokrine System ist ein zentraler Bestandteil während der Entwicklung und sowie der Regulierung physiologischer Prozesse im menschlichen Körper. Eine Dysregulation des endokrinen Systems steht in Verbindung mit der Entwicklung verschiedener Krankheiten einschließlich Krebs. Vom Menschen hergestellte Chemikalien, die in der Lage sind, das endokrine System zu stören und dadurch nachteilige Auswirkungen auf die Gesundheit haben (als endokrin wirkende Chemikalien (EDC) bezeichnet), geben daher Anlass zur Sorge. Verfügbare *in-vitro*-Assays, mit denen EDCs identifiziert und charakterisiert werden können, liefern hauptsächlich Informationen über Mechanismen und Wege der endokrinen Aktivität. Diese Assays decken jedoch in der Regel keine funktionellen Endpunkte ab, die eine Vorhersage zur Krankheitsentwicklung wie hormonbedingte Tumorbildung ermöglichen. Daher müssen komplexe *in-vivo*-Studien durchgeführt werden, für die eine große Anzahl von Testtieren erforderlich ist.

In dieser Arbeit wird der E-Morph-Assay vorgestellt: eine neue robuste und prädiktive *in-vitro*-Testmethode, mit der Chemikalien identifiziert werden können, die den Östrogensignalweg stören. Die Entwicklung dieses Assays basiert auf der Feststellung, dass der Östrogensignalweg die Organisation von *Adherens Junctions* (AJ) in der menschlichen MCF7 Brustkrebszelllinie verändert. Die Spezifität dieses Effekts für den Östrogenrezeptor α (ERα) Signalweg konnte durch Inhibitions- und Knock-Down-Studien verifiziert werden, während die Modulation des G-Protein-gekoppelten Östrogenrezeptors 1 (GPER1) keinen Einfluss hatte. Es konnte gezeigt werden, dass die AJ-Reorganisation durch das ERα-Zielgen Amphiregulin (AREG) vermittelt wird. Zusätzlich sind der epidermalen Wachstumsfaktor Rezeptor (EGFR) und nachgeschaltete Kinase-Signalwege der RhoA- und Src-Familie beteiligt.

Diese krebsrelevanten Signalwege unterstützen die mechanistische und klinische Relevanz der AJ-Organisation als neuen funktionellen Endpunkt im E-Morph-Assay. Die Entwicklung einer Pipeline für die automatisierte Bilderfassung und quantitative Bildanalyse ermöglicht das schnelle Analysieren von Chemikalien. Das Testen von 17 Referenzchemikalien mit bekannten östrogenen Eigenschaften zeigte eine hohe Vorhersagekapazität des E-Morph-Assays.

Zusammenfassend stellt das E-Morph-Assay ein wertvolles *in-vitro*-Assay zur Identifizierung von östrogener Chemikalien unter Verwendung östrogenabhängiger Veränderungen in der AJ-Organisation als funktioneller Endpunkt dar.

1. Introduction

1.1. Estrogens and the endocrine system

In the endocrine system, communication between distal organs is mediated by circulating signaling molecules, i.e. hormones. The interplay of hormones regulates major aspects of development, physiology and behavior. Hormones are synthesized in specific glands such as the adrenal or pituitary gland and secreted into the circulatory system from where they then act on their target organs.

1.1.1. Estrogen function and synthesis

The role of estrogens in the body is diverse. Estrogens are the primary female sex hormones and therefore essential for the development and regulation of the female reproductive system and secondary sex characteristics. During mammary gland development for example they regulate Amphiregulin (AREG) expression, a member of the epidermal growth factor family, which binds to the epidermal growth factor receptor (EGFR) to promote correct ductal growth and branching [1]. Additionally, estrogens play an integral part in other processes in the body e.g. cognitive function or bone homeostasis. Research concerning the effect of estrogens on cognitive function illustrates the complexity of estrogen signaling. Depending on the neural system (hippocampus or striatum), positive as well as negative effects on cognition after estrogen administration can be observed [2]. As it was shown that estrogens can potentially increase neuron viability and reduce amyloid β accumulation and thus, a positive effect of estrogen treatment in Alzheimer disease is currently discussed [3]. Additionally, estrogens are the major hormonal regulator of bone homeostasis independent of sex. Both activation of bone remodeling and bone resorption are inhibited by estrogen action and the loss of estrogen action is connected to an imbalance between bone formation and bone resorption with consequences well documented by the development osteoporosis in post-menopausal women [4].

Estrogen synthesis is regulated through the hypothalamic-pituitary-gonadal axis (HPG axis). Specific neurons in the hypothalamus secret gonadotropin-releasing hormone (GnRH) which stimulates the synthesis of luteinizing hormone (LH) and follicle-stimulating hormone (FSH) in the anterior pituitary gland. Circulating through the blood stream, LH and FSH activate the ovaries to produce testosterone. Testosterone is further metabolized by the Cytochrome P450 enzyme Aromatase (Cyp19A1) to the

main estrogen 17β-estradiol (E2). Estrogens and testosterone in turn influence GnRH, LH and FSH secretion through feedback loops. In addition to the synthesis of estrogens in the ovaries, estrogens are produced in smaller amount in other tissues such as adipose tissue or skin depending on testosterone levels and aromatase expression [5]. Upon entry into menopause, ovaries cease to produce estrogens and the alternative tissues become the only source for estrogens. For men, these alterative tissues are the only source of estrogen. Following synthesis, estrogens are secreted into the blood stream where the majority is bound to albumin or sex hormone-binding globulin. The non-protein bound estrogens are considered biologically active and can freely diffuse through the cell membrane into target cells to initiate estrogen [6].

1.1.2. Estrogen signaling

After passing the cell membrane, estrogens bind to intracellular estrogen receptors (ER) and initiate genomic or non-genomic responses. Three main ER have been identified so far – ERα, ERβ and the G-protein-coupled ER 1 (GPER1).

While the potential existence of a specific ER was already proposed by Elwood Jensen in the early 1960s [7], the ERα complementary deoxyribonucleic acid (cDNA) was only cloned in 1980s, followed by the ERβ ten years later [8]. Both ERα and ERβ are ubiquitously expressed but the ratio of ERα and ERβ is tissue dependent. While ERα is primarily expressed in the mammary gland, uterus, and vagina, the levels of ERβ are higher in ovary, testis, and spleen [9]. Although the genes of ERα (*ESR1*) and ERβ (*ESR2*) are located on different chromosomes, both receptors show – excluding their N-terminal domain – a high degree of sequence homology and similar ligand binding affinities. Like the other members of the nuclear steroid hormone receptor superfamily, ERα and ERβ contain three basic domains – the N-terminal domain, the DNA binding domain, and the ligand binding domain. Transcriptional activity is mediated through the two activation function (AF) domains AF-1 and AF-2 located within the N-terminal and ligand binding domain of ERα, respectively. While AF-1 is constitutively active, the activity of AF-2 is ligand-dependent [10]. ERs primarily localize to the nucleus, with only a small percentage found in the cytoplasm or plasma membrane [11].

In the canonical ER signaling pathway, estrogen binding activates the ERα or ERβ by inducing a conformational change and receptor dimerization. Upon activation, ER can either directly interact with DNA at palindromic estrogen responsive elements (EREs) or indirectly through other transcription factors such as stimulating

protein-1 (SP-1) or activating protein-1 (AP-1) (Figure 1, genomic signaling pathway). A portion of the receptor may already reside inside the nucleus to be directly activated there [12]. For the transcription initiation, additional cofactors such as steroid receptor co-activator-1 (SRC-1) are needed which are recruited by AF-1 or AF-2 in a tissue- and receptor-dependent manner. Furthermore, ligand independent ERα activation through EGF-mediated phosphorylation of Serine 118 residue has been reported (Figure 1, genomic signaling pathway) [9]. Due to their similar structure, ERα and ERβ are able to heterodimerize, thereby influencing each other's signaling activity [8].

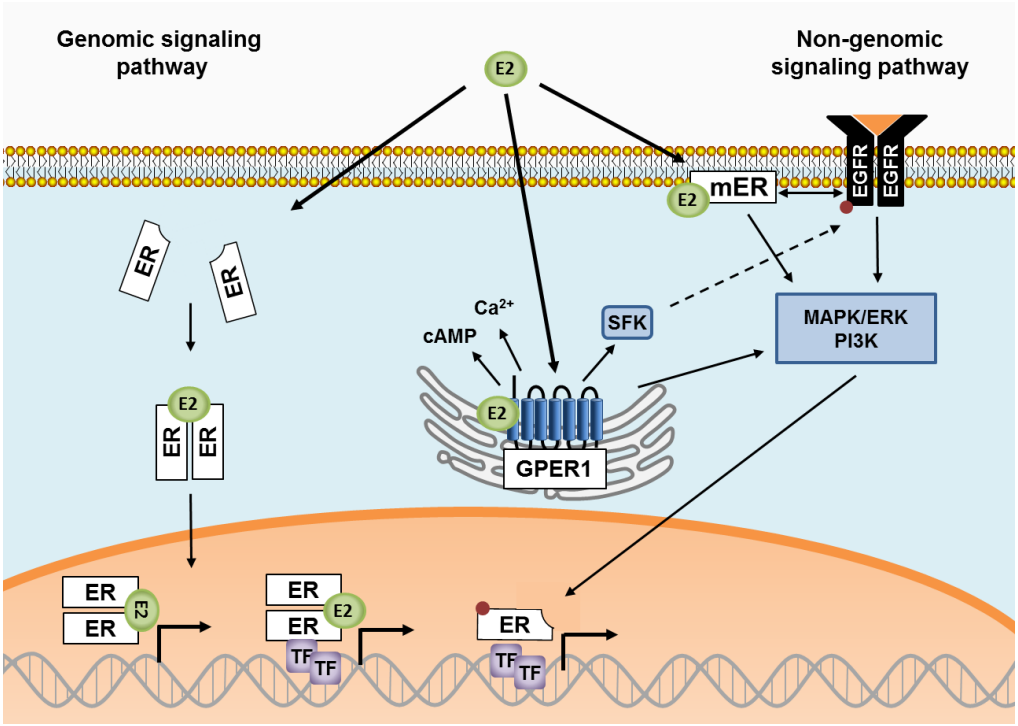

Figure 1: Schematic view of the genomic and non-genomic estrogen signaling pathways.
Estrogen signaling is mediated through the two nuclear estrogen receptors (ER), ERα and ERβ, and the G-protein coupled estrogen receptor 1 (GPER1). Upon activation with 17β-estradiol (E2), the ER can act as transcription factor and either directly or indirectly through transcription factors (TF) induce gene transcription. Ligand-independent ER activation through other signaling pathways is also possible. Non-genomic responses are mediated by membrane associated ER (mER) and the GPER1, which can influence EGFR signaling as well as downstream pathways such as src-family kinases (SFK), mitogen activating protein kinase/extracellular signal-regulated kinase (MAPK/ERK) or phospatidyl-inositol-3-kinase (PI3K) signaling pathway. The red dot indicates phosphorylation.

In addition to the canonical genomic ER signaling pathway, rapid non-genomic responses can be induced through cell-membrane-associated ER. Anchored at the cell membrane via palmitoylation, membrane-associated ERα are able to transactivate the EGFR or influence extracellular signal-regulated kinase (ERK) activity [13, 14]. EGFR or ERK activate downstream signaling pathways which in turn influence gene expression (Figure 1, non-genomic signaling pathway).

The non-genomic signaling route also includes the GPER1, identified only recently. The GPER1 belongs to the family of 7-transmembrane spanning G-protein coupled receptors (GPCR) and is expressed in numerous tissues e.g. mammary gland, cardiovascular system, and bone [15]. Classically, GPCRs are thought to localize at the plasma membrane. Though, this appears to be true for GPER1 in some cell types, commonly GPER1 seems to be primarily localized in intracellular membranes of e.g. the Golgi or endoplasmic reticulum (Figure 1, non-genomic signaling pathway) [11]. While the two nuclear ERs ERα and ERβ have comparable ligand binding affinities, the binding pocket of the GPER1 is distinct. While E2, the main endogenous estrogen, binds to GPER1 with a similar binding affinity as to ERα, Estrone (E1), a slightly weaker endogenous estrogen, does not modulate GPER1 activity at all [11]. Notably, Tamoxifen (Tam) and Fulvestrant (Fulv), two ERα inhibitors commonly used in the treatment of ERα-positive breast cancer, actually activate the GPER1, albeit at lower binding affinities [11, 16]. Coupling to heterotrimeric G-proteins, GPER1 can induce rapid non-genomic responses. The GPER1 was shown to activate multiple pathways like phospatidyl-inositol-3-kinase/Akt (PI3K/Akt) or mitogen activating protein kinase/extracellular signal-regulated kinase (MAPK/ERK) pathway. Through src-family-kinase (SFK)-dependent activation of metalloproteases, GPER1 is also able to transactivate EGFR signaling. Additionally, GPER1-mediated activation of the adenylyl cyclase and calcium mobilization were reported [11].

All three ERs contribute to estrogen signal transduction in the various cells and tissues of the body. Based on their expression profile, dependence on cofactors and cross reactivity, they are able to modulate estrogen signaling in a distinct fashion [11].

1.1.3. Breast cancer

Although estrogen signaling has been shown to be required for breast development under physiological conditions and has beneficial effects on the neural system or bone homeostasis (Section 1.1.1), it also plays a role in the development and progression of endocrine-related cancer such as breast cancer [17]. Breast cancer is one of the most common cancers worldwide and the most common cancer in women independently of the Human Development Index [18, 19]. In Germany, based on the incidence rate reported for 2013/2014, one out of eight women is expected to acquire breast cancer at some point in their life [20]. The global breast cancer incidence rate has been rising by about 3.1 % annually between 1980 and 2010 with over 1.6 million

women newly diagnosed in 2010. In 2018, around 2.1 million women were diagnosed with breast cancer worldwide [21].

In addition to genetic predisposition or family history, which is primary factor in about 10 % of the breast cancer cases, several other factors can contribute to a higher breast cancer risk. Reproductive factors, e.g. early onset of menstruation and late first pregnancy, or lifestyle factors, e.g. high fat diet and lack of physical activity, are known to increase the individual breast cancer risk. Additionally, environmental factors such as hormonal contraceptive drugs or hormone replacement therapy during menopause are thought to elevate the overall risk [18, 19, 21].

Generally, breast cancer is categorized according to its histological appearance and expression of specific marker proteins. Histologically, breast carcinomas are classified according to their origin within the breast (lobule or duct), and their invasion status. Four histological subtypes are defined – preinvasive ductal and lobular carcinoma *in situ*, invasive ductal carcinoma no special type, and invasive lobular carcinoma [21]. With around 70 %, "invasive ductal carcinoma no special type" (NST) is the most common histological subtype [18]. Furthermore, for clinical classification, expression of the marker proteins ERα, progesterone receptor (PGR) and human epidermal growth factor receptor 2 (HER2) are assessed. The receptor status is decisive for later treatment and prognosis. Triple negative ($ER\alpha^-/PGR^-/HER2^-$) breast cancers have for example a generally poor prognosis and are treated by standard chemotherapy that targets rather unspecific quickly dividing cells [21]. Over half of the breast carcinomas are ERα- and PGR-positive and HER2-negative. If the breast cancer is ERα- and/or PGR-positive, endocrine therapy by blocking estrogen signaling has proven to be most beneficial. In endocrine therapy, estrogen signaling is generally blocked by treating patients with antiestrogens like Tam or inhibiting endogenous estrogen synthesis by GnRH analogues in premenopausal women or aromatase inhibitors in postmenopausal woman [21]. The antiestrogen Fulv might be used as a second line antiestrogen when Tam proves to be ineffective [22]. Adjuvant endocrine therapy is recommended for at least five years after surgery in order to reduce the risk for cancer recurrence [21].

1.1.4. Breast cancer at the cellular level

A connection of estrogen and breast cancer was already recognized at the end of the 19th century even before the true nature of cancer was known [23] and is now supported by the renown beneficial effects of endocrine therapy as well as strong experimental evidence from basic research. Next to a general proliferative effect, estrogen signaling is able to influence the expression or activation of marker proteins such as E-Cadherin (E-Cad), EGFR or growth factors known to be involved in cancer progression. Following, these marker proteins as well as their estrogen dependent regulation are described in more detail.

E-Cadherin and adherens junctions

In addition to the hormone receptor status, the expression status of the marker protein E-Cad is generally assessed and used for the classification into lobular and ductal carcinomas. While E-Cad expression is sustained in *in situ* or invasive ductal carcinomas, E-Cad expression is typically lacking in lobular cancer [24]. E-Cad is a transmembrane glycoprotein encoded by the tumor suppressor gene *CDH1*. As essential part of adherens junctions (AJ), it plays an important role in cell-cell contact mediation, apical-basal cell polarity, and mechanotransduction by connecting to the cellular actomyosin network [25]. Additionally, E-Cad interacts with different signal transduction pathways, such as EGFR signaling, and promotes contact inhibition of cell proliferation [26]. Structurally, E-Cad consists of an extracellular (EC) domain of five tandem repeats, a single transmembrane domain, and a cytoplasmic domain. The EC domain is responsible for mediating Ca^{2+}-dependent homotypic interactions between E-Cad proteins of two adjacent cells. Binding of Ca^{2+} induces a conformational change in the EC domain which enables interaction with another Ca^{2+} occupied EC domain of the neighboring cell [25]. Binding of two E-Cad proteins is rather weak but can be strengthened through lateral clustering [27, 28]. The cytoplasmic domain functions as a binding platform for several proteins including p120 and β-catenin. β-catenin in turn mediates interaction with the actin cytoskeleton through force-dependent binding at α-catenin [29].

E-Cad plays an important role in epithelial-mesenchymal transition (EMT) during tissue morphogenesis during in embryonic development but is also implicated in cancer progression [30]. Generally, the loss of E-Cad expression is connected with higher metastatic potential and considered a hallmark of cancer progression, although

recent results also demonstrate a requirement of E-Cad expression for metastases in some cancer models [31, 32]. E-Cad expression is mostly dependent on CpG dinucleotides methylation, differential promotor activity and regulatory elements in exon regions [30]. Estrogen signaling has been shown to directly or indirectly influence E-Cad expression in different ways, including activation or inhibition. ERα can directly regulate E-Cad expression through binding to the half ERE in the promoter region of E-Cad. Whereas ligand-independent ERα binding to the E-Cad ERE was shown to induce E-Cad expression, binding of ligand-activated ERα inhibited E-Cad expression [33, 34]. Additionally, estrogen was shown to indirectly inhibit E-Cad expression by inducing the expression of the transcription factors Slug and Snail, while ERα was also shown to indirectly induce E-Cad expression through metastasis associated gene protein 3 (MTA3) induction. MTA3 is part of the Mi-2/NuRD transcription repression complex, which is a known repressor of *Snail* transcription [32, 35].

In addition to variable E-Cad expression levels, aberrant localization patterns can be observed in some breast cancer samples [24]. The protein levels of E-Cad at cell membranes of AJ are normally regulated through an equilibrium of transport to the membrane, endocytosis, recycling and degradation [36]. AJ formation and maintenance are regulated in part by an interplay of the three Rho family GTPases Rac1, Cdc42 and RhoA. While Rac1 and Cdc42 are responsible for AJ formation, RhoA contributes to AJ maintenance [27]. Additionally, E-Cad is able to bidirectional interact with the EGFR. While E-Cad could inhibit EGFR signaling through NF2/Merlin, EGFR was shown to promote E-Cad endocytosis and thereby reduce the pool of functional E-Cad protein [26, 36].

Epidermal Growth Factor Receptor

EGFR has been shown to be involved in EMT and promotion of other tumor processes such as angiogenesis or metastasis through activating a wide range of different signaling pathways. In breast cancer, EGFR overexpression correlates with larger tumor size and poor clinical outcome and has been discussed as a potential therapeutic target [37]. The sole use of small molecule inhibitors such as Gefitinib in breast cancer treatment seemed so far unsuccessful in clinical trials, but the combination of endocrine therapy and EGFR inhibition in tamoxifen resistant ERα positive breast cancer seems promising at least in animal models [37, 38]. A major problem in breast cancer treatment is the development of Tam resistance which is discussed to be in part

mediated by activation of EGFR signaling, while EGFR inhibition is thought to retain Tam responsiveness [38, 39].

EGFR belongs along with HER2, ErbB-3 and ErbB-4 to the ErbB family of receptor tyrosine kinases. They consist out of an EC ligand binding domain, a single transmembrane domain and a cytoplasmic domain which contains the tyrosine kinase domain. The cytoplasmic domain is highly conserved, whereas the EC domain is heterogeneous indicating differential ligand binding affinities. Generally, the ErbB receptors are activated through binding of growth factors of the EGF family in an autocrine or paracrine fashion. Specific ligands for EGFR include EGF, transforming growth factor α and AREG [40]. Interaction of the receptor with the ligand causes a conformational change within the EC domain which enables dimerization and kinase activation. Homo- as well as heterodimers have been described. Next, specific residues in the cytoplasmic domain are autophosphorylated and can then serve as docking stations for downstream signaling proteins containing a src homology 2 (SH2) domain. This way, several signaling pathways, such PI3K/ERK or SFK are activated. SFKs with c-src as its most prominent member are one of the longest known oncogenes and have been shown to have elevated activity in many breast cancers. Through activating cytoplasmic kinases like the focal adhesion kinase (FAK) or specific GTPase activating proteins, SFKs influence cell motility and cytoskeleton organization [41, 42]. Additionally, SFKs can cause EGFR activation by direct phosphorylation and thus modulating EGFR signaling capacity [40].

As already mentioned, EGFR signaling and estrogen signaling are known to crosstalk with each other and a correct interplay of these pathways is essential during development, in particular of the mammary gland. Crosstalk can happen through various mechanisms. EGFR downstream pathways can influence ERα phosphorylation and thus ERα signaling activity and ligand independent ERα dependent gene expression [9]. The membrane-associated ER and GPER1 in turn can activate the EGFR, either through direct interaction with the receptor or indirectly through SFK-mediated activation of metalloproteases and the subsequent release of EGF-like growth factors [11, 13]. The expression levels of these growth factors are themselves often regulated by ERα. A prime example is the EGF family growth factor AREG.

As mentioned in Section 1.1.1, AREG is essential for correct development of the mammary duct and even though additional response elements exist in its promoter region, the AREG expression is highly estrogen-dependent in breast tissue [43].

In mice, knock down of ERα, EGFR or AREG all lead to a similar phenotype in ductal malformation [1]. Additionally, AREG was shown to stimulate its own expression possibly through EGFR activation as modulation of EGFR activity was shown to influence AREG levels [43, 44]. AREG is overexpressed in many types of cancer, particularly in breast cancer, and was shown to promote cell proliferation, invasion and cancer progression [44]. As it is discussed to play a part in the development of cancer resistance, AREG expression comes more into focus as a prognostic marker and possible target of cancer therapy [44].

In conclusion, as breast cancer is the most frequent cancer in women worldwide, a lot of research was undertaken to understand the underlying molecular mechanisms and possible treatment options. Estrogen and estrogen signaling have long been implicated to play a distinct role in the induction and progression of breast cancer. By dysregulation of key proteins including E-Cad, EGFR or AREG which are important for development and homeostasis of tissues under physiological conditions, estrogen signaling influences cancer cell proliferation, progression and metastasis.

1.2. Endocrine disruption

Ligand dependent activation of the ER is not limited to endogenous estrogens. The discovery of hormones in the beginning of the 20th century was soon followed by the discovery and development of chemicals with estrogenic activity for pharmaceutical use [45-47]. Tissue extracts used in the earlier years for hormonal treatment were substituted with synthesized chemicals [45]. The first contraceptive drug based on a mixture of synthetic estrogens and progestogens was introduced in the late fifties [48]. Only a few years later, environmental chemicals such as pesticides were also suspected to influence the hormonal system and induce adverse health effects in humans and wildlife. The US American biologist Rachel Carson for example described in her book ‘Silent Spring’ the adverse effects of dichlorodiphenyltrichloroethane, dioxin and other man-made chemicals on the endocrine system in wildlife populations [45].

Chemicals responsible for these effects on man and the environment are termed endocrine disrupting chemicals (EDC). In 2002, the World Health Organization (WHO) defined an EDC as “exogenous substance or mixture that alters function(s) of the endocrine system and consequently causes adverse health effects in an intact organism, or its progeny, or (sub)population” [49]. Since then, various direct links between exposure to certain substances and adverse endocrine effects in wildlife populations

have been observed [50]. For example, the high amount of reproductive disorders observed in polar bears could be attributed to the bioaccumulation of organ halogen pollutants [51]. Observed changes in sex ratios of fish correlated with their exposure to environmental chemicals through the effluent from sewage plants [50]. These observations often led to the ban or stricter regulation of these substances. As we are surrounded by a vast number and variety of different man-made chemicals at every moment in our life and effects of EDCs highly dependent on the point and duration of exposure as well as individual susceptibility and sensitivity [52], direct causal links of chemical exposure and endocrine diseases in humans are often difficult to prove yet correlations could be found. For example, exposure to polybrominated diphenyl ethers is connected to non-descended testes in young males and high exposure to polychlorinated dioxins increases the risk of breast cancer [50].

As a reaction to these discoveries in the nineties, governments including the United States of America, Japan, and the European Union put different programs and legislations into place in order to identify and eventually ban EDCs. Close to 1000 chemicals are either known or suspected to have the ability to interfere with the endocrine system through binding to hormone receptors or influencing hormone metabolism, and some of them can be found nearly ubiquitously [50, 52]. Daily, we come into contact with these endocrine active substances (EAS) through common ways of exposure (oral, dermal, inhalation) [53], but as indicated by the definition of the WHO possible endocrine activity alone does not make an EAS an EDC. Only when exposure to an EAS leads to adverse effects through disrupting the endocrine system, this substance would be classified as EDC. Classification of a chemical as EDC has often great impact on its production and marketing. The European regulations for chemicals (REACH (Registration, Evaluation, Authorization and Restriction of Chemicals), Regulation (EC) No 1907/2006), biocides (Regulation (EC) No 528/2012) and plant protection products (Regulation (EC) No 1107/2009) for example strictly impede or prohibit the marketing of chemicals that are classified as EDC in Europe.

In the following section, different chemical classes with known or suspected endocrine disrupting properties are described in more detail. In the final section of the introduction, the regulation of chemicals and available test methods are introduced.

1.2.1. Endocrine active/disrupting chemicals

EAS are structurally diverse and occur in man-made pharmaceuticals (e.g. Diethylstilbestrol (DES)) or in plastic products (e.g. Bisphenol A (BPA)) but also naturally as mycotoxins in fungi (e.g. Zearalenone (Zea)) or as phytoestrogens in plants (e.g. Genistein (Gen) and Daidzein (Dai)). Although a potential endocrine activity of specific substances is often easy to identify, it does not necessary mean that the said substance acts as an EDC and causes an adverse effect. Following, substances from the four mentioned groups are described in more detail.

Diethylstilbestrol (DES)

The 'synthetic estrogen' DES is one of the first recognized EDCs and a prominent example of a link between substance exposure and increased cancer risk in humans. After its strong estrogenic capacity has been described by Dodds *et al* in 1938 [46], it was prescribed for pregnant women to reduce the risk of miscarriages and abortion in the fifties and sixties [45, 54], even though the benefit of this treatment was already controversially discussed at that time [55]. Additionally, it was extensively used in the production of livestock to promote growth [56]. In the early seventies, it came to light that exposure to DES *in utero* is associated with a striking increase of a rare adenocarcinoma of the vagina in daughters at a young age [57]. Consequently, DES was banned for its use on pregnant women and livestock a few years later [56]. Follow-up studies revealed other additional adverse endocrine effects in the daughters exposed *in utreo* such as increased risks for breast cancer, preterm delivery or infertility [56, 58]. Sons exposed with DES *in utero* were found to have an increased risk of developing genital abnormalities [59]. Studies in mice even indicate possible adverse effects in following generations [56, 59].

Bisphenol A (BPA)

While the evidence for endocrine disruption is clear for DES, this is not always the case. The classification of bisphenols as EDCs following the WHO definition is a point of intense discussion. BPA is particularly in the focus because of its widespread usage and high production volume. BPA is essential for the production of polycarbonate plastics and epoxy resins, which are used for various consumer products like food containers, water pipes or medical equipment [60, 61]. The daily intake of BPA through food (the main source of exposure) is estimated to be around 0.48-1.6 µg/kg body weight/day [61] and a study by the US center of Disease Control and Prevention found

BPA in the urine of 95 % of a reference population of 394 American adults indicating a widespread exposure [62].

It has already been shown in 1936 that BPA is endocrine-active and exhibits estrogenic properties [47, 63]. Since it was recognized that EAS might cause adverse health effects, research into possible modes of action of BPA returned into public focus and potential endocrine disrupting properties were investigated. BPA was shown to elicit, for example, antiandrogen action, and interferes with the thyroid system and steroidogenesis [63, 64]. However, correlating BPA exposure to human disease is often difficult because of its widespread exposure and thus the lack of control groups as well as other confounding factors. Current knowledge points towards adverse health effects of BPA including infertility, decreased male sexual function, reduced sperm quality, impact on childhood behavior, and cardiovascular diseases, while no correlation was yet found between BPA exposure and endometrial disorders or birth weight [65].

Therefore, the European Union banned the use of BPA in the production of infant bottles in 2011 (Regulation (EU) 321/2011) and the European Food Safety Authority (EFSA) lowered the tolerable daily intake dose to 4 µg/kg body weight/day in 2015 [66]. Due to the ongoing public debate on a possible total ban of BPA, the production sector has partly switched to the use of other bisphenols like Bisphenol B (BPB) and Bisphenol S (BPS) as BPA alternatives. However, it is not clear if such a ban of BPA would be beneficial for human health as the BPA analogues have not been investigated as extensively yet and the already existing data suggests that these BPA alternatives have at least similar endocrine activity [67, 68].

Zearalenone (Zea)

Zea is an estrogenic mycotoxin produced by *Fusarium* fungi, common soil fungi often found in cereal crops such as corn, maize, barley, or oats. Additionally, Zea is added as a food supplement to promote growth of livestock. Human exposure usually occurs through consumption of plant products or indirectly through contaminated food such as meat or milk [69, 70]. The daily intake of an adult is estimated to range around 0.0008 to 0.029 µg/kg body weight/day with the provisional maximum tolerable daily intake for Zea being set at 0.5 µg/kg body weight by the Joint Committee by the Food and Agriculture Organization of the United Nations and WHO (JECFA) [69, 71].

Although Zea exhibits low acute toxicity, it was found to be strongly estrogenic [70]. Increased hyperoestrogenism observed in pigs, which ate moldy feed led to its discovery and isolation in the sixties [72]. Zea is able to equally bind to ERα

and ERβ and influences estrogen signaling. Though its binding affinity is reported to be lower than that of endogenous estrogens, it is still in range of the binding affinity of phytoestrogens and higher than many potential man-made EDCs [69]. The specific binding affinity depends on the isomer and metabolites were found to be more estrogenic [72]. In addition to or as a result of hyperoestrogenism, various endocrine adverse effects of Zea were observed *in vivo* including decreased fertility, reduced litter size, and changed weight of adrenal, thyroid, testis and pituitary glands [69]. In human, several cases of epidemic premature thelarche and precocious puberty suggest an effect on puberty timing when exposed to Zea in large amounts but a causal link is hard to proof [69].

Genistein (Gen) and Daidzein (Dai)

Plants can be a source for naturally occurring estrogenic substances. Four different structural groups of phytoestrogens are known - lignans, prenylflavonoids, coumestans and isoflavones. While lignans are primarily found in seeds, fruits and vegetables, the primary sources for prenylflavonoids are hops and beer. Coumestan levels are high in peas, certain beans, alfalfa and clover sprouts. Food sources with high isoflavone concentrations are in particular soy and soy-based products. Because of the general switch towards a high soy diet and the usage of soy products in infant food, isoflavones are of particular interest [73].

Similar to Zea, the estrogenic and endocrine disrupting properties of phytoestrogens were first observed in livestock. Sheep grazing in isoflavone-rich red clover fields exhibited fertility problems, increased abortion rates and reproductive abnormalities. Since then, several cases of isoflavone-related endocrine disruption were reported in a multitude of different animals including rodents, birds, fish and cattle [74]. Like all the other previously presented EAS, phytoestrogens are able to interact with the nuclear ERs but tend to show higher affinity for ERβ [73]. Isoflavones like Dai and Gen are additionally thought to influence the steroid and thyroxine biosynthesis, and hormone bioavailability [74]. Gen is known to generally inhibit tyrosine kinases including the EGFR [75]. While endocrine disruption is clearly observed in animals, this is less obvious in humans demonstrating the challenges in dealing with EDCs. Asian countries, where soy is part of the normal diet resulting in higher phytoestrogen exposure levels, generally see lower incidence rates of cardiovascular diseases and breast cancer. Although, many studies were undertaken studying these potential beneficial health effects of phytoestrogens, no clear answer can be made whether

consumption of phytoestrogen-containing food is rather beneficial or harmful as it likely depends on the susceptibility and sensitivity of the population [73]. Soy is also sometimes recommended as an alternative to hormone replacement therapy to lessen menopausal symptoms, however the evidence for positive effects is still inconclusive [73]. As *in vivo* experiments in rodents show clear endocrine-related defects as a result of phytoestrogen exposure, it cannot be excluded that phytoestrogens contribute to estrogen-related adverse health effects.

Although, all the EAS introduced here are able to bind the ER, the ultimate impact on human health is often still controversially discussed. Substances entering the body do not only have one mode of action but often can influence many different cellular pathways. Additionally, the resulting adverse effects depend on susceptibility to exposure, duration and metabolism. Therefore, for a correct classification of EAS many different factors need to be considered.

1.2.2. Chemical regulations and available test methods

Since the recognition of endocrine disruption through EDCs as a serious health issue and establishment of suitable programs and legislations for their regulation, new *in vitro* test methods were developed, and endocrine-related endpoints were integrated into existing *in vivo* assays. Generally, *in vitro* test methods are rather used for the identification of a possible endocrine mode of action and prioritization of chemicals, while *in vivo* assays are able to show an adverse effect. The Organization for Economic Cooperation and Development (OECD) has collated available screening assays for endocrine-related endpoints in form of the Conceptual Framework for Testing and Assessment of EDCs, which is described in OECD Guidance Document (GD) 150 on Standardized Test Guidelines for Evaluating Chemicals for Endocrine Disruption [76].

In this Conceptual Framework, the available assays are sorted according to their strength of evidence and complexity. While the methods and assays in level 1 and 2 are *in silico* or *in vitro*, level 3 to level 5 describe different *in vivo* studies. *In vivo* assays are generally divided according to the species used, i.e. into mammalian and non-mammalian studies.

Level 1 includes an evaluation of already existing data as well as *in silico* non-test information like read across, quantitative structure activity relationships, or absorption, distribution, metabolism and excretion model predictions. Level 2 contains a selection of *in vitro* test methods which are able to provide information on selected

endocrine modes of action. EDCs can perturb the endocrine systems through various mechanisms including receptor binding, transactivation of gene expression or influencing hormone biosynthesis and metabolism. Focusing primarily on estrogenic, androgenic, thyroidal and steroidogenic (EATS) modalities, different *in vitro* test methods were developed and validated. Available test methods to identify substances with estrogenic activity include the analysis of their ER binding affinity (OECD Test Guideline (TG) 493: "Performance-based Test Guideline for Human Recombinant Estrogen Receptor (hrER) – *In Vitro* Assays to Detect Estrogen Receptor Agonists and Antagonists" [77]), their ability to modulate ER transactivation (OECD TG 455: "Performance-based Test Guideline for Stably Transfected Transactivation – *In Vitro* Assays to Detect Estrogen Receptor Agonists and Antagonists" [78]), and effects on estrogen synthesis (OECD TG 456: H295R Steroidogenesis Assay). Level 3 describes *in vivo* assays that are specific for selected endocrine mechanisms including the mammalian Uterotrophic Assay (OECD TG 440) and Hershberger Assay (OECD TG 441) to detect xenoestrogens and xenoandrogens, respectively, but also include a selection of non-mammalian assays including the Short Term Fish Reproductive Assay (OECD TG 229). Level 4 and 5 include *in vivo* studies which provide data on relevant adverse effects concerning endocrine-related endpoints. While level 4 studies focus on the adverse endocrine effects, level 5 assays provide data concerning an adverse effect over a longer time span / life cycle. The Combined Chronic Toxicity/Carcinogenicity Studies (OECD TG 451-453) and the Combined 28-Day Reproductive Screening Tests (OECD TG 421 and 422) are both examples of level 4 assays while the Two-Generation Reproduction Toxicity Study (OECD TG 416) and the Extended One-Generation Reproductive Toxicity Study (OECD TG 443) represent level 5 test methods. Nation-specific regulations and assessment procedures of chemicals build on these different methods described in OECD GD 150.

The protection of humans and wildlife from exposure to EDCs is a central part of several regulations in the European Union (EU) including the Plant Protection Product Regulation (EU No 1107/2009), the Biocidal Product Regulation (EU No 528/2012), the Water Framework Directive (2000/60/EC), REACH (EU No 1907/2006), and the Cosmetics Regulation (2009/1223/EC). As mentioned (Section 1.2), the classification of a substance as an EDC often triggers its exclusion from further use and production. In 2018, the EFSA published a GD on the identification of endocrine disruptors in the context of plant protection and biocidal

products [79]. In this document, the different assays already described in OECD GD 150 are considered as the basis for assessment of potential endocrine effect. They are sorted into four groups according to their contribution towards information of mechanism and adversity – *in vitro* mechanistic (Level 2), *in vivo* mechanistic (level 3 and selected endpoints of level 4 and 5), EATS-mediated (level 4 and 5, selected level 3 assays) and sensitive to, but not diagnostic of, EATS (level 4 and 5). Following the definition of the WHO, a substance is classified as an EDC when a) it shows an adverse effect in an intact organism related to a change in morphology, physiology, growth, development, reproduction or life span, b) a endocrine mode of action could be shown, and c) it is plausible, that the observed adverse effect is caused through the endocrine mode of action. Identification and classification of EDC are conducted based on the existing data in a weight-of-evidence approach.

In the late nineties, the United States (US) Environmental Protection Agency (EPA) founded the Endocrine Disruptor Screening Program (EDSP). The Endocrine Disruptor Screening and Testing Advisory Committee (EDSTAC) as part of said program set up a two-tiered testing strategy. Similar to the Conceptual Framework described in OECD GD 150, it divides the same and some additional assays into two groups, one providing the mode of action and one showing the adversity. The tier 1 testing battery contains a selection of *in vitro,* and simple *in vivo* assays for mode of action identification and prioritization, while the tier 2 testing battery shows the adverse effect *in vivo* using complex animal-intensive studies [80].

Currently, over 10,000 unique chemicals are included in the EDSP and in need of testing. Completing the tier 1 assays for all chemicals is not feasible as it would require decades, a large amount of money and a high number of animals. One chemical undergoing the full tier 1 testing battery would mean the sacrifice of about 130 rats, 30 tadpoles or frogs and 60 fish even before entering tier 2 testing [81]. Similarly, in the EU, even though the last deadline for a registration under REACH ended in 2018, it is expected that several dossiers will fail at initial evaluation and additional information and testing will be required [82]. Due to the high intrinsic animal-to-animal variation of some endpoints, many *in vivo* studies require large group numbers. Additionally, inter-species differences need to be considered.

During the last decades, there has been a general drive towards the reduction and replacement of animal experiments through the use of alternative non-animal test methods. In addition to being more ethical, alternative test methods are often more time

efficient and cost effective. Additionally, they might be more predictive for human health effects as many of these alternative test methods are based on human cells. Still alternative test methods have the inherent limitation that they cover only specific endpoints and do not represent an entire organism. For example, the OECD TG 493 Estrogen Receptor Binding Assay uses recombinant human ER either full length produced in insect cells (Freyberger-Wilson Assay) or only the human ER binding domain produced in *Escherichia coli* (Chemical Evaluation and Research Institute (CERI) Assay) [77]. Based on competitive binding between the test chemical in comparison to E2, this test method provides information about the ER binding affinity of the test chemical but does not consider any functional consequence. Distinction between estrogen and antiestrogen action of test substances is possible with the OECD TG 455 Estrogen Receptor Transactivation Assay utilizing either Michigan Cancer Foundation-7 (MCF7) (VM7-Luc-ER Transactivation (TA) Assay) or human-ERα-HeLa-9903 (Stably Transfected TA (STTA) Assay) cells that were stably transfected with an ERE-regulated luciferase gene [78]. However, as the luciferase expression depends on the activation of a rather idealistic ERE, the transactivation assay still does not cover more complex modes of ER-dependent transactivation, which would require multiple cellular systems with an endogenous ER signaling pathway.

It is common agreement that the currently available alternative test methods alone do not suffice for full replacement of animal tests. The Adverse Outcome Pathway (AOP) concept has been introduced by the OECD in 2012 to overcome these limitations but also to identify knowledge gaps in toxicologically relevant modes of action. AOPs are built on the understanding that a Molecular Initiating Event (MIE) leads through a series of Key Events (KEs) across increasing layers of biological complexity to an adverse outcome in an organism [83]. The MIE and the KEs can be covered by one or multiple alternative test methods but may still also include animal testing. Efforts to fully replace animal testing by using AOP-based testing strategies that include multiple alternative test methods and fixed data interpretation procedures are currently underway.

Following along the canonical ERα signaling pathway (Section 1.1.2), Browne *et al*, as part of the ToxCast and Tox21 program, developed the ToxCast ER model [84]. This model integrates results of 18 different high-throughput screening assays to derive a score for ER activity. The assays are selected to follow the mode of action of ER activation analyzing the different ER signaling-relevant endpoints

including ER binding, dimerization and transactivation. Cell proliferation (E-SCREEN assay [85]) is included as the only functional endpoint. Comparison with existing data from the Uterotrophic Assay (OECD TG 440) showed a high predictive capacity of the ER score. The ToxCast ER model is therefore an accepted alternative for the Uterotrophic Assay in the context of Tier 1 substance prioritization [80]. Additionally, the ToxCast ER model, with a reduced number of 16 assays, is also a central part of the OECD Case Study on the Use of an Integrated Approach to Testing and Assessment (IATA) for Identifying Estrogen Receptor Active Chemicals that was published in 2019 [86].

2. Purpose

We are surrounded by a huge variety of chemicals every day. Some chemicals are suspected to disrupt and adversely affect our endocrine system. The endocrine system is an integrate part during development and the regulation of most bodily functions. As dysregulation of the endocrine system is connected to adverse health effects such as cancer, EDC are of high concern. Although several *in vitro* test methods exist that cover the initial events of ER activation only the E-SCREEN assay has a functional endpoint. Following the AOP and the drive towards replacement of animal experiments with alternative methods, there is a need for new *in vitro* test methods with functional endpoints.

The starting point of this thesis was the observation that inhibition of estrogen signaling causes AJ reorganization in a human breast cancer cell line. Hence, a first goal of this thesis was to further characterize the observed AJ reorganization by studying the underlying cellular mechanism and its functional consequences. A second goal was to develop a high throughput (HT) compatible alternative test method that uses this AJ reorganization as a novel endpoint for the identification of substances with estrogenic properties, and to analyze its predictive capacity in comparison to existing data of yet available test methods using well-established reference substances.

3. Results

3.1. Characterization of adherens junction organization as a novel estrogen specific endpoint

3.1.1. Antiestrogen treatment causes adherens junction reorganization

Based on the finding that ERα signaling modulates AJ organization in MCF7/vBOS breast cancer cells [87], the objective of this thesis was to develop a test method in a HT compatible assay set-up for the identification of estrogenic substances using AJ organization as endpoint.

As a first step, the ERα responsiveness of MCF7/vBOS cells was verified. MCF7/vBOS cells were treated with different concentrations of the estrogen E2 and the two antiestrogens Fulv and 4-hydroxytamoxifen (4-OHT) for 48 h. Figure 2 shows the resulting effects on gene expression levels of the estrogen-responsive genes *TFF1*, *PGR*, and *EGR3*. While E2 treatment did not influence gene expression of the three target genes, both antiestrogens caused an inhibition of their expression levels in a dose-dependent manner and at clinically relevant concentrations of 1 and 10 nM, respectively. Even though gene expression was not induced by E2, estrogen signaling could be modulated by antiestrogen treatment. The poor responsiveness to ERα stimulation may be explained by sufficiently high levels of residual estrogens in the cell culture medium to fully activate estrogen signaling capacity in MCF7/vBOS cells. The high estrogen responsiveness is not surprising since the original MCF7-BOS cells were selected for high E2-sensitivity [88]. Notably, the inhibition of target gene expression was more pronounced upon Fulv treatment compared to 4-OHT, which agrees with Fulv to be a selective ER downregulator (SERD) whereas 4-OHT to acts as selective ER modulator (SERM).

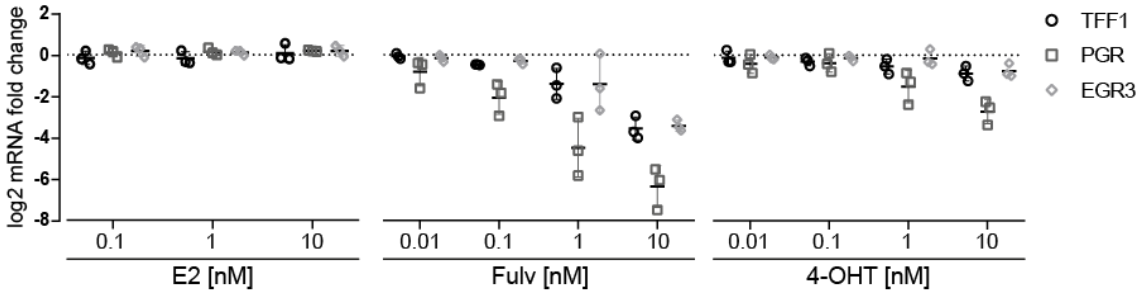

Figure 2: Antiestrogens are able to modulate estrogen responsive gene expression.
Log2 mRNA fold change of *TFF1*, *PGR*, and *EGR3* of MCF7/vBOS cells treated with different concentrations of 17β-estradiol (E2), Fulvestrant (Fulv) or 4-hydroxytamoxifen (4-OHT) for 48 h. qPCR-data was normalized against *YWHAZ* as housekeeper and the solvent control (ΔΔCT-method). One dot represents one biological replicate, the line indicates the mean and error bars the standard deviation.

The ERα protein disrupting properties of Fulv could be further verified by Western blot (Figure 3 a). In line with previously published data [89, 90], treatment with Fulv efficiently reduced ERα protein levels while no effect on *ESR1* transcription was detectable (Figure 3 b). Interestingly, 4-OHT caused an increase in ERα protein but not messenger ribonucleic acid (mRNA) levels suggesting that binding of 4-OHT stabilized ERα in a post-transcriptional manner (Figure 3 a, b). In order to test if ERα signaling can modulate E-Cad expression in MCF7/vBOS cells, the effect of antiestrogen treatment on *CDH1* mRNA and E-Cad protein expression was analyzed (Figure 3 a, b). Treatment with Fulv caused a twofold increase in E-Cad protein levels, while no effect on *CDH1* mRNA level was detectable suggesting a post-transcriptional stabilization of E-Cad. Notably, the increase in E-Cad levels was rather not detectable upon 4-OHT treatment, which may be due to the smaller capacity of 4-OHT to inhibit ERα signaling compared to Fulv (see Figure 2).

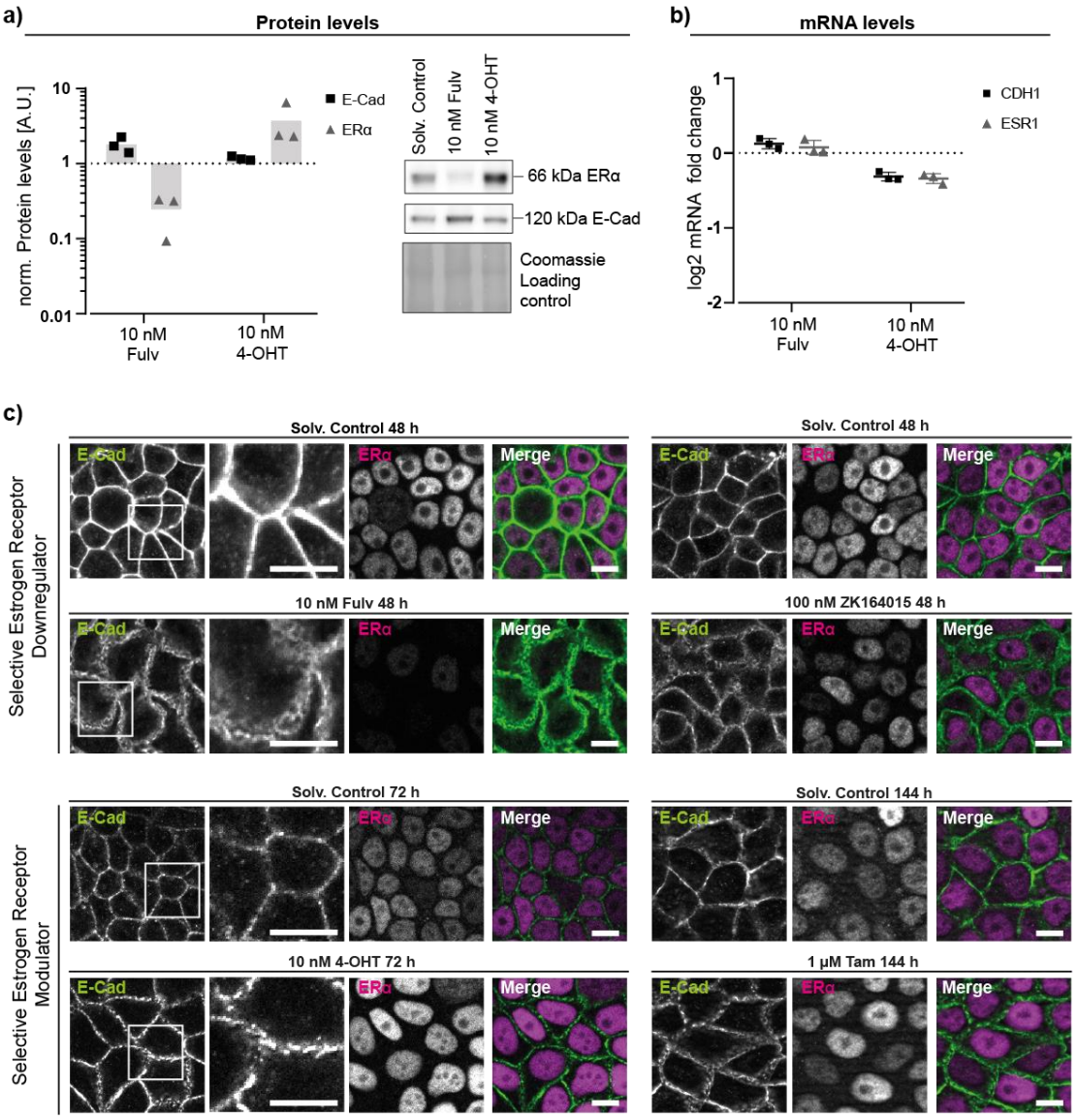

Figure 3: Antiestrogen treatment does not cause an increase in E-Cadherin expression but adherens junction reorganization.
a) Protein levels of E-Cadherin (E-Cad) and estrogen receptor α (ERα) after treatment with Fulvestrant (Fulv) and 4-Hyrdoxytamoxifen (4-OHT). Protein levels were normalized to the Coomassie blue loading control and the solvent control, n= 3. Treatment and Western blot were conducted under supervision by Ivana Lazic as part of her master thesis. b) Log2 mRNA fold change of MCF7/vBOS cells treated with different concentrations of Fulv and 4-OHT for 48 h, normalized as in Figure 2. c) MCF7/vBOS cells treated with different antiestrogens (Fulv, 4-OHT, ZK164015, Tamoxifen (Tam)). Cells were stained for E-Cad (green) and ERα (magenta), scale bar= 10 µm.

As a next step, the effect of ERα signaling modulation on AJ organization was analyzed by immunofluorescence staining (Figure 3 c). MCF7/vBOS cells were again treated with Fulv and 4-OHT and stained for ERα and E-Cad as a marker for AJs. While E-Cad uniformly localized across cell membranes (i.e. regular AJs) in the solvent control, treatment with Fulv and 4-OHT resulted in the formation of E-Cad clusters and AJ reorganization (i.e. irregular AJs). Again, Fulv appeared to be more potent than 4-OHT as AJ reorganization occurred after 48 h upon Fulv treatment but only after 72 h

upon 4-OHT treatment. The effect of the two antiestrogens on ERα protein levels (see Figure 3 a) was also clearly visible in immunofluorescence staining, when comparing the staining intensity of ERα between treatment and the respective solvent control. In order to confirm the effect of antiestrogens on AJ organization, two additional antiestrogens, the SERD ZK164015 (ZK) and the SERM Tam, the metabolic precursor of 4-OHT, were tested. Upon treatment of MCF7/vBOS cells with ZK and Tam, the AJs reorganized in a similar fashion as compared to Fulv and 4-OHT. Although AJ reorganization upon Fulv and ZK treatment occurred on a similar timescale, a 10-fold higher concentration of ZK was required. Tam was the weakest antiestrogen. Notably, ZK and Tam also decreased and increased ERα staining intensity, respectively, as already seen with Fulv and 4-OHT. Together, these data confirm the responsiveness of MCF7/vBOS cells used in this project to the antiestrogen-mediated depletion of the ERα signaling pathway in terms of target gene expression and AJ organization.

In order to use AJ organization as endpoint in a test method for the identification of estrogenic substances, changes in AJ organization need to be quantifiable. Therefore, fluorescence microscopy images needed to be turned into numbers. For this, an image analysis pipeline was built using the CellProfiler (CP) and CellProfiler Analyst (CPA) open-source software [91, 92]. This pipeline consisted of three main steps – CP-based cell segmentation and determination of morphological parameters, and CPA-based cell classification (Figure 4 a; see 7.5 for more details). During the classification step, cells were categorized into two distinct groups, i.e. regular AJs and irregular AJs, by supervised machine learning (training) on control images. The training set of cells was then used as a reference for classification of all other images from the same experiment. This way, each image could be represented as a number, i.e. the Morphology Index (MI). The MI is defined as the fraction of cells showing regular AJs normalized to the solvent control, which is set to 1.0 (Figure 4 b).

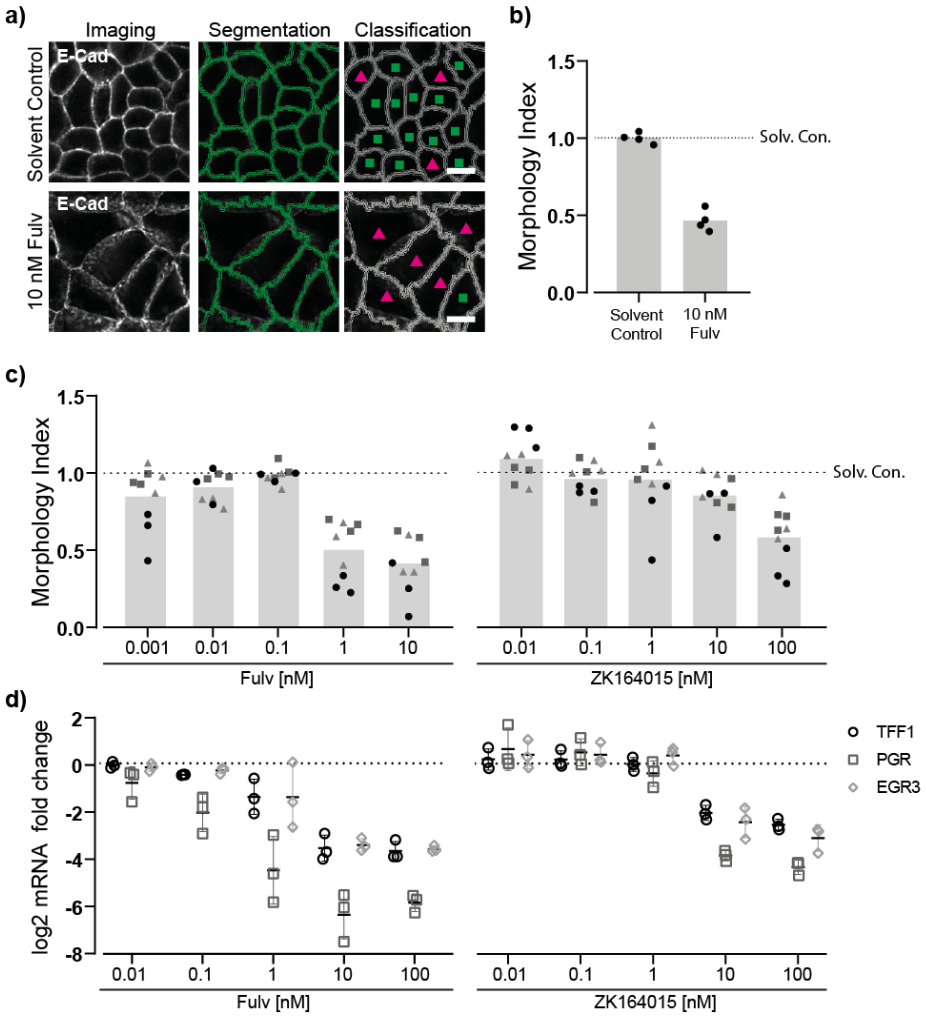

Figure 4: Quantification of adherens junction reorganization.
a) MCF7/vBOS cells were treated with 10 nM Fulvestrant (Fulv) for 48 h and stained for E-Cadherin (E-Cad), scale bar= 10 µm. Following, the images were analyzed with a CellProfiler/CellProfiler Analyst image analysis pipeline (see main text for details). Cells were segmented (green line) and classified into having regular (■) or irregular adherens junction (AJ) (▲) organization. b) The Morphology Index (MI) of MCF7/vBOS cells treated with 10 nM Fulv for 48 h. The MI is defined as the fraction of cells showing regular AJ organization normalized to the solvent control. One data point represents the mean of one analyzed image. c) The MI of MCF7/vBOS cells treated with different concentrations of Fulv and ZK164015. One data point represents the mean of one analyzed image and ■, ●, ▲ the three biological replicates. d) Log2 mRNA fold change of *TFF1*, *PGR*, und *EGR3* of MCF7/vBOS cells treated for 48 h with different concentrations Fulv (data from Figure 2) and ZK164015 normalized as in Figure 2.

Treatment of MCF7/vBOS cells with 10 nM Fulv caused a switch from regular to irregular AJ organization and thus a decrease of the MI. To test the performance of the image analysis pipeline, cells were treated with different concentrations of Fulv and ZK, stained for AJs with E-Cad as marker protein and analyzed as described above (Figure 4 c). Both antiestrogens caused a decrease of the MI in a dose-dependent manner. While Fulv treatment decreased the MI to a mean value of about 0.5 at 1 nM, ZK needed a concentration of 100 nM to reach a similar effect level. These differences in activity were also observed when comparing the effects of the two antiestrogens on

the expression of estrogen-responsive genes (Figure 4 d). Furthermore, the inhibition of estrogen-responsive genes correlated well with the reduction of the MI and therefore formation of irregular AJs. Additionally, the MI reduction seemed to be a robust read-out since similar dose-response relationship could be detected in independent experiments. Together, these data demonstrate the applicability of the image analysis pipeline to accurately detect AJ organization and its usability as an indicator for the ERα signaling status in MCF7/vBOS cells.

Taken together, it was verified, that ERα signaling can be modulated in MCF7/vBOS cells by treatment with antiestrogens. Additionally, it was shown that inhibition of estrogen signaling caused a reorganization of AJs, which could be quantified using a CP/CPA image analysis pipeline.

3.1.2. Adherens junction reorganization is estrogen receptor α specific

In order to use AJ organization as endpoint for the identification of estrogenic substances, the specificity of Fulv-induced AJ reorganization for the ERα signaling pathway needs to be clearly shown. Thus, it was tested whether addition of an estrogen such as E2 can prevent Fulv-mediated formation of irregular AJs. MCF7/vBOS cells were cotreated with 10 nM Fulv in combination with different concentrations of E2, and the MI and estrogen responsive gene expression were analyzed (Figure 5 a, b). With increasing E2 concentrations, an increase in the normalized MI was observed. Note that, in addition to normalizing the fraction of cells showing regular AJs to the solvent control (1.0) as described above, a second normalization to 10 nM Fulv (0) has been performed to derive a normalized MI. Hence, Figure 5 a shows that Fulv-mediated AJ reorganization was already partially prevented at 0.01 nM E2. At a concentration of 1 nM E2, the normalized MI value reached the level of the solvent control indicating full prevention of AJ reorganization by 10 nM Fulv. The mRNA levels of estrogen responsive genes showed a similar trend. Although, an inhibition of estrogen-responsive gene expression was still detectable at 0.01 nM E2, mRNA expression levels were higher than compared to treatment with 10 nM Fulv alone indicating a partial prevention of Fulv-mediated inhibition of ERα signaling. Starting at a concentration of 0.1 nM E2, estrogen-responsive gene expression reached the level of the solvent control. Interestingly, in contrast to cells treated with E2 only (see Figure 2), the mRNA levels of *PGR* even increased over the level of the solvent control at E2 concentrations of 1 and 10 nM suggesting that ERα signaling can indeed be stimulated in MCF7/vBOS

cells under certain circumstances, such as cotreatment with an ERα inhibitor. Together, these data points towards ERα dependency of AJ reorganization and illustrate again, that the MI can be used as a reliable measure to assess the ERα signaling status of MCF7/vBOS cells.

In order to further pinpoint Fulv-mediated reorganization of AJs to a specific inhibition of the ERα signaling pathway, the ERα was directly depleted by silencing RNA (siRNA) knock down (KD) targeting *ESR1*. MCF7/vBOS cells were transfected with four different siRNAs individually and in combination for 72 h. To first check for KD efficiency, the *ESR1* mRNA levels and the ERα protein levels were analyzed (Figure 5 c, d). While *ESR1* mRNA levels remained unchanged upon Fulv treatment as already shown before (see Figure 3 b), its expression was reduced by most individual *ESR1* siRNAs, except ESR1_10, and their combination (Figure 5 c). A concurrent reduction of the estrogen responsive gene *TFF1*, though less striking as for Fulv, was also observed indicating an inhibition of ERα signaling. Combination of the four siRNAs led to a strong reduction in ERα protein levels which was comparable to the effect of the SERD Fulv. Taken together, the protein and mRNA expression data indicate an effective KD of ERα. (Figure 5 d).

To analyze the effect of ERα KD on AJ organization MCF7/vBOS cells were again transfected with the four *ESR1* siRNAs individually and in combination for 72 h, followed by immunofluorescence staining for E-Cad and ERα (Figure 5 e, f). Image analysis was performed as described in Section 3.1.1. The siRNA-mediated KD of ERα resulted in an efficient reduction of ERα staining intensity as well as a similar clustering of E-Cad and AJ reorganization as previously observed upon Fulv treatment (Figure 3 c). Compared to the transfection reagent and scrambled controls, the normalized MI decreased significantly upon ERα KD and partly even reached the normalized MI level of cells treated with 10 nM Fulv. Together, these data show that downregulation of the ERα protein levels is sufficient to induce AJ reorganization and thus verify that antiestrogen-mediated reorganization of AJs is specific to inhibition of the ERα signaling pathway.

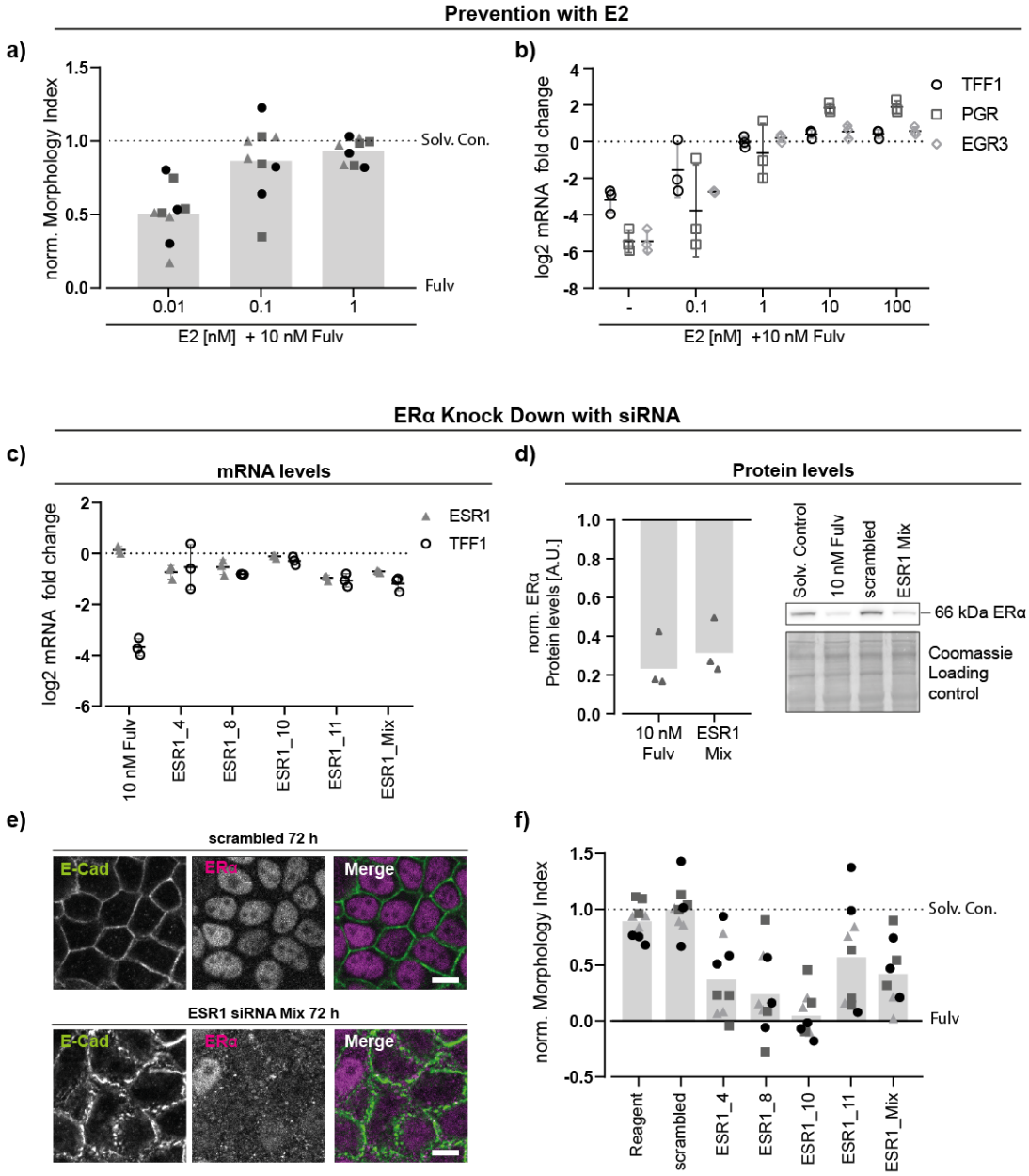

Figure 5: Adherens junction reorganization is prevented by estrogen addition and induced by ERα siRNA knock down.

a-b) MCF7/vBOS cells were treated with 10 nM Fulvestrant (Fulv) and different concentrations of 17β-estradiol (E2) for 48 h. a) The normalized Morphology Index (norm. MI) of MCF7/vBOS cells. The norm. MI is defined as the fraction of cells showing regular adherens junctions (AJ) normalized to the means of solvent control (1.0) and 10 nM Fulv (0). One data point represents the distribution of one analyzed image and ■, ●, ▲ the three biological replicates. b) Log2 mRNA fold change of *TFF1*, *PGR*, and *EGR3* normalized as described in Figure 2. c-f) MCF7/vBOS cells transfected with different siRNAs targeted against *ESR1*. c) Log2 mRNA fold change normalized to the corresponding controls as described in Figure 2. d) Estrogen receptor α (ERα) protein expression of cells either treated with 10 nM Fulv or transfected with a mix of *ESR1* siRNA. Protein levels were normalized to the Coomassie blue loading control and the corresponding control, n= 3. e) Representative images of transfected cells (scrambled/*ESR1* siRNA) stained for E-Cadherin (green) and ERα (magenta), scale bar= 10 µm. f) Norm. MI normalized as described above.

Though ERα is the primary target of Fulv and 4-OHT, it was shown that both antiestrogens can act on the GPER1. Interestingly, while both compounds act as antagonists for ERα, they were shown to act as agonists for the GPER1 and activate its downstream signaling cascades [16]. To test for a potential effect of Fulv and 4-OHT on GPER1 with regard to AJ reorganization, it was first analyzed whether the specific GPER1 agonist G1, which was reported not to act on ERα, would induce AJ reorganization. MCF7/vBOS cells were treated with different G1 concentrations alone or in combination with 10 nM Fulv, followed by analysis of AJ organization (Figure 6 a, b). In the tested concentration range, the normalized MI of G1 alone remained close to the solvent control and in combination with 10 nM Fulv around the level of the Fulv-treated cells. Higher concentrations could not be tested because of cytotoxicity of the substance. Thus, it can be concluded that the GPER1 agonist G1 does likely not have an effect on AJ organization.

Next, the effect of the two GPER1 antagonists G36 and G15 on Fulv-mediated AJ reorganization was tested. Both have been reported to specifically inhibit GPER1 induced effects such as PI3K or ERK activation. Whereas G15 has been reported to have limited binding affinity to ERα, G36 should be a more specific GPER1 antagonist [93, 94]. MCF7/vBOS cells were cotreated with either of the two GPER1 antagonists in combination with 10 nM Fulv, followed by analysis of AJ organization (Figure 6 c, d). While upon G36 treatment the normalized MI only slightly increased (Figure 6 c), G15 treatment did fully prevent Fulv-induced AJ reorganization at a concentration of 5 µM (Figure 6 d).

As it has been reported that G15 may also act as ERα agonist at high concentrations of around 10 µM [93], the effect of G15 and G36 on the expression of estrogen responsive genes was further investigated. Interestingly, neither cotreatment with G36 nor G15 could prevent the Fulv-mediated inhibition of estrogen responsive gene expression (Figure 6 e, f) suggesting that G15 could prevent AJ reorganization through a mechanism that was independent of ERα signaling inhibition.

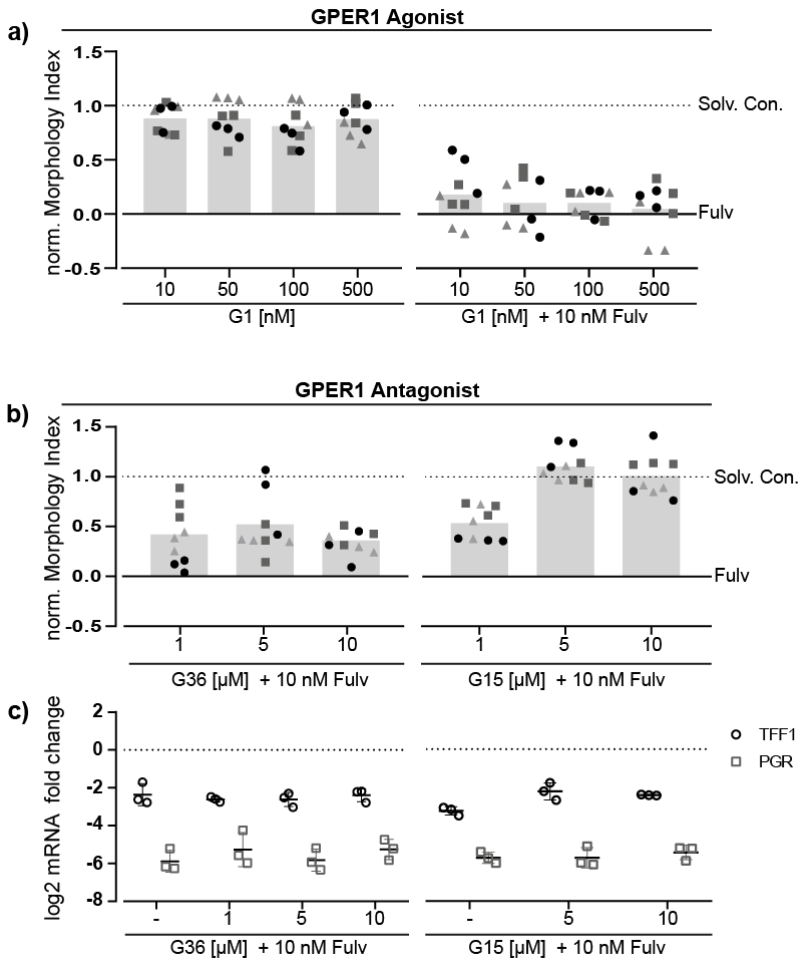

Figure 6: GPER1 antagonists influence adherens junction organization in contrast to GPER1 agonists.
a) Normalized Morphology Index (norm. MI) of cells treated with different concentrations of the GPER1 agonist G1 with or without 10 nM Fulvestrant (Fulv) for 48 h normalized as described in Figure 5. b-c) MCF7/vBOS cells treated with the two GPER1 antagonists G36 or G15 and 10 nM Fulv. b) Norm. MI normalized as described in Figure 5. c) Log2 mRNA fold change of *TFF1* and *PGR* normalized as described in Figure 2.

To further investigate the G15 effect on Fulv-induced AJ reorganization, MCF7/vBOS cells were treated with different Fulv concentrations alone or in combination with 5 µM G15, followed by analysis of AJ organization. As expected, starting from 1 nM Fulv, the normalized MI decreased in the cells treated with Fulv alone with slightly less efficient MI reduction at very high concentrations (Figure 7 a; note that the normalized MI was normalized to 10 nM Fulv alone). Treatment of cells with different concentrations of Fulv in combination with 5 µM G15 showed again a full prevention of AJ reorganization up until 10 nM Fulv. However, starting from 100 nM Fulv, the mean normalized MI decreased again to a value of around 0.6-0.7 indicating that higher concentrations of Fulv can at least partially compensate for G15-mediated prevention of AJ reorganization. Due to increased cytotoxicity, higher

concentrations of Fulv, at which the G15-mediated prevention of AJ reorganization might be fully compensated, could not be identified, though.

To test whether G15 could also prevent ERα KD-mediated AJ reorganization, MCF7/vBOS cells were transfected with a mixture of four *ESR1* siRNAs and treated with different concentrations of G15 (Figure 7 b). Transfection of cells with *ESR1* siRNA alone again resulted in a decrease of the normalized MI to about the level of Fulv treatment. In contrast to the observed effect of G15 on Fulv treatment, the addition of increasing concentrations of G15 to cells transfected with *ESR1* siRNA did not increase the normalized MI indicating that AJ reorganization was not prevented. To control for G15 reactivity in this experiment, cells were also cotreated with 10 nM Fulv in combination with different G15 concentrations. While at 5 µM G15 only a slight increase of the normalized MI was observed, the normalized MI reached the level of the scrambled control at 10 µM G15 indicating that Fulv-mediated AJ reorganization was fully prevented. Although G15 was slightly less reactive compared to previous experiments (Figure 6 b; Figure 7 a), it still sufficed to analyze the effect of G15 on ERα KD-mediated AJ reorganization. The findings that high Fulv concentrations could at least partially compensate for G15-mediated prevention of AJ reorganization and the lack of an effect of G15 on ERα KD-induced AJ reorganization suggest that G15 may interfere at least in part with Fulv through a competitive mechanism.

In order to address the role of GPER1 for Fulv-induced AJ reorganization more directly, MCF7/vBOS cells were transfected with a combination of four different siRNAs targeting *GPER1* siRNA and treated with 10 nM Fulv (Figure 8 a, b). If Fulv-induced AJ reorganization depends on the GPER1 activation, the simultaneous KD of the GPER1 should at least partially prevent AJ reorganization. However, while GPER1 KD caused a slight reduction in the normalized MI on its own, the normalized MI of the cells additionally treated with 10 nM Fulv remained at the level of the Fulv positive control.

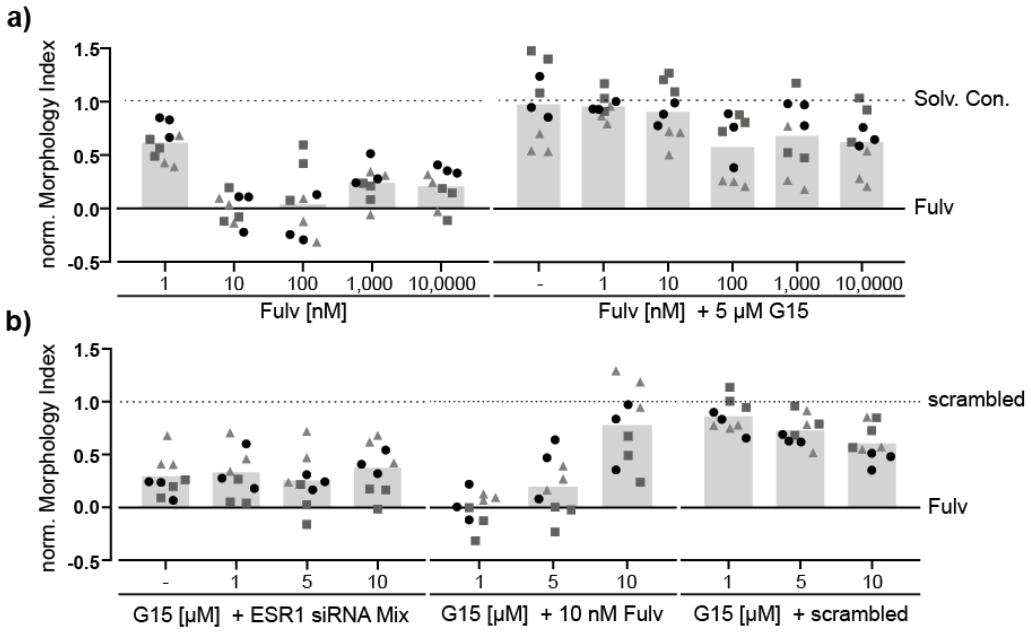

Figure 7: G15 can prevent Fulvestrant-induced adherens junction reorganization but not ERα knock down induced.
a) Normalized Morphology Index (norm. MI) of MCF7/vBOS cells treated with a fixed G15 concentration and different Fulvestrant (Fulv) concentrations for 48 h normalized as described in Figure 5. Treatment of cells and immunofluorescent staining done under supervision by Carolina Hurtado during her bachelor thesis. b) Norm. MI of MCF7/vBOS transfected with *ESR1* siRNA or scrambled and treated with different G15 concentration for 72 h. Cells cotreated with Fulv and G15 were included as G15 activity control. The MI was normalized on the scrambled solvent control and Fulv otherwise as described in Figure 5.

To control for GPER1 KD efficiency, *GPER1* mRNA levels were analyzed (Figure 8 b). In both conditions, *GPER1* mRNA level were downregulated by about twofold. Interestingly, while the expression of the estrogen responsive gene *TFF1* remained unaffected, the KD of GPER1 caused a slight upregulation of *PGR* mRNA. The previously described Fulv-mediated inhibition of *PGR* and *TFF1* mRNA levels (see Figure 4 d) remained however rather unaffected by GPER1 KD. The KD efficiency could only be checked on the mRNA level as no suitable antibody could be identified for Western blot analysis. Furthermore, MCF7/vBOS cells were transfected with a mixture of *ESR1* and *GPER1* siRNAs separately and in combination (Figure 8 c, d). The ERα KD caused the expected decrease of the normalized MI to a level around the Fulv positive control, while again no striking effect on AJ reorganization was observed for the GPER1 KD. Although, the normalized MI of the cells transfected with both *ESR1* and *GPER1* siRNA was slightly increased compared to the Fulv positive control and the cells transfected with *ESR1* siRNA only, it needs to be noted that the MI was in a similar range in previous experiments (see Figure 5 f; Figure 7 b). To control for KD efficiency, the *ESR1* and *GPER1* mRNA levels were analyzed. As expected,

ESR1 mRNA levels were decreased by about two-fold in cells transfected with *ESR1* siRNA alone and with both *ESR1* and *GPER1* siRNA. The corresponding inhibition of estrogen responsive gene expression can also be observed. However, the KD effect of *GPER1* mRNA was less clear as in both KD conditions only a weak downregulation of *GPER1* was observed. Thus, the influence of *GPER1* depletion on ERα KD-induced AJ reorganization remained rather unclear in this experiment as the GPER1 KD may possibly have not been effective enough.

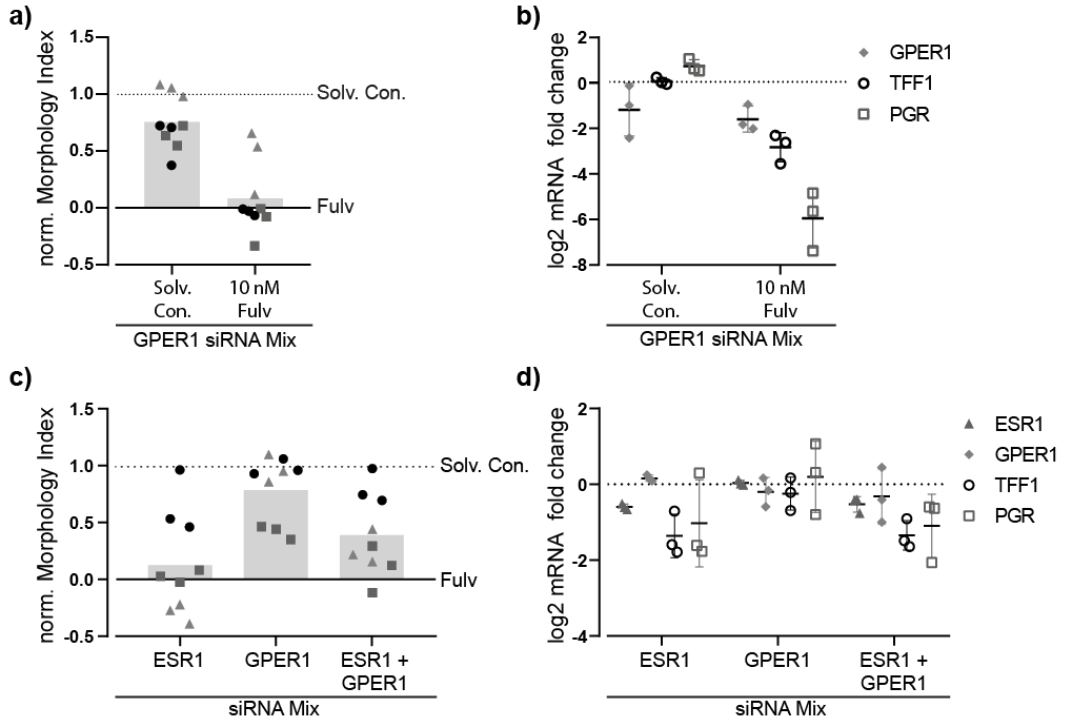

Figure 8: GPER1 KD does not influence adherens junction organization.
a-b) MCF7/vBOS cells transfected with a mixture of different *GPER1* siRNAs and treated with 10 nM Fulvestrant (Fulv) for 72 h. a) The normalized Morphology Index (norm. MI) normalized to the with scrambled siRNA transfected cells with or without Fulv treatment otherwise as in Figure 5. b) Log2 mRNA fold change of *GPER1* and estrogen responsive genes *TFF1* and *PGR* normalized on the scrambled control otherwise as described in Figure 2. c-d) MCF7/vBOS cells transfected with mixture of different *GPER1* siRNAs and *ESR1* siRNAs, separately and together. c) The norm. MI normalized to the cells transfected with scrambled siRNA with or without Fulv treatment otherwise as in Figure 5. d) Log2 mRNA fold change of *GPER1*, *ESR1* and estrogen responsive genes *TFF1* and *PGR* normalized on the scrambled control otherwise as described in Figure 2.

Taken together, these data show that Fulv-induced AJ reorganization was primarily caused by an inhibition of the ERα signaling pathway. This was demonstrated by the findings that the addition of an estrogen can prevent Fulv-induced AJ reorganization and, more importantly, that the specific depletion of ERα was sufficient for AJ reorganization. Although a potential role of the GPER1 signaling pathway in Fulv-induced AJ reorganization could not be completely excluded, the data suggests that GPER1 rather did not play an essential role in this process.

3.1.3. Adherens junction reorganization is a relevant functional endpoint

Changes in cell-cell adhesion play an important role in the development and progression of cancer, particularly in epithelial types of cancer such as breast cancer. As an inhibition of ERα signaling caused a striking reorganization of AJs in MCF7/vBOS breast cancers cells, the underlying molecular mechanisms and functional consequences of this reorganization were investigated in more detail.

Adherens junction reorganization results in increased cell-cell contact stability

The described reorganization of AJs is characterized by increased clustering of E-Cad at the cell membrane. The functional relevance of this E-Cad clustering was analyzed using two different assays – the Trypsin Resistance Assay and the quantitative Calcium Switch Resilience Assay. The Trypsin Resistance Assay was performed in a similar fashion as described in the paper by Shewan *et al* [95]. The susceptibility of E-Cad for Trypsin digestion can be used as a proxy for the fraction of E-Cad that is not directly involved in cell-cell contacts. Fulv-treated cells were incubated with Trypsin/ethylenediaminetetraacetic acid (EDTA) for 4 min prior to protein lysis and the levels of the full length E-Cad protein as well as the resulting fragments were analyzed by Western blot (Figure 9 a). Fulv treatment generally caused a slight increase of full length (120 kDa) E-Cad protein levels confirming previous observations (Figure 3 a). Trypsin treatment resulted in the detection of two additional bands at around 90 kDa and 60 kDa. These bands were strikingly less prominent upon Fulv treatment compared to solvent control cells indicating a reduced Trypsin susceptibility (Figure 9 a'). Along this line, the level of full-length E-Cad did not decrease in Fulv treated cells compared to solvent control cells upon Trypsin digestion (Figure 9 a''). The reduced Trypsin susceptibility of Fulv-related cells suggests that an increased fraction of E-Cad was involved in cell-cell contact formation, which may be reflected by the clustering of E-Cad at the cell membrane.

In Order to test if the reduced susceptibility of Fulv-treated cells to Trypsin digestion and the formation of E-Cad clusters influenced cell-cell contact stability, the quantitative Calcium Switch Resilience Assay was performed. In this assay, addition of the calcium chelating agent ethylene glycol-bis (β-aminoethyl ether)-N,N,N′,N′-tetraacetic acid (EGTA) reduces free calcium ions in the medium that are essential for E-Cad binding between cells. MCF7/vBOS cells were treated with Fulv as described above to allow formation of irregular AJs and then stained with the live cell imaging-

compatible dye CellTrace to visualize the cells. Upon EGTA addition, cells started to lose their cell-cell contacts and rounded (Figure 9 b, c). For each captured time point, the fraction of rounded cells was determined using an image analysis pipeline that was built within the PerkinElmer Harmony high content (HC) analysis software (see Section 7.5 for more details). While the fraction of rounded cells immediately increased in solvent control cells, in Fulv-treated cells it only started to increase after 40 min. Even after 120 mins, the fraction of rounded cells in the Fulv treatment condition was considerably smaller compared to solvent control cells indicating an increased resilience to calcium deprivation.

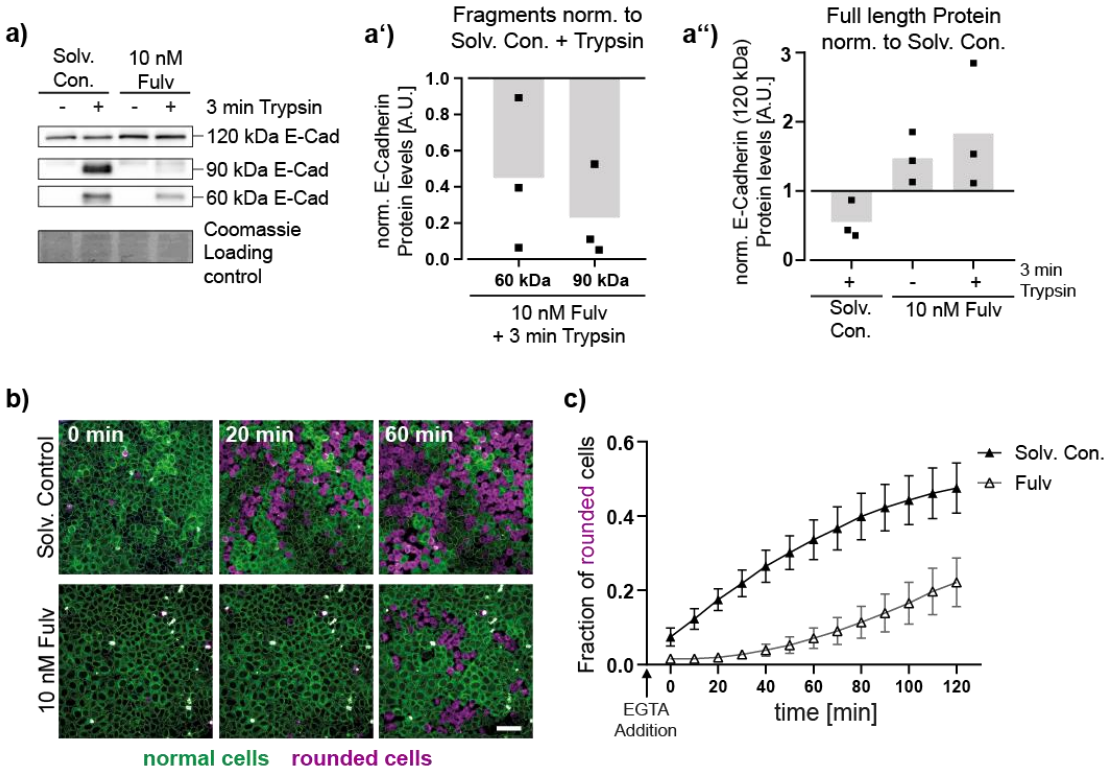

Figure 9: Adherens junction reorganization results in increased cell-cell contact stability.
a) E-Cadherin (E-Cad) protein level full length and fragments of MCF7/vBOS cells treated with 10 nM Fulvestrant (Fulv) and incubated with Trypsin/EGTA solution for 3 min (antibody for intracellular domain monoclonal mouse IgG2a, k Anti-E-Cadherin C36). Protein levels were normalized to the Coomassie blue loading control and a') the solvent control incubated with Trypsin or a'') to the standard solvent control, n= 3. b-c) Fulv treated MCF7/vBOS cells were stained with CellTrace and incubated with 8 mM EGTA for 120 min. Images were taken every 10 mins and analyzed with the Harmony analysis pipeline. Cells were classified into normal (green) and rounded (magenta) cells. b) Representative images of the cell classification at different time points, scale bar= 50 µm. c) Fraction of rounded cells over time, n= 3.

Together, the decreased susceptibility to Trypsin digestion and an increased resilience to the calcium chelating agent EGTA together suggest that an increased fraction of E-Cad was involved in cell-cell contact formation upon Fulv treatment, which eventually resulted in increased cell-cell contact stability.

Adherens junction reorganization is regulated by Amphiregulin

ERα can act directly or indirectly as transcription factor and regulate gene expression. As AJ reorganization was caused by ERα signaling inhibition (see Section 3.1.2), it was investigated which changes in gene expression correlate with the process of AJ reorganization using a time course microarray analysis. This way, AREG, a ligand of the EGFR, was identified as a possibly relevant target (data not shown). *AREG* was one of the earliest genes that showed a response to ERα signaling inhibition and the protein is known to be essential in breast development (reviewed in [1]). Hence, the results from the microarray analysis were verified by performing quantitative polymerase chain reaction (qPCR) for the same time points after the start of Fulv treatment (Figure 10 a). Whereas *ESR1* expression remained unchanged across all collected time points, the mRNA levels of the ERα target gene *TFF1* started to decrease after 24 h. Notably, *AREG* mRNA levels were already decreased by nearly four-fold after 4 h and even by 100-fold after 48 h. To confirm the regulation of *AREG* expression by ERα signaling, MCF7/vBOS cells were either treated for 48 h with different concentrations of Fulv alone or cotreated with a fixed concentration of 10 nM Fulv in combination with different E2 concentrations (Figure 10 b). With increasing concentrations of Fulv, *AREG* mRNA level decreased in a dose-dependent manner, while cotreatment with increasing concentrations of E2 resulted in an increase of *AREG* expression levels. At a concentration of 0.1 nM E2, the Fulv-mediated inhibition of *AREG* expression was fully prevented, which was also the case for the ERα target genes as shown before (see Figure 5 b). Interestingly, *AREG* expression level even increased over the level of the solvent control at E2 concentrations of 1 and 10 nM in a similar manner as shown for *PGR* (see Figure 5 b). These data indicate that *AREG* expression levels were very tightly regulated by ERα signaling activity also in our cell system.

To test whether inhibition of *AREG* expression is sufficient for AJ reorganization, MCF7/vBOS cells were transfected with a combination of four different *AREG* siRNAs for 72 h (Figure 10 c, d). While E-Cad was uniformly distributed across cell membranes in the scrambled control, transfection of cells with *AREG* siRNA resulted in an E-Cad distribution similar to Fulv treated cells (Figure 10 c). This observation was confirmed across multiple images as the normalized MI of the scrambled transfected cells was close to the solvent control, whereas the normalized MI of the AREG KD cells was close to the level of the Fulv positive control. Thus,

depletion of *AREG* by siRNA appears to be sufficient for the induction of AJ reorganization.

To address the possibility that AREG KD interfered with ERα signaling, thereby causing AJ reorganization, the mRNA levels of *AREG* and *TFF1* were compared between ERα and AREG KD cells (Figure 10 d). *AREG* mRNA levels were decreased in both KD conditions verifying KD efficiency and ERα-dependency of *AREG* expression. Notably, *TFF1* expression was only inhibited in ERα KD cells confirming that AREG KD-induced AJ reorganization was not caused by direct interference with the ERα signaling pathway. Furthermore, AREG protein levels were reduced in cells transfected with *AREG* or *ESR1* siRNA, albeit to a smaller extent than compared to Fulv treatment (Figure 10 f).

As AREG depletion was sufficient to induce AJ reorganization, it was next tested whether an AREG overexpression could also prevent the Fulv-induced formation of AJ reorganization. MCF7/vBOS cells were transfected with a plasmid encoding for a green fluorescent protein (GFP)-tagged human AREG (hAREG-GFP) and then treated with 10 nM Fulv. Analysis of AJ organization revealed that the normalized MI of cells overexpressing AREG and not treated with Fulv was in the range of the solvent control indicating that AJ organization was not affected (Figure 10 g). However, the normalized MI of cells overexpressing AREG that were treated with Fulv was considerably increased over the level of the Fulv positive control although it did not fully reach the level of the solvent control in all three biological replicates. This data shows that overexpression of AREG was able to at least partly prevent Fulv-mediated AJ reorganization.

In order to verify that AREG overexpression did not interfere with Fulv-mediated inhibition of ERα signaling, thereby possibly preventing AJ reorganization, mRNA levels of *AREG* and *TFF1* were measured in a single control experiment (Figure 10 h). As expected, cells overexpressing AREG showed a striking increase in *AREG* mRNA levels and could fully compensate for Fulv-mediated reduction of *AREG* mRNA levels. Notably, *TFF1* mRNA levels were decreased in Fulv-treated cells irrespective of AREG overexpression confirming that the partial prevention of AJ reorganization was not caused by interference with the Fulv-mediated inhibition of the ERα signaling pathway. The expression levels of hAREG-GFP were further analyzed by Western blot (Figure 10 i). In line with similar mRNA expression levels, hAREG-GFP (70 kDa) was also rather equally expressed at the protein level in both

solvent control and Fulv-treated cells. Furthermore, a smear of bands was detected right above the hAREG-GFP band (70 kDa) suggesting that hAREG-GFP was post-translationally modified, potentially glycosylated, and therefore correctly processed. Interestingly, hAREG-GFP overexpression may have stimulated expression of endogenous AREG as the protein level of endogenous AREG (bands at 35 kDa and 43 kDa) were elevated and their Fulv-mediated reduction was not detectable.

Taken together, these data clearly show that AREG is an ERα-responsive gene, which is in line with previously published data [96-98]. The findings that the KD of AREG induced AJ reorganization in a similar fashion as ERα KD or Fulv-treatment but without inhibiting ERα signaling, and that the overexpression of AREG at least partly prevented Fulv-induced AJ reorganization suggest that ERα signaling controls AJ organization through AREG.

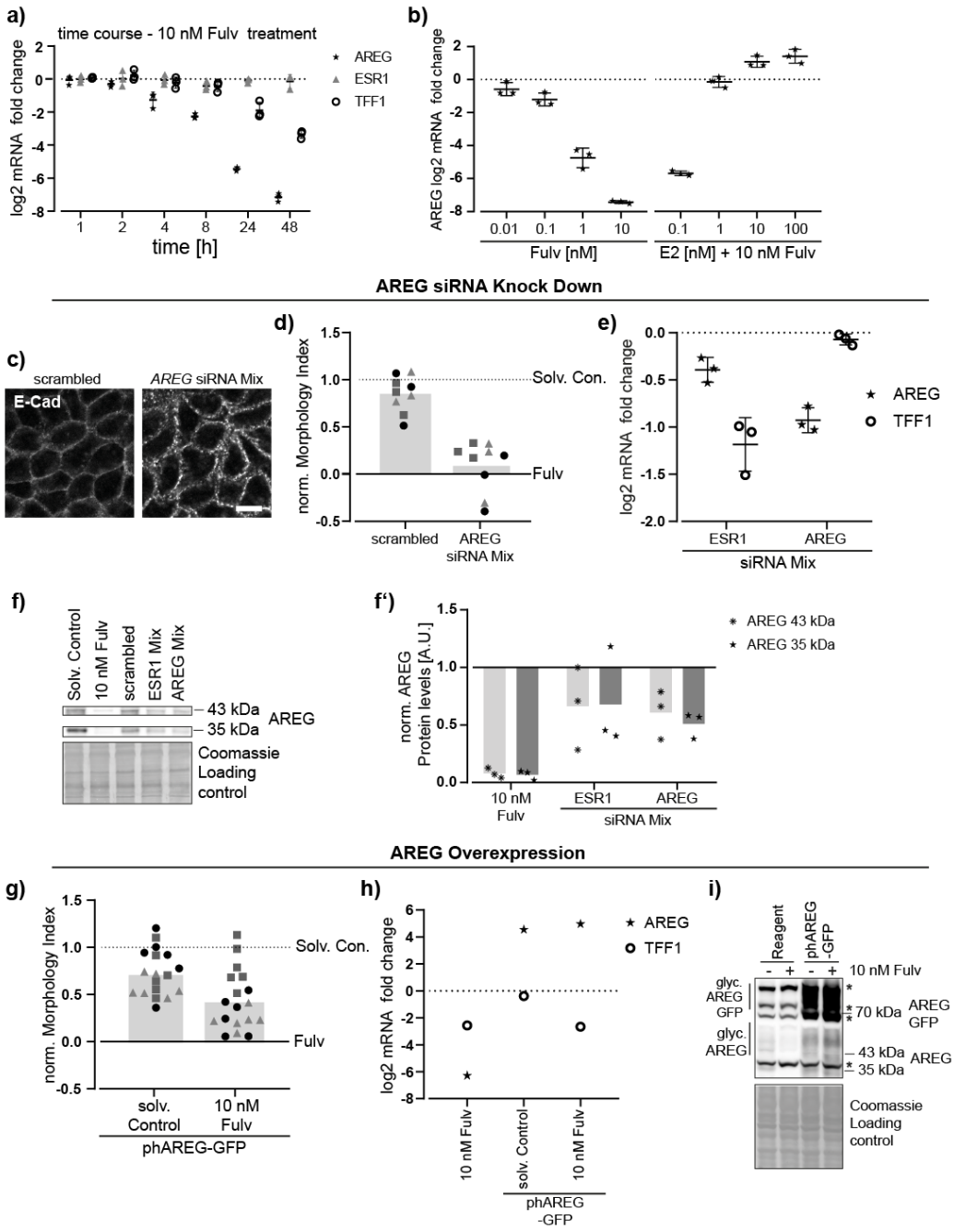

Figure 10: Adherens junction reorganization is depended on Amphiregulin expression.
a) Log2 mRNA fold change of *AREG, ESR1* and *TFF1* of MCF7/vBOS cells after different incubation times with 10 nM Fulvestrant (Fulv) normalized on solvent control of the corresponding time point otherwise as described in Figure 2. b) Log2 mRNA fold change of *AREG* of MCF7/vBOS cells treated with different Fulv concentrations or different concentrations of 17β-estradiol (E2) and 10 nM Fulv normalized as described in Figure 2. c-g) MCF7/vBOS cells transfected with a mixture of different *AREG* siRNAs for 72h. c) Representative images of transfected cells (scrambled/*AREG* siRNA) stained for E-Cadherin, scale bar= 10 µm. d) The normalized Morphology Index (norm. MI) normalized as described in Figure 5. e) Log2 mRNA fold change of *AREG* and *TFF1* of cells transfected with *AREG* or *ESR1* siRNA normalized described in Figure 2. f) Protein expression of cells transfected with a mixture of either four *ESR1* or *AREG* siRNA. Protein levels were normalized to the Coomassie blue loading control and the scrambled control, n= 3. g-i) MCF7/vBOS transfected with phAREG-GFP to overexpress AREG. Cells treated with 10 nM Fulv for 48 h. g) The norm. MI normalized to the Fulv-treated or solvent control with six images per replicate, otherwise as in Figure 5. h) Log2 mRNA fold change of *AREG* and *TFF1* of cells normalized as described in Figure 2, n= 1. i) Protein expression of transfected and 10 nM Fulv treated cells. * indicates unspecific bands.

Adherens junction reorganization involves EGFR signaling

AREG is a known ligand of the EGFR, which regulates in concert with the ERα signaling pathway the organization of cells during mammary gland development [1]. To test if AJ reorganization also involves the EGFR signaling pathway, EGFR protein and mRNA level were analyzed in cells treated with Fulv and 4-OHT (Figure 11 a, b), or transfected with *ESR1* siRNA or *AREG* siRNA (Figure 11 c, d). EGFR protein levels were strikingly elevated in cells treated with 10 nM Fulv or transfected with *ESR1* siRNA, while a less prominent increase was observed in cells treated with 10 nM 4-OHT or transfected with *AREG* siRNA (Figure 11 a, c). Interestingly, this increase in protein level was not necessarily reflected by the *EGFR* mRNA expression levels (Figure 11 b, d). Only in *ESR1* siRNA cells, the *EGFR* mRNA level was elevated compared to the corresponding control. Treatment with 10 nM Fulv or transfection with *AREG* siRNA rather decreased *EGFR* mRNA levels, while treatment with 4-OHT did not have any effect. Thus, the increase in EGFR protein level upon AJ reorganization was likely regulated on a post-transcriptional level potentially involving changes in protein stability.

Considering that AREG is known to activate EGFR signaling and downregulation of *AREG* resulted in AJ reorganization, it was tested whether inhibition of EGFR activity alone might be sufficient to induce AJ reorganization. Hence, MCF7/vBOS cells were treated with the EGFR inhibitor Gefitinib, a drug that is used in breast cancer therapy [37, 38], for 72 h and the effect on AJ organization was analyzed (Figure 11 e, f). E-Cad distribution upon treatment with 1 µM Gefitinib was similar to that observed for Fulv-treated cells. Quantification of multiple replicates revealed that the normalized MI of Gefitinib-treated cells was reduced to a value of around 0.4 suggesting that inhibition of EGFR signaling activity was sufficient for the induction of AJ reorganization, albeit less efficient than inhibition of ERα signaling. However, an increase of the Gefitinib concentration did not result in further reduction of the normalized MI value. To verify this observation, two additional EGFR inhibitors, PD153035 and BIBX1382, were tested (Figure 11 g, h). Both PD153035 and BIBX1382 also caused AJ reorganization at a concentration of 1 µM, albeit less widespread and striking as compared to Fulv or Gefitinib treatment.

In order to investigate the possibility that EGFR inhibition interfered with ERα signaling, thereby causing AJ reorganization, the mRNA level of the ERα target gene *TFF1* were analyzed (Figure 11 i). All three inhibitors showed a similar dose-dependent

reduction of the *TFF1* expression level, which was at least not caused by a transcriptional depletion of *ESR1* (Figure 11 i). Moreover, *EGFR* and *AREG* mRNA levels were also downregulated in a dose-dependent manner. The similar changes in expression through all three inhibitors indicate that the observed effects were specific to EGFR signaling inhibition but not off-target effects. Though, AREG was shown to play an instructive role in AJ reorganization, the identification of a causal link between EGFR inhibition and AJ reorganization requires further studies. Nevertheless, these data point towards an essential crosstalk between the EGFR and ERα signaling pathways in the regulation of AJ morphology.

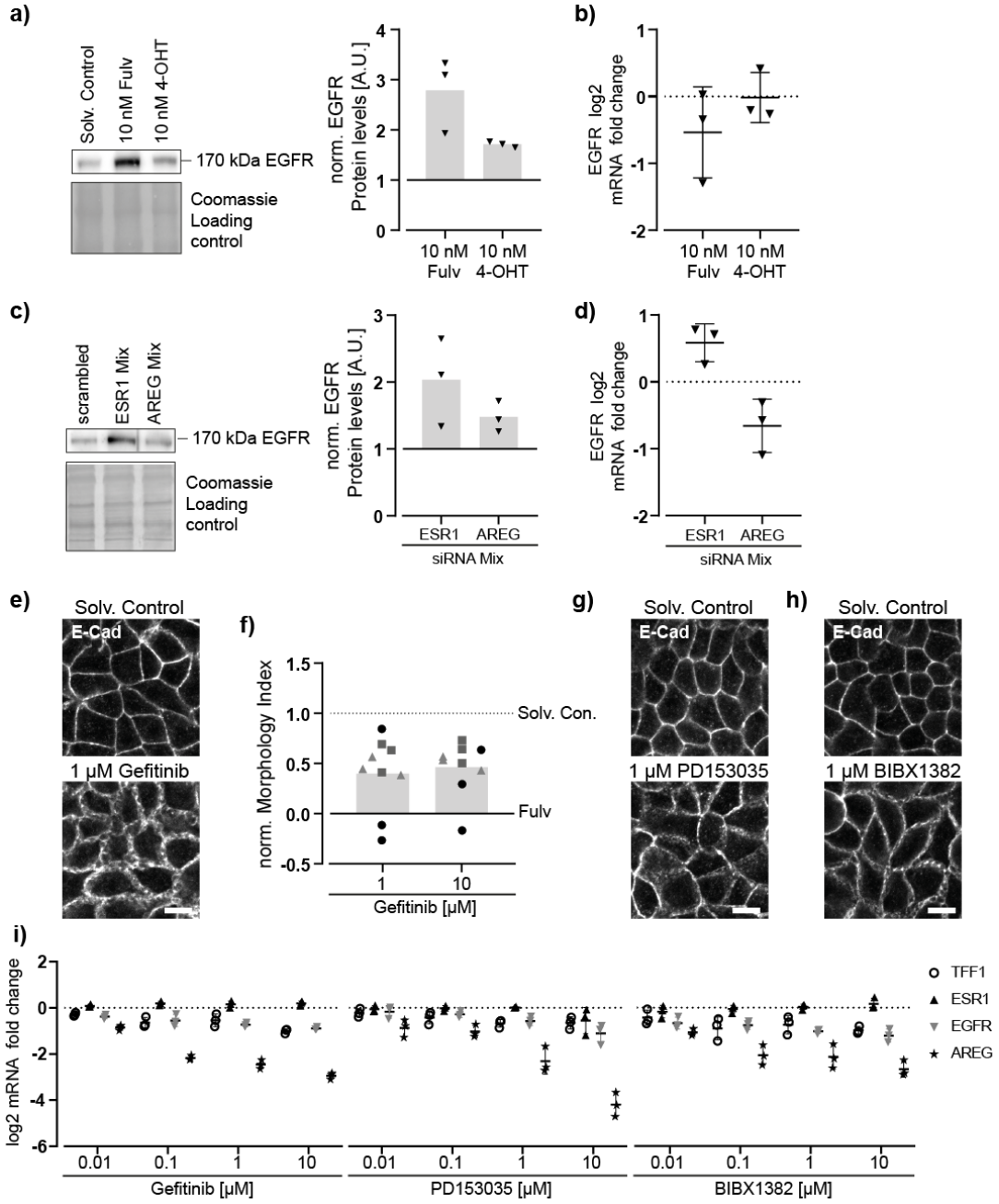

Figure 11: The EGFR protein level is increased in cells with adherens junction reorganization.
a,b) MCF7/vBOS cells treated with Fulvestrant (Fulv) and 4-hydroxytamoxifen (4-OHT) for 48 h. Protein sampling and Western blot done under supervision by Ivana Lasic as part of her master thesis. c,d) MCF7/vBOS cells transfected with a mix of *ESR1* or *AREG* siRNA for 72 h. a,c) Protein expression of transfected cells. Protein levels were normalized to the Coomassie blue loading control and the corresponding control (solvent control or scrambled), n= 3. b,d) Log2 mRNA fold change of *EGFR* in MCF7/vBOS cells normalized as described in Figure 2. e-h) MCF7/vBOS cells treated with the EGFR inhibitors Gefitinib, PD153035 and BIBX1382 for 72 h. e) Representative images of cells treated with 1 µM Gefitinib stained for E-Cadherin (E-Cad), scale bar= 10 µm. f) Normalized Morphology Index (norm. MI) of Gefitinib-treated cells normalized as described in Figure 5. g) Representative images of cells treated with 1 µM PD153035 or BIBX1382 stained for E-Cad, scale bar= 10 µm. h) Log2 mRNA fold change of *TFF1*, *ESR1*, *EGFR*, and *AREG* of MCF7/vBOS cells normalized as in Figure 2.

Inhibition of Src family kinases decreases *AREG* expression and induces adherens junction reorganization

EGFR is known to regulate and to be regulated by SFK (as reviewed in [99], [100]). Additionally, it was reported, that SFKs are an essential mediator of the crosstalk between EGFR and ERα [101]. In order to test whether SFKs also play a role in AJ organization, MCF7/vBOS cells were treated with three different inhibitors of SFKs – kb-src4, PP1, and PP2 (Figure 12 a-d). PP3 was included to control for potential side effects on EGFR signaling as reported for the structurally related PP1 and PP2 SFK inhibitors. Whereas no effect on AJ organization was observed upon treatment with the c-Src specific inhibitor kb-src4, AJ reorganization was induced in cells treated with the general SFK inhibitors PP1 and PP2 at 10 µM. Notably, cells treated with 100 µM PP3 did also show subtle changes in AJ organization, albeit not to the same extent as observed for PP1 and PP2, which may be explained by its inhibitory effect on EGFR signaling (reported IC50 of 2.7 µM [102]). While the normalized MI of kb-src4-treated cells remained close to the normalized MI of the solvent control, the normalized MI of PP1- and PP2-treated cells decreased to the level of the Fulv control at 5 µM. Interestingly, the normalized MI of PP3-treated cells was rather in the range of the solvent control across all concentrations tested indicating that the image analysis pipeline was not capable to detect the subtle changes in AJ organization described above.

In order to test whether SFK inhibition also interferes with ERα signaling as shown for EGFR inhibition, gene expression of *ESR1*, *TFF1*, *PGR*, and *AREG* were analyzed upon treatment with PP1, PP2, and PP3 (Figure 12 e). All three substances showed comparable effects on gene expression levels, which were less pronounced in PP3-treated cells. In contrast to all other substances described so far, a slight dose-dependent increase of *ESR1* was observed. Moreover, while *TFF1* remained constant, *PGR* expression was induced to a similar extent as shown in Figure 5 b (cotreatment of Fulv and E2 with E2 concentrations of 1 and 10 nM). Interestingly, *AREG* expression was considerably downregulated under these conditions. Due to the contradictory results of ERα-dependent gene expression, the effect of SFK inhibition on ERα signaling remained unclear. These findings underline again the connection of AJ reorganization, AREG expression and EGFR activity. However, the role of SFK for AJ organization remains unclear.

The inhibitor kb-src4 is reported to be highly specific for c-Src while PP1 and PP2 also inhibit other SFKs such as Fyn [103, 104]. As kb-src4 did not cause AJ reorganization, which rendered an essential role of c-Src rather unlikely, it was tested whether disrupting the function of Fyn influences AJ organization. Hence, cells were transfected with a mixture of four *FYN* siRNA alone or under cotreatment with Fulv for 72 h (Figure 12 f-g). Under both conditions, *FYN* mRNA levels were clearly decreased in cells transfected with *FYN* siRNA. Despite the efficient KD of Fyn, no striking effect on the normalized MI was observed in untreated Fyn KD cells compared to the scrambled solvent control. However, the normalized MI of Fyn KD cells cotreated with Fulv was slightly elevated compared to the scrambled Fulv control, which also correlated with a slight increase in *AREG* expression levels.

To summarize, the SFK inhibitors PP1 and PP2 were able to induce AJ reorganization while also causing downregulation of *AREG* expression levels. Whether the downregulation is mediated through ERα signaling inhibition remains to be elucidated. The c-Src-specific inhibitor kb-src4 and a Fyn KD however did not cause any AJ reorganization while *AREG* gene expression levels also remained unaffected. Since the activity of SFK appears to be directly connected to AREG expression, future studies have to unravel the complex interplay of SFK, AREG and EGFR activity in the formation of ERα-dependent AJ re-organization.

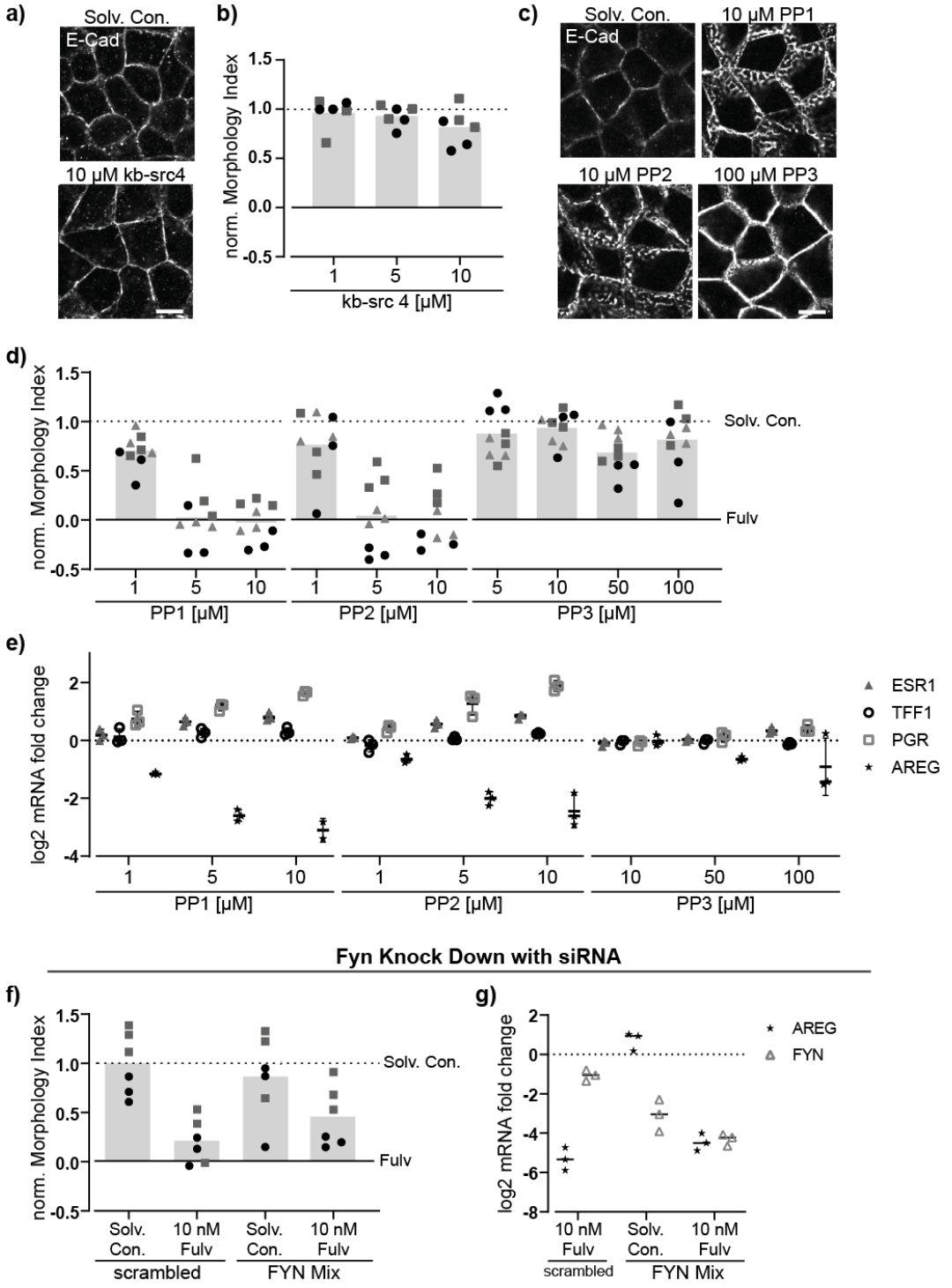

Figure 12: Src family kinase inhibitors PP1 and PP2, but not knock down of Fyn, induced adherens junction reorganization.
a) MCF7/vBOS cells treated with kb-src4 for 144 h. Representative images stained for E-Cad, scale bar= 10 µm. b) The normalized Morphology Index (norm. MI) was normalized as described in Figure 5, n= 2. Treatment and immunofluorescence staining were conducted under supervision by Carolina Hurtado during her bachelor thesis. c-d) MCF7/vBOS cells treated with PP1, PP2, and PP3 for 48 h. Treatment and immunofluorescent staining was conducted under supervision by Carolina Hurtado during her bachelor thesis c) Representative images stained for E-Cad, scale bar = 10 µm. d) Norm. MI normalized as described in Figure 5. e) Log2 mRNA fold change of *ESR1*, *TFF1*, *PGR*, and *AREG* normalized as in Figure 2. f-g) MCF7/vBOS cells transfected with a mix of four *FYN* siRNA for 72 h. f) The norm. MI normalized as described in Figure 5. g) Log2 mRNA fold change of *AREG* and *FYN* normalized as described in Figure 2.

Next, it was tested whether substances that can prevent Fulv-induced AJ reorganization (see Figure 5 and Figure 6) were also capable of preventing PP1- and PP2-induced AJ reorganization. As the effects of PP1 and PP2 on AJ organization and gene expression levels were almost indistinguishable, the following experiments were performed using the more broadly used PP2 inhibitor only. MCF7/vBOS cells were cotreated with 10 µM PP2 and different concentrations of E2, G15, or G36 and the AJ organization was analyzed (Figure 13 a, b). The normalized MI of PP2 only treated cells was in this experiment slightly higher compared to the Fulv control (Figure 13 a). Cotreatment of cells with PP2 and E2 at 0.01 nM or G15 at 5 nM was sufficient to reach the normalized MI of the solvent control, while cotreatment with G36 did not fully prevent PP2-induced AJ reorganization at any concentration. Although these data generally resembled the results of the cotreatment with Fulv (see Section 3.1.2, Figure 6), some qualitative differences in the appearance of AJs and E-Cad membrane distribution could still be observed (Figure 13 b).

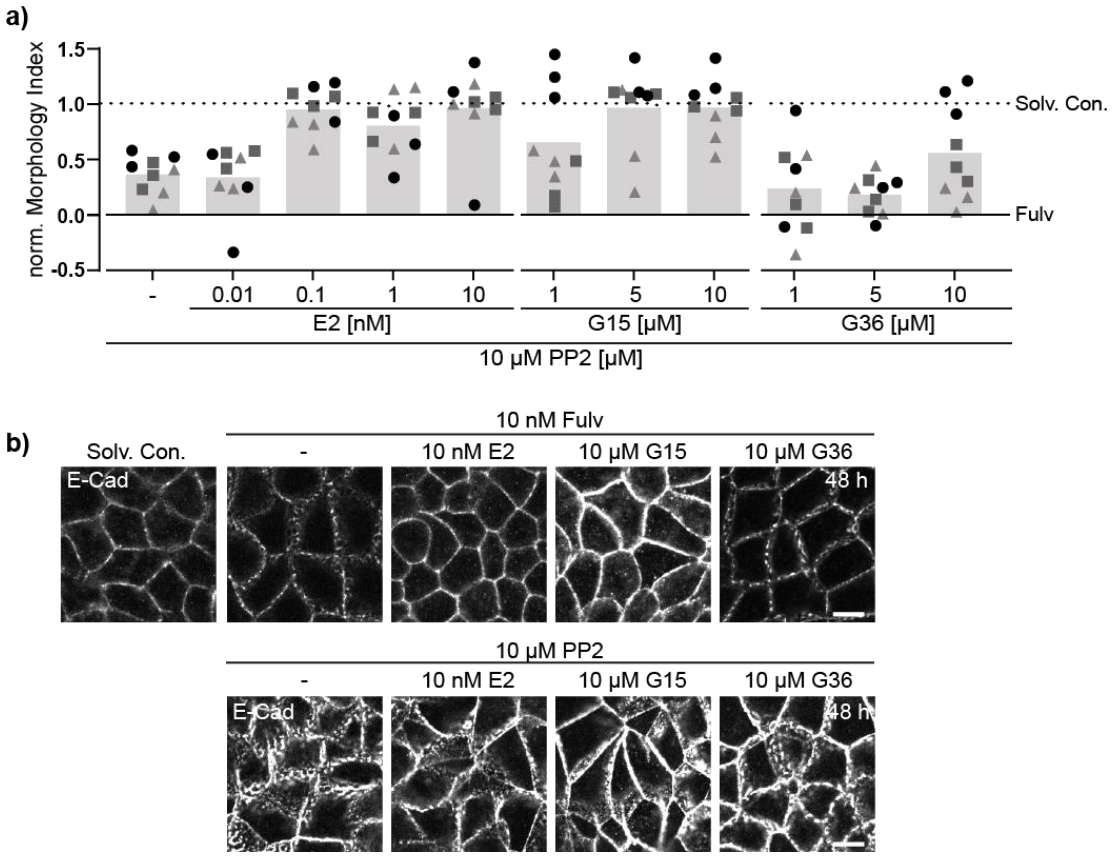

Figure 13: G15 and E2 can partially prevent PP2-induced adherens junction reorganization.
a) MCF7/vBOS cells cotreated with PP2 and different concentrations of E2, G15 and G36 for 48 h. The normalized Morphology Index (norm. MI) normalized as described in Figure 5. b) Representative images of MCF7/vBOS cells cotreated PP2 or Fulvestrant (Fulv) (for the quantification of all replicates of the Fulv treated cells see Figure 5 and Figure 6) and different concentrations of E2, G15 and G36 for 48 h stained for E-Cadherin (E-Cad), scale bar= 10 µm.

In conclusion, these data indicate that the effect of the SFK inhibitors PP1 and PP2 on AJ organization was at least partially mediated by an interplay between the SFK, ERα and potentially the EGFR signaling pathways. Although it appears rather unlikely that either c-Src or Fyn alone are sufficient for regulating AJ organization, the identity of a central SFK member or combination of multiple essential SFK members involved in AJ reorganization remain to be identified.

RhoA activation influences adherens junction reorganization

SFKs are known to be at the heart of the crosstalk between integrins and the Rho-family of small GTPases in adhesion signaling and cytoskeleton rearrangement (reviewed in [41]). Thus, a possible role of the Rho-family of small GTPases in AJ reorganization was investigated further.

As a first experiment, it was tested whether RhoA activation affects AJ reorganization. MCF7/vBOS cells were pretreated with 10 µM PP2 for 72 h or 10 nM Fulv for 48 h to induce AJ reorganization (Figure 14 a, b). Subsequently, cells were treated for 8 h with different concentrations of the RhoA activator CN03. CN03 is acts specifically on RhoA by catalyzing the deamidation of glutamine-63 (Q63), thereby blocking GTPase activity and resulting in constitutively active RhoA [105]. Whereas no effect of CN03 on AJ organization was observed in the solvent control, CN03 efficiently reverted the PP2/Fulv-induced AJ reorganization to regular AJ organization. Quantification of the AJ organization of Fulv pretreated cells across three replicate experiments confirmed these observations as the addition of CN03 for 8 h sufficed to raise the normalized MI value of Fulv treated cells to nearly 0.5 (Figure 14 c). These results point towards an involvement of RhoA in AJ reorganization.

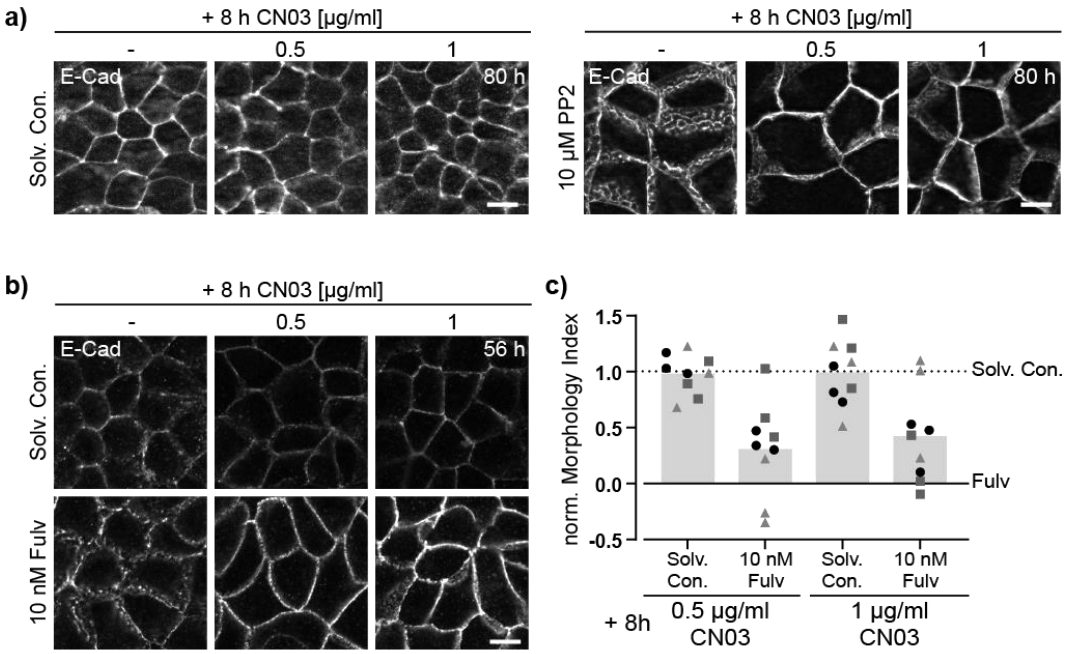

Figure 14: RhoA activator CN03 can rescue normal adherens junction organization after Fulvestrant or PP2 treatment.
a) Representative images of MCF7/vBOS cells pretreated with PP2 for 72 h and then cotreated with CN03 another 8 h stained for E-Cadherin (E-Cad), scale bar= 10 µm. b-c) MCF7/vBOS cells pretreated with Fulvestrant (Fulv) for 48 h and then cotreated with CN03 another 8 h. Treatment and immunofulorescence staining was done under supervision by Carolina Hurtado as part of her bachelor thesis. b) Representative images of MCF7/vBOS cells stained for E-Cad, scale bar= 10 µm. c) The normalized Morphology Index (norm. MI) normalized as described in Figure 5.

As RhoA activation was able to revert PP2/Fulv-induced AJ reorganization, it was tested next, whether RhoA inhibition might induce AJ reorganization. Thus, cells were treated with the two RhoA inhibitors Y16 and Rhosin at 10 µM and 50 µM for 48 h and 72 h, respectively (Figure 15 a). While Rhosin binds directly to RhoA to generally inhibit RhoA activation (GDP-GTP exchange) by Guanine nucleotide exchange factors (GEFs), Y16 only prevents activity of the Rho-specific RhoGEF12/Leukemia-associated Rho guanine nucleotide exchange factor (LARG) [106, 107]. It needs to be noted that CN03, Y16, and Rhosin are reported to also act on the closely related RhoC. Whereas no differences in AJ organization were observed between solvent control and Y16-treated cells, E-Cad clusters formed at 10 µM Rhosin and AJs reorganized at 50 µM Rhosin. To test if Rhosin-mediated AJ reorganization can be reverted by CN03 in a similar fashion as shown for PP2 and Fulv, MCF7/vBOS cells were pretreated with 50 µM Rhosin for 48 h followed by treatment with CN03 for 8 h at 0.5 and 1 µg/ml (Figure 15 b). Treatment with 50 µM Rhosin decreased the normalized MI to the level of the Fulv control indicating a similar type of AJ reorganization. Addition of CN03 for 8 h caused an increase of the normalized MI of

Rhosin-treated cells to a level that was similar to the corresponding CN03-treated Fulv control indicating a similar mechanism of AJ reorganization. Again, a potential interference of RhoA inhibition with the ERα signaling pathway was analyzed by measuring the gene expression levels of *ESR1*, *TFF1*, and *AREG* upon treatment with Rhosin (Figure 15 c). Though, no changes in the expression of *ESR1* were observed, both *TFF1* and *AREG* were downregulated suggesting that, similar to the EGFR inhibitors (Figure 11 i), AJ reorganization upon RhoA inhibition may also involve ERα signaling. In order to test whether Fulv-mediated AJ reorganization may have been caused by repression of *RHOA* expression, the mRNA levels of *RHOA* and the closely related *RHOC* were analyzed, along with *CDH1* whose expression levels were usually not affected by any treatment condition (Figure 15 c'). Again, no changes in the mRNA levels of *CDH1* were observed. Notably, Rhosin treatment resulted in a reduction of *RHOA* and *RHOC* levels at high concentrations, which was not the case for Fulv-treatment. Interestingly, *RHOC* expression levels even increased upon Fulv-treatment, while *RHOA* remained unchanged. Therefore, it was investigated whether modulation of RhoA or RhoC expression levels have an effect on AJ organization.

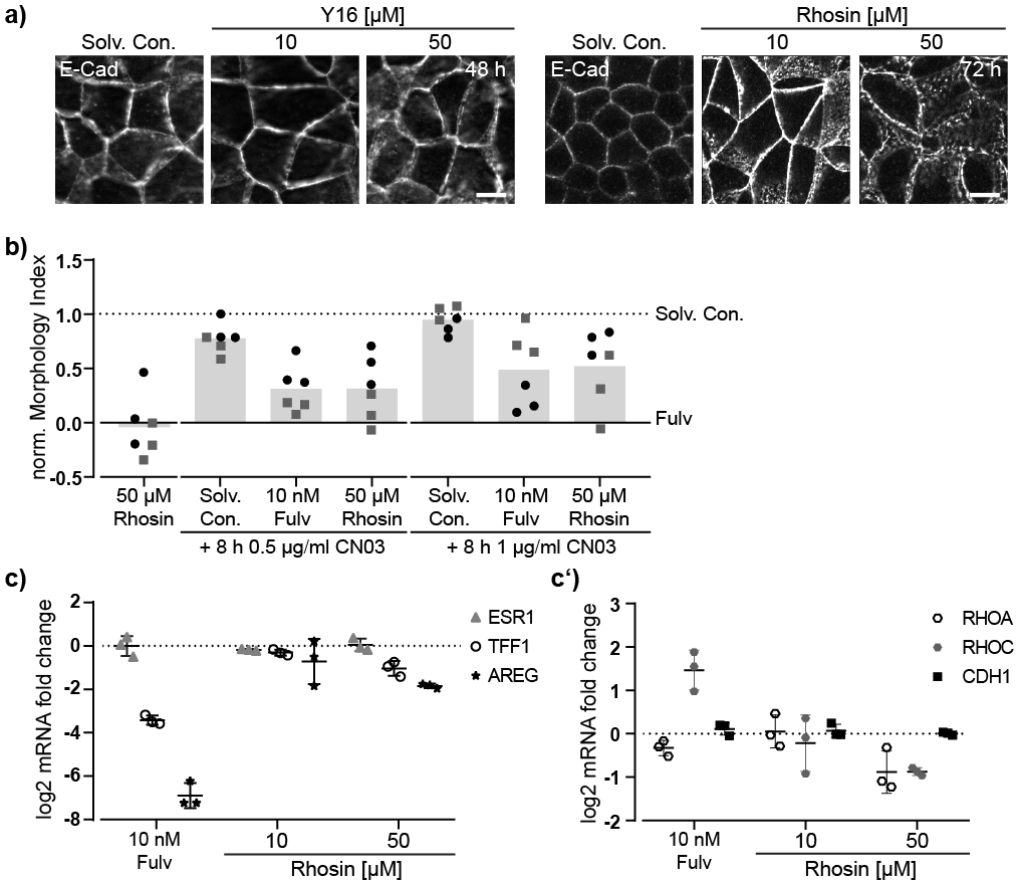

Figure 15: Inhibition of RhoA through Rhosin induces adherens junction reorganization.
a) Representative images of MCF7/vBOS cells treated with Y16 and Rhosin for 48 h and 72 h, respectively, stained for E-Cadherin (E-Cad), scale bar= 10 µm. b) The normalized Morphology Index (norm. MI) of MCF7/vBOS cells pretreated with 50 µM Rhosin or 10 nM Fulvestrant (Fulv) for 48 h and then cotreated with CN03 for 8 h normalized as described in Figure 5, n= 2. Treatment and immunofulorescence staining was done under supervision by Carolina Hurtado as part of her bachelor thesis. c) Log2 mRNA fold change of *ESR1*, *TFF1*, and *AREG* and c') *RHOA*, *RHOC*, and *CDH1* of MCF7/vBOS cells treated with Rhosin for 72 h normalized as described in Figure 2. Treatment and RNA extraction was done under supervision by Carolina Hurtado as part of her bachelor thesis.

To test whether downregulation of RhoA would induce AJ reorganization, MCF7/vBOS were transfected with a mixture of four different siRNAs and AJ organization and mRNA levels were analyzed (Figure 16 a, b). Although, *RHOA* was efficiently downregulated, its KD neither induced the characteristic AJ reorganization nor prevented the effect of Fulv. Analysis of the mRNA levels also demonstrated the specificity of the RhoA KD as the *RHOC* levels remained unchanged. Interestingly, the *AREG* mRNA levels were slightly elevated compared to the corresponding untransfected control cells, which closely resembled the results of the Fyn KD (Figure 12 e).

Next, it was investigated whether overexpression of wild-type (WT) and mutant RhoA might influence AJ organization. MCF7/vBOS cells were transfected with plasmids encoding for GFP-RhoA^{WT} or two RhoA mutants, the constitutive active GFP-RhoA^{Q63L} and the constitutive inactive GFP-RhoA^{N19T}. Subsequently, the transfected cells were treated with 10 nM Fulv for 48 h and the AJ organization was analyzed (Figure 16 c). Neither the overexpression of RhoA^{WT} nor constitutive inactive RhoA^{N19T} seemed to influence AJ organization in control or Fulv-treated cells. Notably, in line with previous experiments using the RhoA activator CN03 (Figure 14, Figure 15 b), Fulv-treated cells overexpressing the constitutive active RhoA^{Q63L} did not show AJ reorganization (green arrow), while the surrounding untransfected cells did (white arrow). Interestingly, AJ reorganization was also reduced in untransfected cells directly connected to several RhoA^{Q63L} overexpressing cells suggesting that neighboring cells may influence each other regarding AJ organization.

To summarize, modulation of RhoA protein levels by KD or overexpression of RhoA^{WT} did not influence Fulv-induced AJ reorganization. However, manipulation of RhoA activity by expression of mutant RhoA constructs indicates that RhoA was not sufficient to induce AJ reorganization but apparently rather played a permissive role as the overexpression of the constitutive active mutant RhoA^{Q63L} prevented Fulv-induced AJ reorganization.

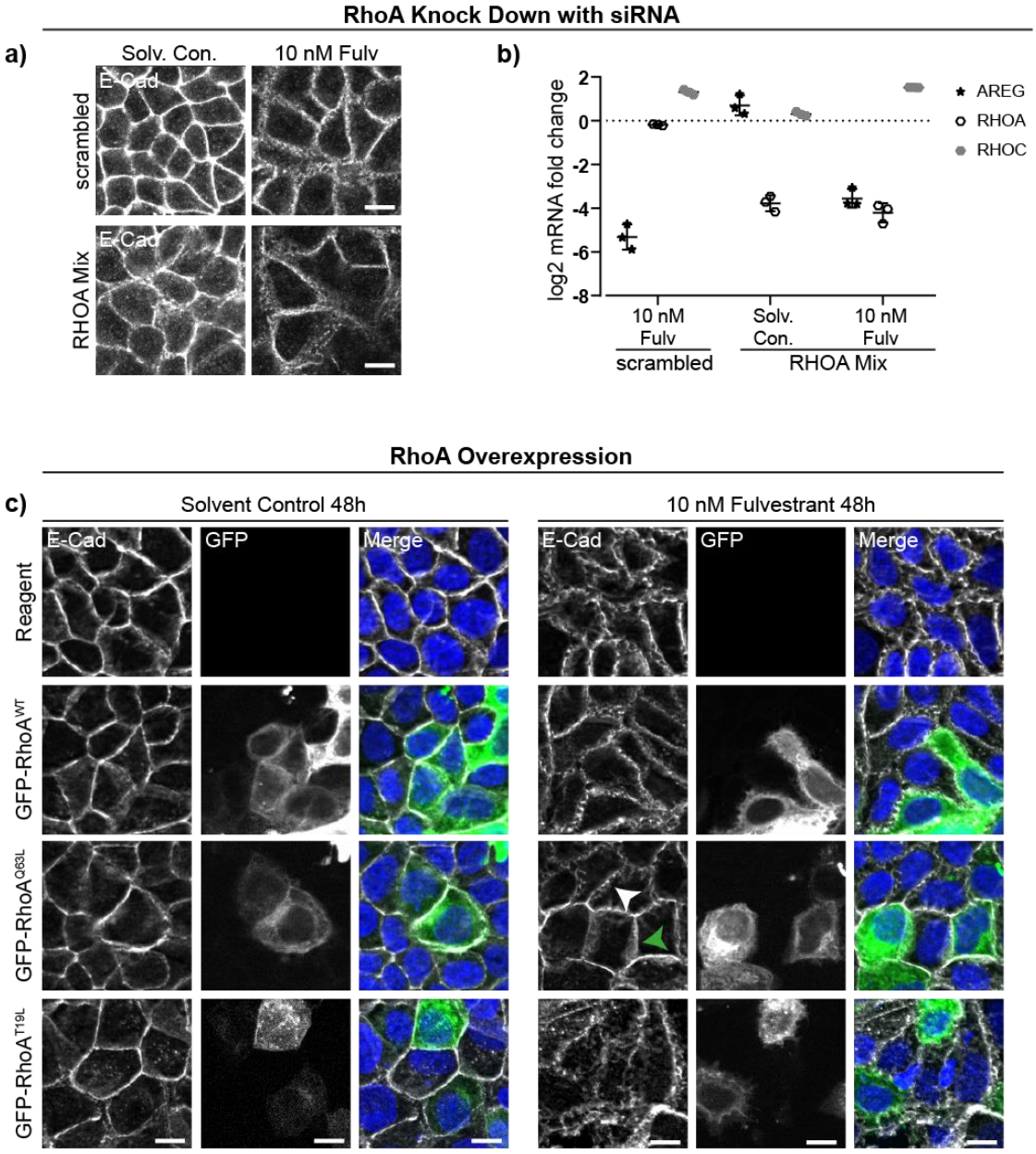

Figure 16: Overexpression of constitutive active RhoA prevents adherens junction reorganization
a-b) MCF7/vBOS cells transfected with a mix of *RHOA* siRNA for 72 h. a) Representative images of MCF7/vBOS cells stained for E-Cadherin (E-Cad), scale bar= 10 µm. b) Log2 mRNA fold change of *AREG*, *RHOA* and *RHOC* normalized as described in Figure 2. c) Representative images of MCF7/vBOS cells transfected with GFP-RhoA^{WT}, GFP-RhoA^{Q63L}, and GFP-RhoA^{T19L} stained for E-Cad, scale bar= 10 µm. White arrow indicates adherens junction (AJ) reorganization; green arrow indicates regular AJ organization.

Following, as the RhoA modulators are reported to also act on RhoC and quantitative differences in its gene expression levels were observed as described before, RhoC was also analyzed in more detail. As a downregulation of the *RHOC* mRNA level was shown upon Rhosin treatment (Figure 15 c), it was tested whether a KD of *RHOC* might induce AJ reorganization. MCF7/vBOS cells were transfected with a mixture of *RHOC* siRNAs and treated with 10 nM Fulv for 72 h (Figure 17 a). Although, *RHOC*

was efficiently downregulated, its KD neither induced the characteristic AJ reorganization nor clearly prevented the effect of Fulv since the normalized MI of KD cells was similar compared to the corresponding controls. Again, the specificity of the RhoC KD could be confirmed as the *RHOA* expression levels remained unchanged (Figure 17 b). Notably, in this experiment *AREG* mRNA levels were rather decreased upon RhoC KD when compared to the corresponding control, which is in contrast to the increased gene expression levels observed for Fyn KD and RhoA KD. Since an upregulation of *RHOC* was observed upon Fulv treatment, it was further tested whether RhoC overexpression might induce or influence AJ reorganization (Figure 17 c). MCF7/vBOS cells were transfected with a plasmid encoding for GFP-RhoC^{WT} and treated with 10 nM Fulv for 48 h. Similar to RhoA, no effect of RhoA^{WT} overexpression on AJ reorganization was observed for Fulv treated or solvent control cells.

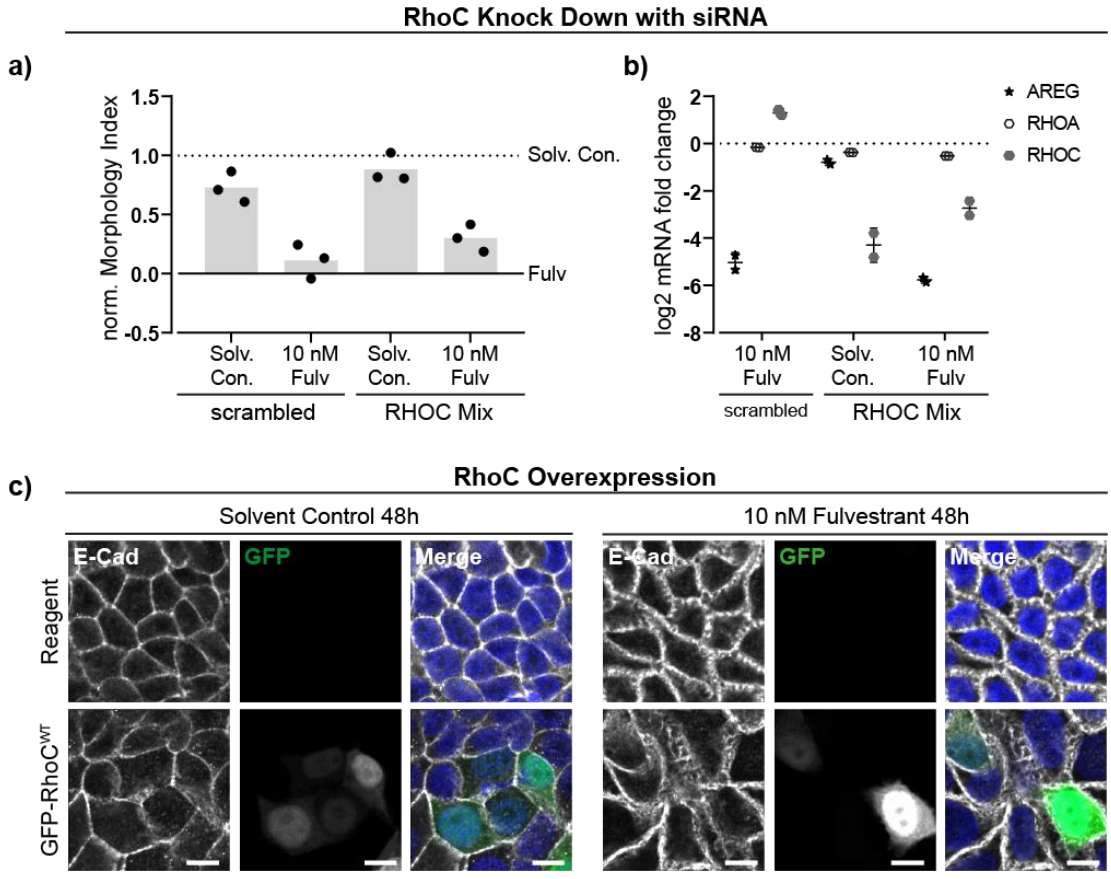

Figure 17: RhoC expression did not influence adherens junction reorganization.
a-b) MCF7/vBOS cells transfected with a mix of *RHOC* siRNA for 72 h. a) The normalized Morphology Index (norm. MI) normalized as described in Figure 5. b) Log2 mRNA fold change of *AREG*, *RHOA* and *RHOC* normalized as described in Figure 2. c) Representative images of MCF7/vBOS cells transfected with RhoA^{WT}-GFP, stained for E-Cad, scale bar= 10 µm.

During development of new cell contacts and cell-cell adhesion, RhoA acts in concert with two other members of the Rho family of small GTPases, namely Rac1 and Cdc42, both of which are also influenced by SFK signaling (reviewed in [27]). As Rac1 and Cdc42 are known to negatively influence RhoA activity, it was finally tested whether inhibition of these two GTPases might interfere with AJ reorganization. MCF7/vBOS cells were treated with three different inhibitors of Rac1 and Cdc42 for 48 h with or without Fulv (Figure 18). However, none of these inhibitors showed any effect on AJ organization in Fulv-treated or control cells at sub-toxic concentrations.

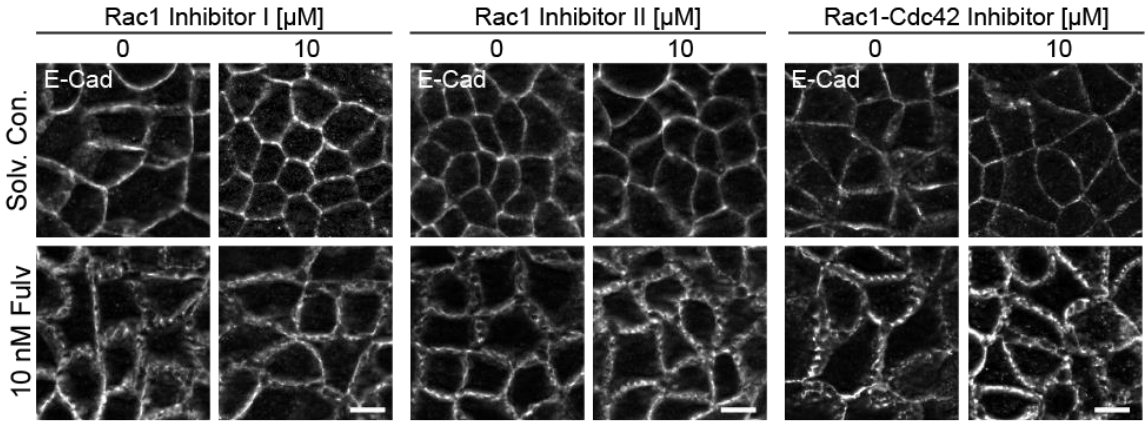

Figure 18: Inhibition of Rac1 or Cdc42 does neither induce nor prevent adherens junction reorganization.
Representative images of MCF7/vBOS cells treated with Rac inhibitor I, Rac1 inhibitor II and Rac1-Cdc42 inhibitor with or without 10 nM Fulvestrant (Fulv) in the background for 48 h stained for E-Cadherin (E-Cad), scale bar= 10 µm.

Taken together, though RhoA activation through CN03 cotreatment or overexpression of the constitutive active mutant GFP-RhoA^{Q63L} was able to revert or prevent AJ reorganization, it did not play an instructive role in Fulv-induced AJ reorganization. As RhoA is a major hub in cytoskeleton regulation, its activation might just cause general changes in the regulation of the cytoskeleton. While the RhoA inhibitor Rhosin did induce AJ reorganization, it also downregulated *AREG* and inhibited ERα responsive gene expression. The protein expression levels of RhoA and RhoC *per se* did not appear to influence AJ reorganization. Therefore, the specific role of Rho family GTPases for AJ organization remains to be addressed in more detail in further studies.

3.2. Development of a high throughput compatible assay set-up

In addition to the investigation of the underlying mechanism for AJ reorganization, a main objective of this thesis was the development of an HT-compatible assay set-up for the identification of estrogenic substances using AJ reorganization as the endpoint. A useful HT screening assay needs to be automatable, time efficient and reliable. Following, the different development and optimization steps leading to a HT compatible estrogen-morphology (E-Morph) assay set-up are described.

3.2.1. Optimization of staining method and computational analysis

As a first step, seeding and treatment of cells was scaled up from a 6- or 12-well plate format to a 96-well plate format, and the imaging of cells was moved from manual imaging using a Zeiss LSM 880 AiryScan Confocal Microscope to automated imaging of predefined sections with the Opera Phenix HC Screening System.

First, it was tested whether AJ reorganization upon Fulv treatment could still be robustly detected in this new set-up. MCF7/vBOS cells seeded into 96-well plates were treated for 48h and stained for E-Cad by immunofluorescence staining (Figure 19 a). Notably, the previously described AJ reorganization could again be observed upon Fulv treatment showing that the new plate format as well as the imaging modality did not have any influence on the detection of the effect. Next, the images were analyzed with the integrated image analysis software Harmony following the same principle as the CP/CPA pipeline described above (Section 3.1.1). The cells were again classified into regular and irregular AJ organization and the MI was calculated.

Essential for a good test method is a sufficiently high dynamic range, which is represented by the signal separation between the positive and negative controls. Thus, the signal window (SW) and Z' value (Z') of Fulv treated cells and the solvent control were determined. Indicators for a good signal separation are a SW above 2 or a Z' above 0.4 [108]. With scores of 6.99 and 0.48 respectively, both SW and Z' indicated sufficient signal separation. Hence, scaling to a 96-well plate format, automation of the imaging, and image analysis pipeline was deemed successful.

As immunofluorescence staining is time consuming and involves many sample preparation steps, alternative and more efficient cell staining methods were tested. MCF7/vBOS cells were again treated with 10 nM Fulv for 48 h and stained with the two live cell stains LysoTracker and CellTrace (Figure 19 b, c). In contrast to the E-Cad staining by immunofluorescence, the two live cell stains do not visualize the cell

membrane but the cytoplasm to indicate cell morphology. More specifically, LysoTracker specifically stains, as the name already suggests, the lysosomes while CellTrace covalently binds to intracellular proteins *per se* and thus represents a more general staining method to visualize the cytoplasm. In accordance, the LysoTracker staining was generally more granular than CellTrace. Whereas the outlines of individual cells were difficult to discriminate in solvent control cells in both staining methods, the cells appeared to be clearly separated upon Fulv treatment. The irregular AJ organization detected by E-Cad staining correlated with an increased spacing between cells upon LysoTracker and CellTrace staining. Subsequently, the images were analyzed using the Harmony image analysis software. For the three different staining methods, cells could be successfully classified into regular and irregular AJ organization and the MI determined. Generally, the determined MI values were in a similar range as with low throughput set-up. Additionally, calculation of the SW and Z' revealed a similar signal separation for LysoTracker staining and a better separation for CellTrace when compared to immunofluorescence staining.

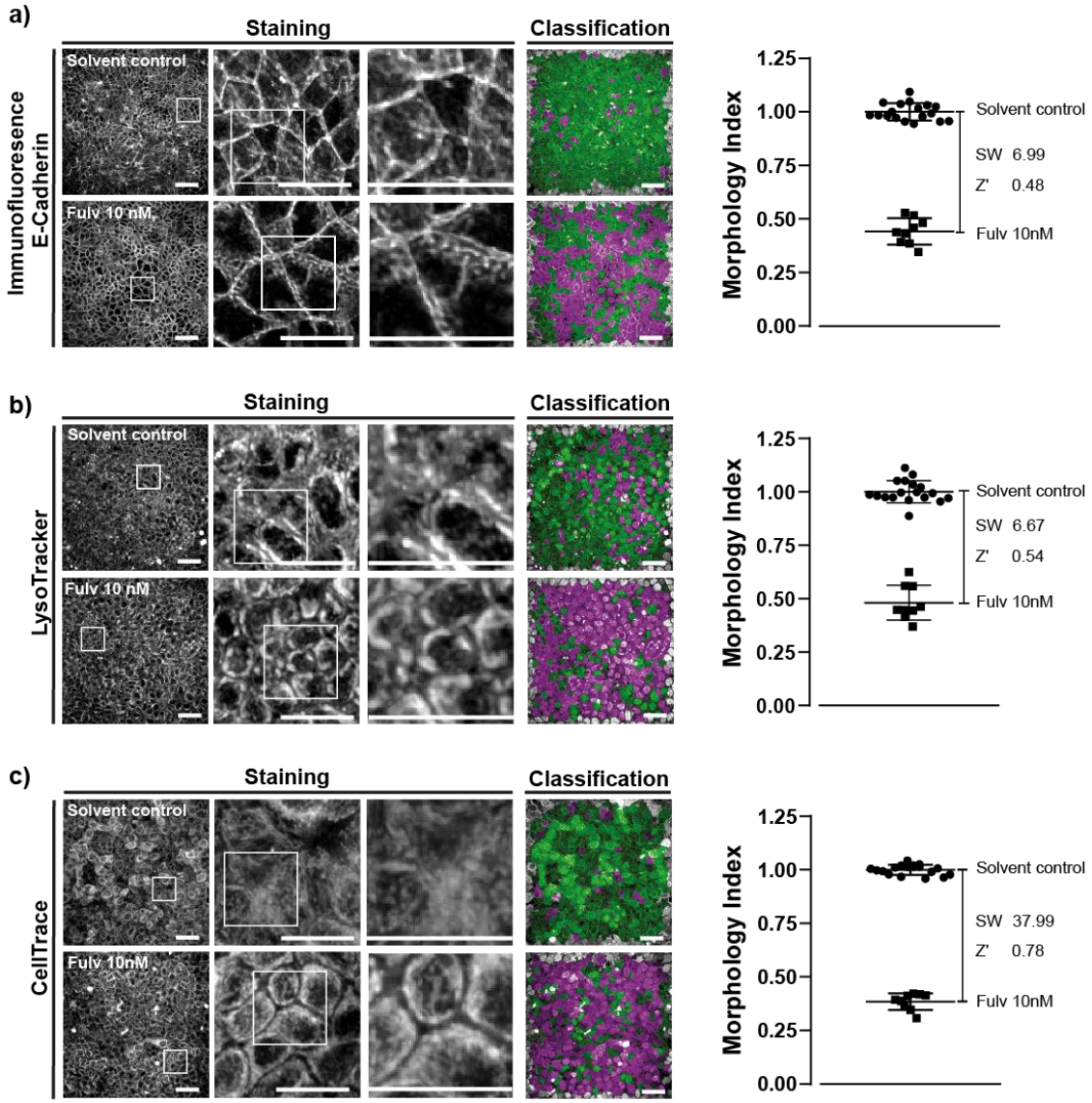

Figure 19: CellTrace cytoplasmic staining is sufficient for differentiation between regular and irregular adherens junction organization.
a-c) MCF7/vBOS cells were treated with 10 nM Fulv for 48 h and stained a) for E-Cad with immunofluorescent staining, b) with LysoTracker and c) CellTrace (scale bar= 25 µm). Image analysis and cell classification was done with the integrated image analysis software Harmony. The Morphology Index is defined as the fraction of cells showing regular adherens junction organization normalized to the solvent control. The line indicates the mean distribution with error bars indicating the standard deviation. One dot represents one well with analyzed 9 images. The results of three biological replicates are shown. Signal window (SW) and Z' were calculated as described by Iversen *et al* [108]. The values represent the mean value of the three biological replicates.

Next, the performance of the three different staining methods were further compared in two different dose response set-ups – phenotype formation and prevention. In the phenotype formation set-up, MCF7/vBOS cells were treated with different concentrations of Fulv for 48 h (Figure 20 a-c). In the phenotype prevention set-up, the cells were co-treated with 10 nM Fulv and different concentrations of E2 for 48 h (Figure 20 d-f). Subsequently, cells were stained with the three different staining methods and the images analyzed using the Harmony software (Figure 20).

In the phenotype formation set-up, the MI values remained close to the solvent control at low Fulv concentrations in all three staining methods (Figure 20 a). They slowly started decreasing at 0.5 nM, before reaching a plateau at Fulv concentrations between 10 nM and 100 nM Fulv, thus showing a similar trend as can be seen in Figure 2 and Figure 4 shown above for the low-throughput CP image analysis set-up. No striking differences between the staining methods concerning MI values or the dose response curve were observed and the IC50 values were all in the same range. The MI of the immunofluorescence-stained cells reached its plateau slightly sooner, but also at a higher MI score of 0.5, while the MI of LysoTracker and CellTrace decreased to a value of around 0.25 indicating an increased sensitivity. Notably, staining with CellTrace resulted in the smallest within-plate and between-plate variance across technical and biological replicates.

In the phenotype prevention set-up, at low concentrations of E2, the MI value across the different staining methods was around 0.5 and slowly increased before reaching 1.0 at 10 nM E2. These results are again in agreement with results shown in Figure 5. Similar to the phenotype formation set-up, all MI values of the different staining methods were in same range and showed comparable dose-response curves and EC50 values. Notably, CellTrace staining again showed the least variance of the three staining methods.

Taken together, these results show that quantification of the AJ organization is also possible by visualizing the cytoplasm using the two live cell stains LysoTracker and CellTrace. As quantification of the CellTrace-stained cells showed the lowest variance and the best signal separation, all subsequent assay development steps for the E-Morph Assay were performed using CellTrace staining.

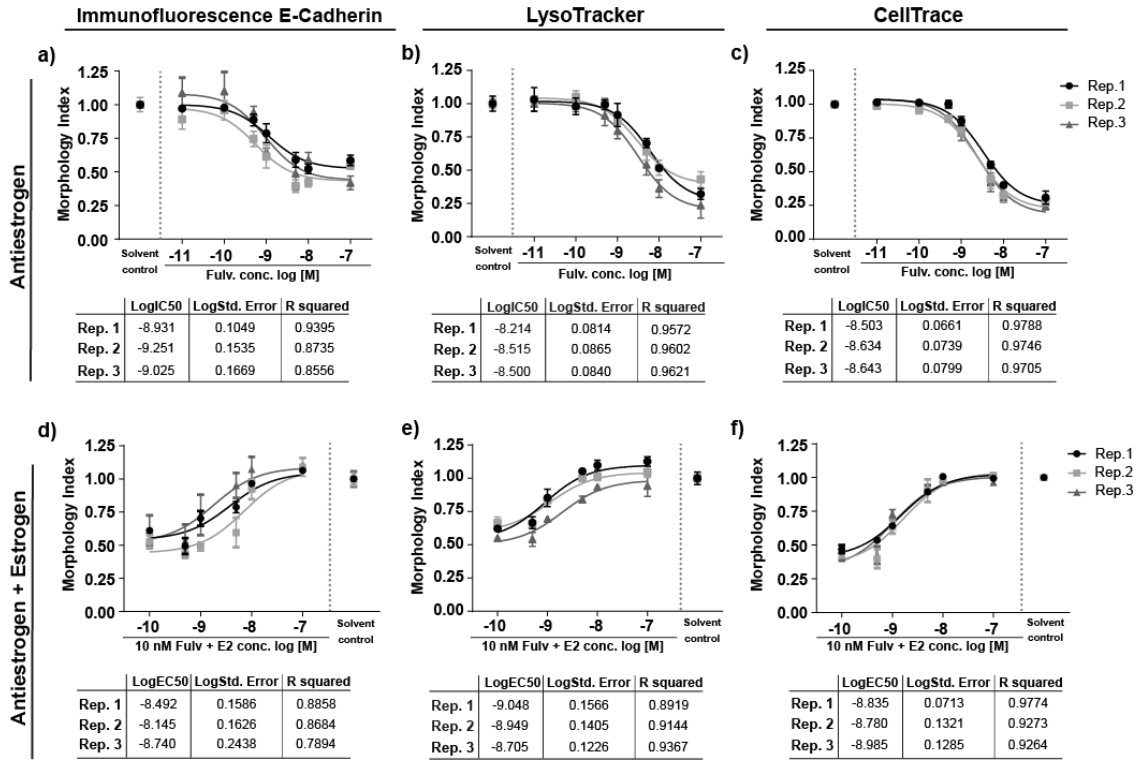

Figure 20: The different staining methods show all similar dose-response curves.
a-c) MCF7/vBOS cells treated with different concentrations of Fulvestrant (Fulv) for 48 h. d-f) MCF7/vBOS cells treated with 10 nM Fulv and different concentrations of 17β-estradiol (E2). a-f) Cells were stained for E-Cadherin for immunofluorescent staining, with LysoTracker and CellTrace. Image analysis and cell classification was done with the integrated image analysis software Harmony. The Morphology Index is defined as the fraction of cells showing regular adherens junction organization normalized to the solvent control. One dot represents one biological replicate consisting out of three different wells with nine images each. The dose response curves were fitted using the non-linear fit algorithm (three parameters, hill slope= 1) by GraphPad. The error bars indicate the standard deviation.

As already mentioned, quantification of AJ reorganizations was conducted using the integrated commercial image analysis software Harmony, while previous experiments described in the first part of this thesis were analyzed using an analysis pipeline based on the free CP/CPA software. To show that quantification of AJ reorganization is independent of the software used, the images of the CellTrace staining were additionally exported and evaluated using a CP/CPA pipeline (Figure 21). The SW and Z' values were nearly indistinguishable from the values obtained with the Harmony software while the minor differences between the obtained IC50 or EC50 values were within the variance of the biological replicates. To conclude, it was also possible to analyze the images using the free CP/CPA software as an alternative to the commercial Harmony software.

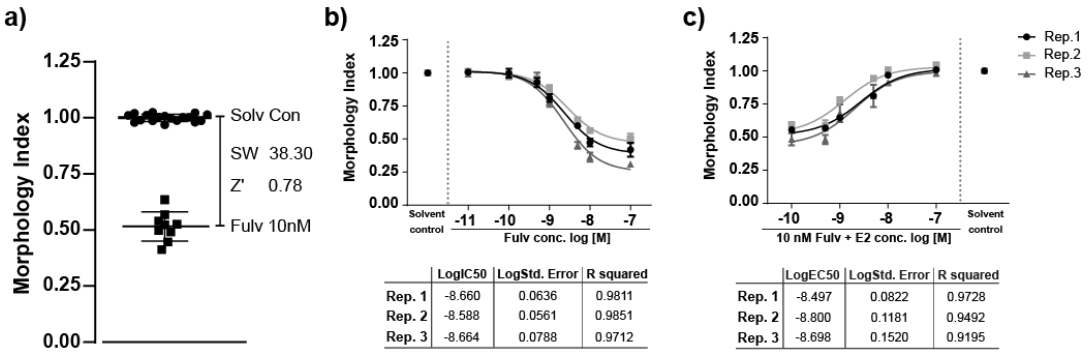

	LogIC50	LogStd. Error	R squared
Rep. 1	-8.660	0.0636	0.9811
Rep. 2	-8.588	0.0561	0.9851
Rep. 3	-8.664	0.0788	0.9712

	LogEC50	LogStd. Error	R squared
Rep. 1	-8.497	0.0822	0.9728
Rep. 2	-8.800	0.1181	0.9492
Rep. 3	-8.698	0.1520	0.9195

Figure 21: Quantification of CellTrace stained cells can also be conducted with a CellProfiler/ CellProfiler Analyst analysis pipeline.
a) MCF7/vBOS cells were treated with 10 nM Fulv for 48 h. The results of three biological replicates are shown. Signal window (SW) and Z' were calculated as described by Iversen *et al* [108]. The values represent the mean value of the three biological replicates. b) MCF7/vBOS cells treated with different concentrations of Fulvestrant (Fulv) for 48 h. c) MCF7/vBOS cells treated with 10 nM Fulv and different concentrations of 17β-estradiol (E2). a-c) Cells were stained with CellTrace. Image analysis and cell classification was done with CellProfiler/CellProfiler Analyst. The Morphology Index is defined as the fraction of cells showing regular adherens junction organization normalized to the solvent control. One dot represents one biological replicate consisting out of three different wells with 9 images each. The dose response curves were fitted using the non-linear fit algorithm (three parameters, hill slope= 1) by GraphPad.

3.2.2. Optimization of the measuring time point

Next to being easy in handling, a test method should be as time efficient as possible. Additionally, shorter incubation times might also decrease unspecific toxicity of the test substance and, thus, might allow testing of higher concentrations. In the experiments described in the first part of this thesis (Section 3.1), 48 h were used as the standard incubation time. Here, it was now tested whether the incubation time could be further optimized.

To get a first approximation of the timing of the morphological changes, MCF7 cells stably expressing GFP-tagged E-Cad (MCF7/E-CadGFP) were used in a time course experiment. The cells were treated with 10 nM Fulv for 24 h and then imaged every 2 h using the HC microscope Opera Phenix. The images were analyzed using the Harmony software and the MI was determined (Figure 22 a). At 24 h, the MI of the treated cells was still at the level of the solvent control but decreased to a level of around 0.25 after 40 h of treatment. Although the two biological replicates slightly differed in the early kinetics of phenotype development, the MI of both replicates reached a plateau at a value of 0.25 indicating that full AJ reorganization can be generally expected after about 40 h.

From these results, selected time points were analyzed in the MCF7/vBOS cell line. For the selection of incubation periods, the increased responsiveness of the

MCF/vBOS was taken into account by also including a period below 40 h. MC7vBos cells were treated with different concentrations of Fulv for five different incubation periods – 30 h, 40 h, 48 h, 72 h, and 144 h – and subsequently imaged and analyzed (Figure 22 b). For all five incubation periods, a Fulv concentration of 0.1 nM did not induce AJ reorganization. The MI started to decrease at 1 nM Fulv and reached a plateau at around 100 nM. The different incubation times mainly differed in the MI value that was reached at the highest Fulv concentration. The maximum signal separation (dynamic range) was obtained at the 30 h and 48 h time points, while the 72 h time point had only a minor additional benefit. Thus, the 30 h and 48 h time points were further validated according to the requirements for a HC screening assay published by Iversen *et al* [108]. In three independent biological repeat experiments, each three 96-well plates of MCF7/vBOS cells were treated with 10 nM Fulv (representing the *"Min" signal* range), the solvent control (representing the *"Max" signal* range) and a combination of 10 nM Fulv and 3 nM E2 (representing the *"Mid" signal* range) for 30 h and 48 h, then imaged and quantified. The results were analyzed with regard to the within-day and between-day signal distribution as well as signal-to-noise ratio (SW and Z'). The MI distribution of the different plates and replicates as well as the corresponding SW and Z' is shown in Figure 22 c-d. While the within-day and between-day signal distribution (variance) was sufficiently small for the 48 h time point, the 30 h time point did not pass this validation requirement for a HC screening assay. Additionally, whereas for the 48 h time point, all plates had a $SW > 2$ or a $Z' > 0.4$, several plates of the 30 h time point fell short on this criterion. These results show that a 30 h treatment period was not sufficient to reliably and stably induce AJ reorganization as compared to an incubation period of 48 h, which was used for the following substance testing.

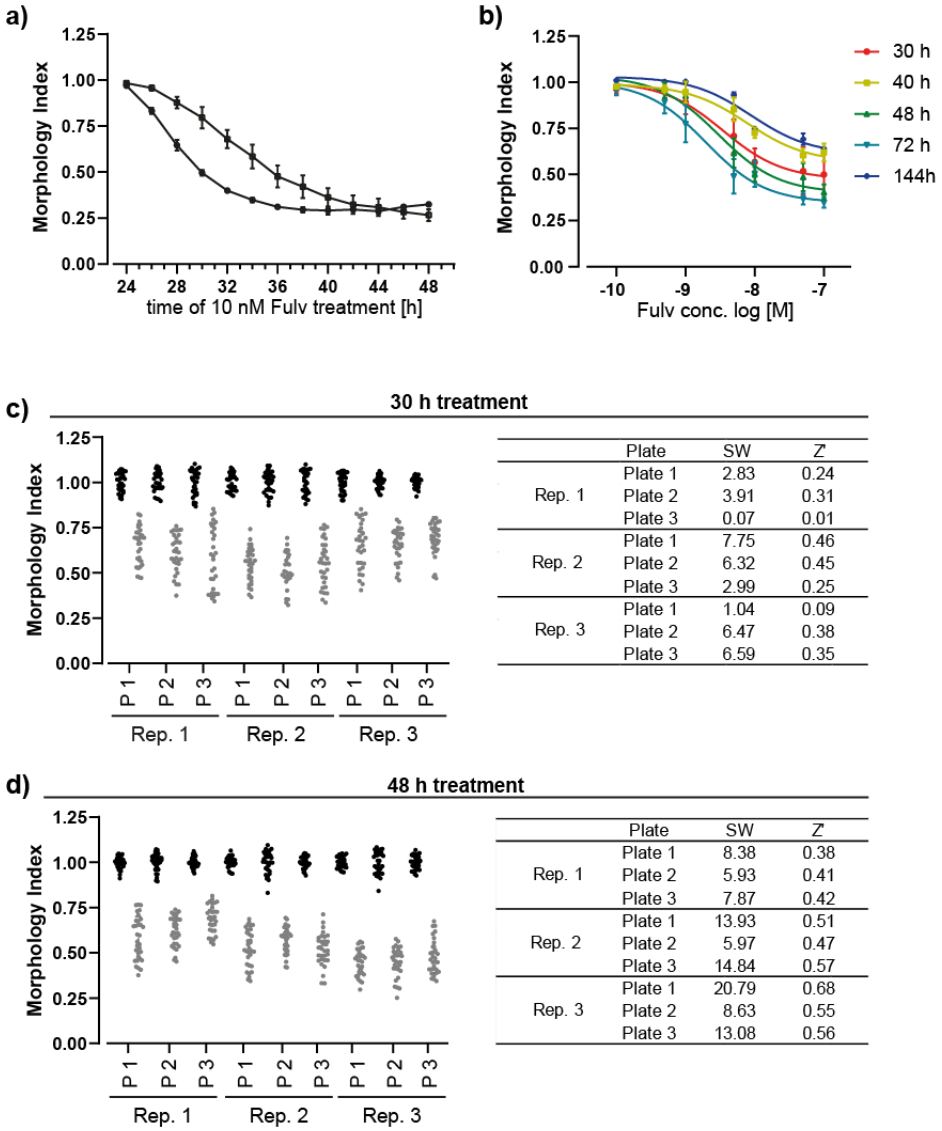

	Plate	SW	Z'
Rep. 1	Plate 1	2.83	0.24
	Plate 2	3.91	0.31
	Plate 3	0.07	0.01
Rep. 2	Plate 1	7.75	0.46
	Plate 2	6.32	0.45
	Plate 3	2.99	0.25
Rep. 3	Plate 1	1.04	0.09
	Plate 2	6.47	0.38
	Plate 3	6.59	0.35

	Plate	SW	Z'
Rep. 1	Plate 1	8.38	0.38
	Plate 2	5.93	0.41
	Plate 3	7.87	0.42
Rep. 2	Plate 1	13.93	0.51
	Plate 2	5.97	0.47
	Plate 3	14.84	0.57
Rep. 3	Plate 1	20.79	0.68
	Plate 2	8.63	0.55
	Plate 3	13.08	0.56

Figure 22: Treatment of the cells for 48 h is the ideal time point.
a) MCF7/E-CadGFP cells were treated with 10 nM Fulvestrant (Fulv), stained for the nuclei with Hoechst 33342 and imaged at 37 °C every 2 h for 24 h, n= 2. b) MCF7/vBOS cells treated with different concentrations of Fulv for different time periods (30-144 h). Cells were stained with CellTrace, n= 1. c-d) MCF7/vBOS treated with 10 nM Fulv (gray) and solvent control (black) for c) 30 h or d) 48 h in three different plate layouts and in three independent runs following the validation protocol suggested by Iversen *et al* [108]. a-d) The Morphology Index is defined as the fraction of cells showing regular adherens junction organization normalized to the solvent control. Image analysis and cell classification was done with the integrated image analysis software Harmony. One dot represents one biological replicate consisting out of three different wells with nine images each; error bars show the standard distribution between wells.

3.2.3. Definition of a cytotoxicity read-out

A key confounder of results in *in vitro* testing is unspecific cytotoxicity of the test substance. Thus, an endpoint addressing potential cytotoxicity is ideally included in the E-Morph Assay set-up to directly exclude results of those test substance concentrations or to define the maximal, relevant testing concentration. There are different assays or endpoints to demonstrate cytotoxicity available that differ in their sensitivity, specificity, and applicability for a given assay set-up. Here, the applicability of three different endpoints – CellTox Green intensity (addressing membrane integrity), number of cells (addressing proliferation or general cytotoxicity), and conversion of the CellTiter Blue reagent (addressing proliferation, metabolism) – was analyzed. An overview of these readouts is shown in Figure 23 a. CellTox Green is non-membrane permeable dye that upon intercalation into the DNA can be excited at a wavelength of 485-510 nm. As it can only penetrate the cell and interact with the DNA when the cell membrane is disrupted, high CellTox Green intensity in the nuclei corresponds to cytotoxicity of the substance (Figure 23 b). This endpoint could easily be integrated into the assay set-up by adding the dye after staining with Hoechst 33342 and CellTrace, and measuring the mean CellTox Green intensity in the area of nuclei. The number of cells is an accepted marker for cytotoxicity and cell proliferation. Determination of this parameter was already part of the image analysis pipeline as described so far and did not require any adaptation of the assay set-up. The CellTiter Blue assay is a measure of the redox potential and metabolic capability of the cells as it depends on the conversion of the redox dye resazurin into the fluorescent resorufin. As the resulting amount of resorufin also directly depends on the incubation time and its fluorescence spectrum additionally would interfere with the other fluorescence signals, this cytotoxicity assay was not integrated into the imaging set-up but was performed after (see Section 7.2 for more detail). The three endpoints were evaluated by treating MCF7/vBOS cells with three cytotoxic substances – Triton X 100, 5-fluorouracil, and sodium azide – with known mechanisms of cytotoxicity (Figure 23 c-e). As expected, the CellTox Green intensity increased with increasing substance concentrations, while the number of cells, defined by the number of nuclei, declined. The CellTiter Blue readout decreased in a similar fashion for 5-fluorouracil and sodium azide, while remaining constant for Triton X 100. The most sensitive endpoint was the number of nuclei, generally showing an effect even before significant changes could be detected in CellTox Green or CellTiter Blue assays. Based on the standard deviations of these results, appropriate

cytotoxicity thresholds were defined for CellTox Green (two-fold signal induction) and number of cells (15 % reduction of cell number) endpoints that are indicated in Figure 23 c-d by the dotted lines.

Subsequently, it was tested whether Fulv treatment on its own affected any of the selected cytotoxicity endpoints. While no striking differences between Fulv treatment and the solvent control were observed for CellTox Green intensity or number of cells endpoints, the signal of the CellTiter Blue assay was consistently lower in Fulv-treated cells than the solvent control. Estrogen signaling is known to influence proliferation and the metabolism of cells [85, 109]. As the cells were seeded to reach confluence before treatment, the inhibiting effect of Fulv on cell proliferation should be minimal. Therefore, the lower CellTiter Blue signal for Fulv was likely not due to cytotoxicity of the substance but a decrease in estrogen-dependent cell metabolism. In addition, the mean CellTiter Blue signal appeared to vary greatly between individual replicates something not observed for the other two endpoints.

To conclude, although all three endpoints were able to indicate cytotoxicity, CellTiter Blue appeared to be the least predictive. The CellTiter Blue assay was not able to correctly identify the cytotoxicity of Triton X 100 and showed effects in Fulv treated cells. Furthermore, additional incubation and measurement steps would be needed. Therefore, only CellTox Green and number of cells were included as cytotoxicity endpoints in the updated assay set-up and used for the following testing of substances.

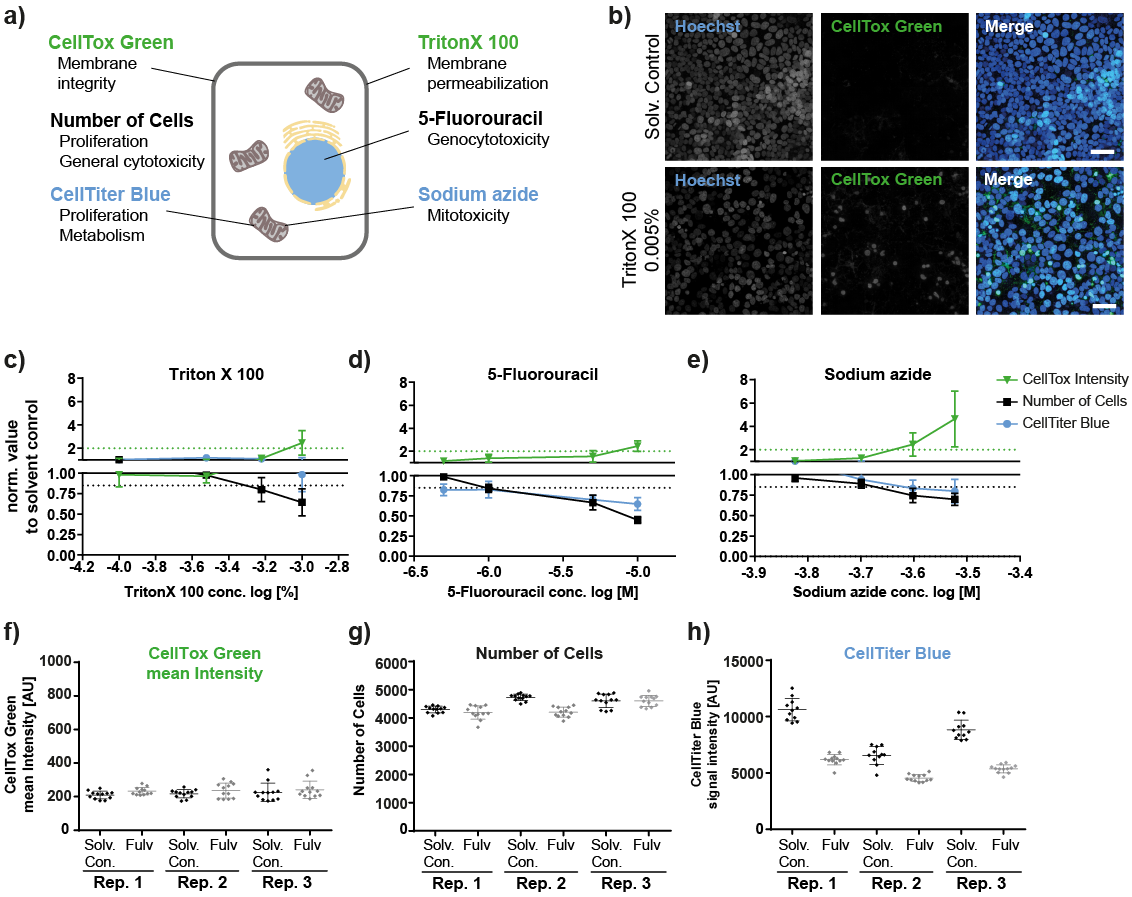

Figure 23: Number of cells and CellTox Green are appropriate markers for cytotoxicity.
a) Overview of the different cytotoxicity endpoints as well as substances that were tested. b) MCF7/vBOS cells treated with 0.005 % Triton X 100 for 48 h and stained with Hoechst and CellTox Green, scale bar= 50 µm. c)-e) The line indicates the mean value and the error bars the standard deviation. One dot represents one well consisting out of 9 images. f) MCF7/vBOS cells treated with different concentrations of Triton X 100 48 h. g) MCF7/vBOS cells treated with different concentrations of 5-Fluorouracil for 48 h. h) MCF7/vBOS cells treated with different concentrations of sodium azide for 48 h. f)-h) Cells were first stained for CellTrace, Hoechst 33342 and CellTox Green, imaged and then incubated for 120 min with the CellTiter Blue reagent. The fluorescence signal of CellTiter Blue reagent was then measured separately. The dotted lines represent the cytotoxicity thresholds for CellTox Green (2, green) and number of cells (0.85, black). f) CellTox Green mean intensity value of cells treated with Fulvestrant (Fulv) and the solvent control stained with CellTox Green. g) Number of segmented cells in the wells treated with Fulv and the solvent control and stained with Hoechst 33342. h) CellTiter Blue signal intensity after 120 min incubation with cells treated with Fulv and the solvent control for 48 h. c)-h) The values were normalized on the mean value of the solvent control. The experiment was conducted in biological replicates with 3 wells per treatment and 9 images per well. The error bars show the standard deviation.

3.2.4. Definition of a prediction model using a test set of six substances

After optimization of the staining procedure and integration of the two cytotoxicity endpoints, the E-Morph Assay was then used for pilot testing of six reference chemicals with known estrogenic potential – two strong estrogenic substances (17α-Ethinylestradiol (EE), DES), two weak estrogenic substances (Gen, BPA) as well as two negative substances (Atrazine (Atra), Reserpine (Reserp)). MCF7/vBOS cells were treated with 10 nM Fulv and the six substances in twelve concentrations for 48 h. Following, the cells were stained with Hoechst 33342, CellTox Green and CellTrace, imaged and analyzed with the image analysis software Harmony (Figure 24 a-c; Figure 25 a-c). Apart from Atra, all substances crossed the predefined cytotoxicity thresholds for the number of cells and CellTox Green intensity endpoints (see Section 3.2.3) at the highest concentrations as indicated by the grey area. The number of cells often decreased already at slightly lower concentrations than an increase in CellTox Green intensity was observed. Under treatment of Atra, the number of cells rather increased than decreased and CellTox Green intensity remained constant (Figure 24 a-b), indicating that Atra is not toxic in the tested concentration range. At non-cytotoxic concentrations, the MI of the two strong estrogenic substances EE and DES reached the level of the solvent control already at low concentrations between 10 nM and 100 nM, while a higher concentration of 1 µM of the weak estrogen Gen was needed. The MI of the BPA-treated cells increased with higher concentrations to a value between 0.75 and 0.8 but did not fully reach the level of the solvent control. The MI of Atra and Reserp increased at low concentrations but reached a plateau at a value of 0.7.

To verify the results from the pilot testing and define an appropriate threshold of the MI readout that indicates estrogenicity, the six tested substances were further tested for their estrogenic potential by analyzing their gene expression profile (Figure 24 d; Figure 25 d). MCF7/vBOS cells were cotreated with 10 nM Fulv and the six substances at selected concentrations for 48 h, and the expression of the estrogen responsive genes *PGR*, *EGR3*, and *PDZK1* was analyzed. For EE, DES, and Gen, the cotreatment completely prevented the Fulv-induced inhibition of the gene expression at 1 nM, 10 nM, and 10 µM, respectively, while only a slight induction of gene expression was observed for BPA at 10 µM. No effect on the gene expression was detected for the two negative substances Atra and Reserp. Notably, comparing the MI values and the gene expression data for the estrogenic substances, the MI was often just above a value of

0.75 at concentration where a rescue of the gene expression was observed. Thus, the threshold for the classification of a test substance as estrogenic/positive was set to an MI value of 0.75, which is indicated by a dashed line in Figure 24 c and Figure 25 c.

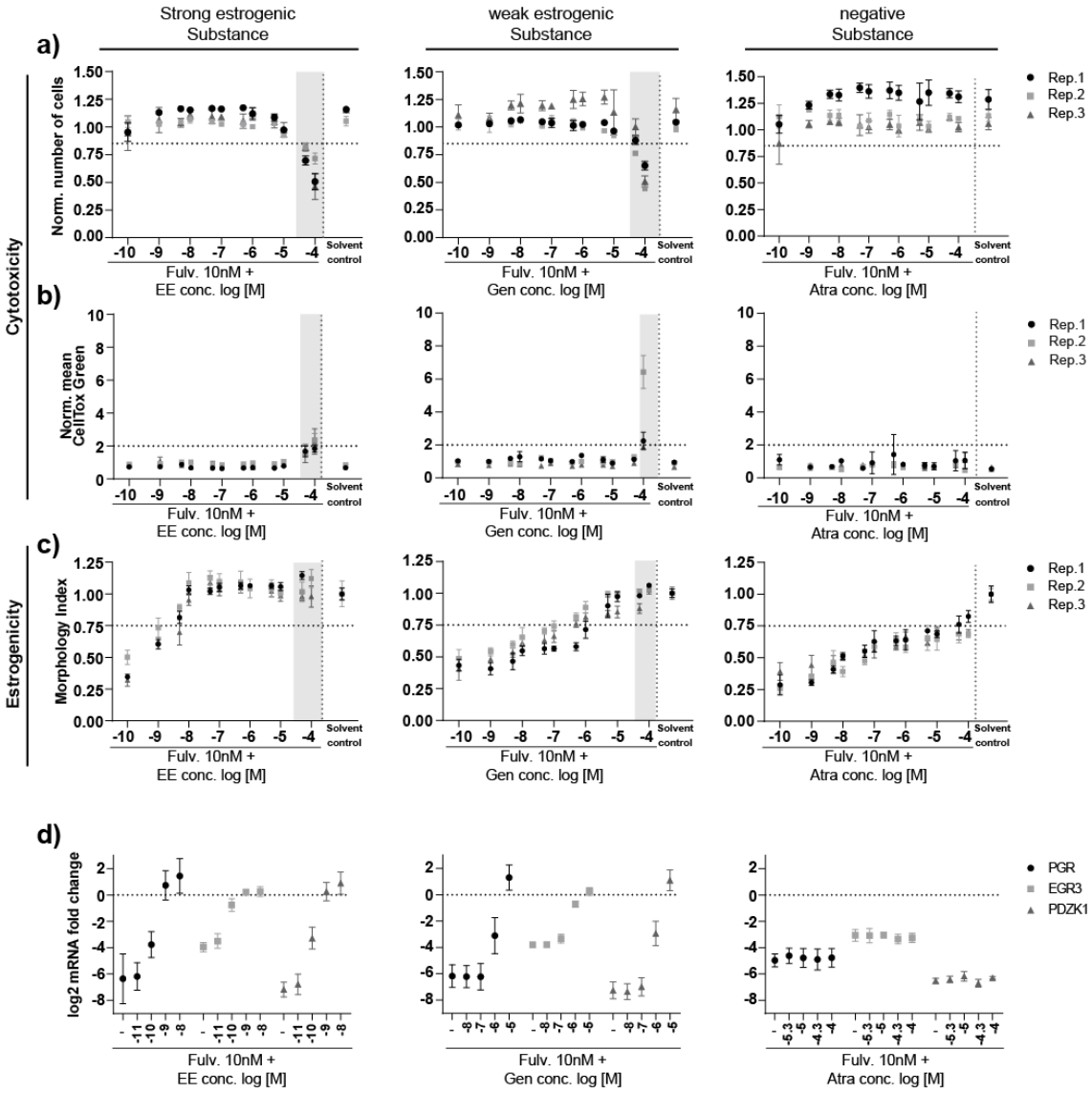

Figure 24: Testing of three substances with different estrogenic potential.
a-d) MCF7/vBOS cells treated with 10 nM Fulvestrant (Fulv) and different concentrations of 17α-Ethinylestradiol (EE), Genistein (Gen), and Atrazine (Atra) for 48 h. a)-c) Cells stained for Hoechst 33342, CellTox Green, and CellTrace and analyzed with the image analysis software Harmony. The experiment was conducted in biological replicates with 3 wells per treatment and 9 images per well. The error bars show the standard deviation. The horizontal dotted lines represent the defined thresholds for number of cells (0.85), CellTox Green (2), and the Morphology Index (0.75). The grayed-out area indicates concentrations with cytotoxicity. a-b) values were normalized to 10 nM Fulv control. c) The Morphology Index is defined as the fraction of cells showing regular adherens junction organization normalized to the solvent control. d) Log2 mRNA fold change of *PGR*, *EGR3*, and *PDZK1* of MCF7/vBOS cells normalized as described in Figure 2.

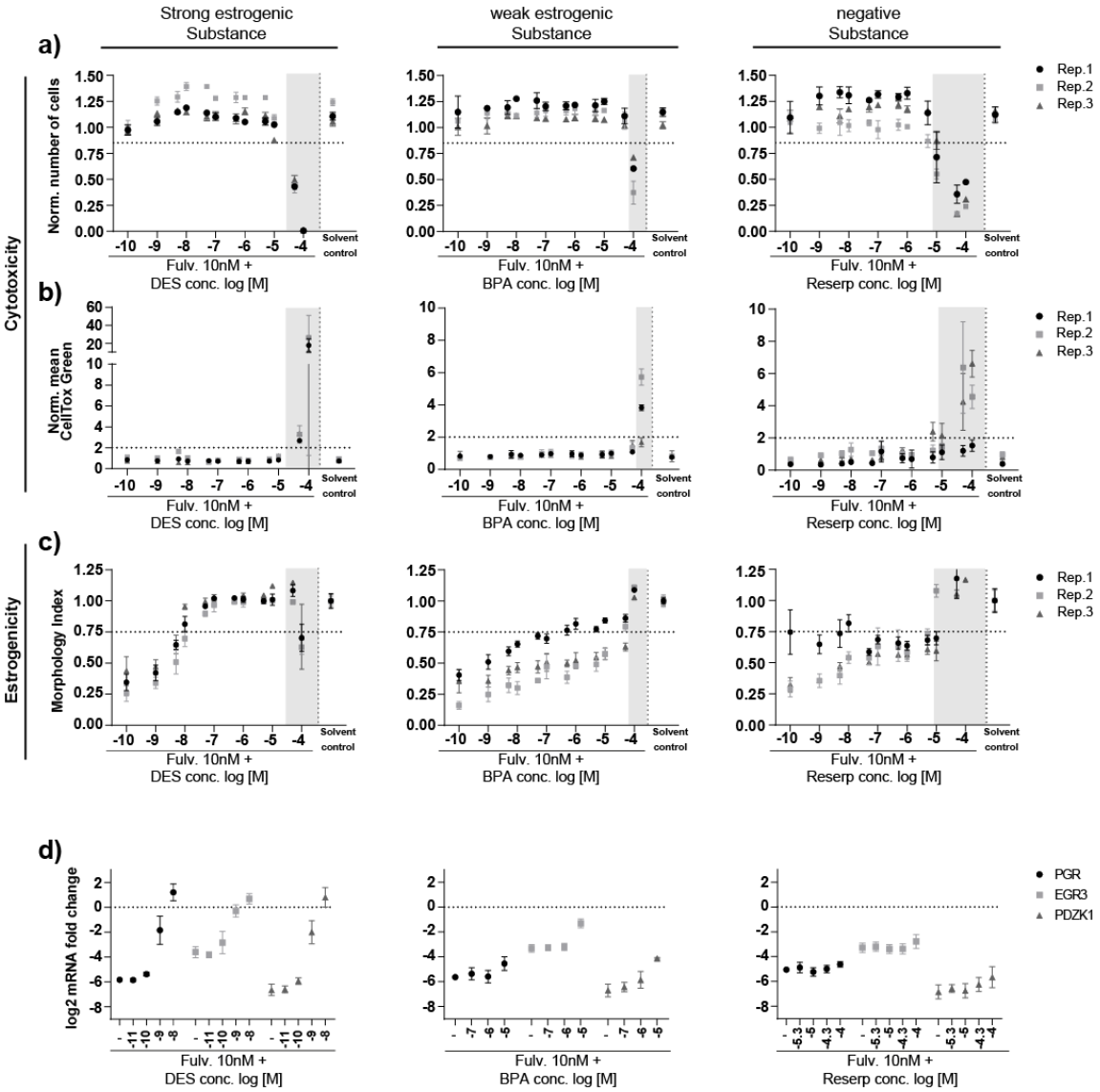

Figure 25: Testing of three substances with different estrogenic potential.
a-d) MCF7/vBOS cells treated with 10 nM Fulvestrant (Fulv) and different concentrations of Diethylstilbestrol (DES), Bisphenol A (BPA), and Reserpine (Reserp) for 48 h. a)-d) Cells stained for Hoechst 33342, CellTox Green, and CellTrace and analyzed with the image analysis software Harmony. The experiment was conducted in biological replicates with 3 wells per treatment and 9 images per well. The error bars show the standard deviation. The horizontal dotted lines represent the defined thresholds for number of cells (0.85), CellTox Green (2), and the Morphology Index (0.75). The grayed-out area indicates concentrations with cytotoxicity. a-b) Values were normalized to 10 nM Fulv control. c) The Morphology Index is defined as the fraction of cells showing regular adherens junction organization normalized to the solvent control. d) Log2 mRNA fold change of *PGR*, *EGR3*, and *PDZK1* of MCF7/vBOS cells normalized as described in Figure 2.

Based on the results shown in Sections 3.2.3 and 3.2.4, it was possible to define appropriate acceptance criteria to assess the results of the test method and to establish a prediction model to identify substances with estrogenic potential. A schematic overview is shown in Figure 26. For a valid run, a sufficient signal separation (SW > 2 or Z' > 0.4) needs to be present in the controls (10 nM Fulv and solvent control). Next, cytotoxic concentrations of the test substance are excluded from further analysis. The prediction model describes the criteria for a final classification of a test substance as estrogenic/positive or negative. A substance is classified as estrogenic if in at least two out of three runs the MI crossed the threshold of 0.75 at least at one tested concentration. Based on this prediction model, all six tested substances were correctly classified.

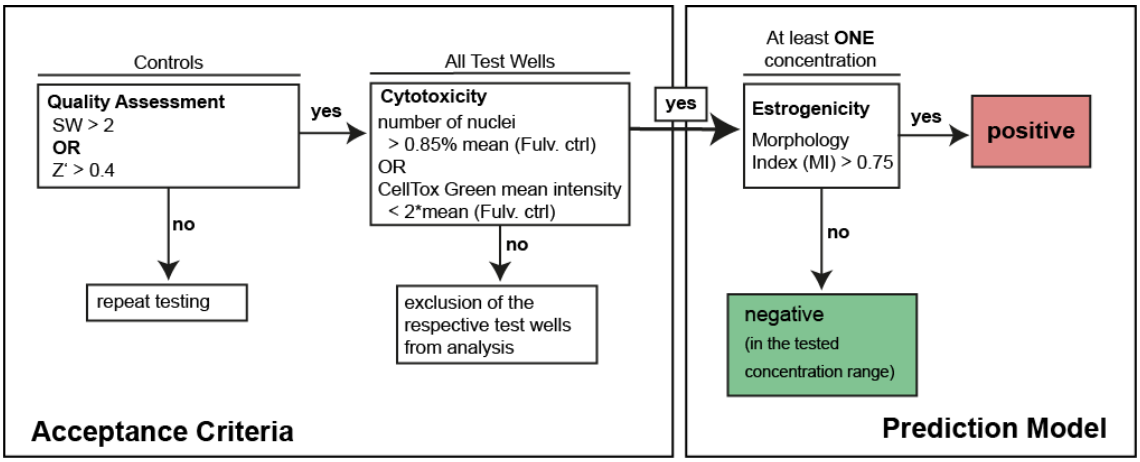

Figure 26: Schematic view of the acceptance criteria and the prediction model for the testing of potentially estrogenic substances in the E-Morph Assay.

As weakly estrogenic substances were not able to show a full dose-response curve before being cytotoxic, it was not possible to calculate an EC50 value for this class. Therefore, to estimate the relative potency of all tested substances, the logarithmic concentration where the MI equals 0.75 was calculated (referred to as MI75). The calculated MI75 values of the four estrogenic substances showed the expected order of estrogenic potency, with EE being the strongest and BPA being the weakest estrogenic substance (Table 1).

Table 1: Classification and MI75 of the six tested substances.
MCF7/vBOS cells treated with 10 nM Fulvestrant and the listed six substances for 48 h. Cells were stained with Hoechst 33342, CellTox Green, and CellTrace and analyzed with the image analysis software Harmony. The experiment was conducted in three biological replicates with three wells per treatment and nine images per well. The MI75 is defined as the calculated logarithmic concentration where the Morphology Index (MI) equals 0.75.

Substance	Chemical class	Classification	MI75			
			Rep. 1	Rep. 2	Rep. 3	Mean
17α-Ethinylestradiol (EE)	Steroid	POS	-8.42	-8.86	-8.22	-8.50
Diethylstilbestrol (DES)	Stilbestrol	POS	-8.09	-7.68	-8.18	-7.98
Genistein (Gen)	Isoflavone	POS	-5.76	-6.84	-6.34	-6.31
Bisphenol A (BPA)	Phenol	POS	-6.38	-4.38	-	-5.38
Atrazine (Atra)	Triazines	NEG	-4.36	-	-	-
Reserpine (Reserp)	Indole	NEG	-8.2	-	-	-

3.2.5. Validation of the E-Morph Assay with eleven additional substances

With a prediction model now in place, eleven additional substances were tested. The substances were selected for their known estrogenic potential and their diversity in structure (Table 2). Additionally, different bisphenols were included, that are discussed as alternatives for BPA. MCF7/vBOS cells were cotreated with 10 nM Fulv and the eleven substances at different concentrations for 48 h, stained, imaged and analyzed as described above. Upon applying the acceptance criteria and prediction model described in Section 3.2.4 and summarized in Figure 26, the substances were classified as estrogenic/positive and negative, and the MI75 was calculated. The results are listed in Table 2. As expected, E2 and E1 had the lowest MI75 value with -8.62 and -7.97, respectively, followed by Coumestrol (Coum) (MI75= -6.85) and Zea (MI75= -6.59). BPB and BPS had the highest MI75 values, while Progesterone and Ketoconazole were classified as negative.

Table 2: Classification and MI75 of the eleven additionally tested substances.
MCF7/vBOS cells treated with 10 nM Fulvestrant and the listed eleven substances for 48 h. Cells were stained with Hoechst 33342, CellTox Green, and CellTrace and analyzed with the image analysis software Harmony. The experiment was conducted in three biological replicates with three wells per treatment and nine images per well. The MI75 is defined as the calculated logarithmic concentration where the Morphology Index (MI) equals 0.75.

Substance	Chemical class	Classification	MI75			
			Rep. 1	Rep. 2	Rep. 3	Mean
17β-Estradiol (E2)	Steroid	POS	-8.36	-8.68	-8.82	-8.62
Estrone (E1)	Steroid	POS	-8.01	-7.99	-7.93	-7.97
5α-Dihydro-testosterone (DHT)	Steroid	POS	-5.02	-5.64	-6.82	-5.82
Zearalenone (Zea)	Lactone	POS	-6.77	-6.51	-6.49	-6.59
Bisphenol AF(BPAF)	Phenol	POS	-6.37	-5.21	-5.27	-5.62
Bisphenol B (BPB)	Phenol	POS	-4.52	-4.33	-4.35	-4.40
Bisphenol S (BPS)	Phenol	POS	-4.51	-4.08	-4.48	-4.36
Daidzein (Dai)	Isoflavone	POS	-4.89	-5.52	-6.14	-5.52
Coumestrol (Coum)	Isoflavone	POS	-7.02	-6.87	-6.65	-6.85
Progesterone (PG)	Steroid	NEG	-	-	-5.81	-
Ketoconazole(KetoC)	Piperazines	NEG	-	-	-5.38	-

To better compare and visualize the data of the in total 17 tested substances, the MI75 values were normalized to the mean MI75 value of the known potent estrogen EE (Figure 27). Four different categories could be defined – strong (rel. MI75 > 0.9), medium (0.9 > rel. MI75 > 0.6), weak (0.6 > rel. MI75), and negative (rel. MI75= 0). The tested endogenous and pharmaceutical estrogens completely made up the category of the strong estrogens, while the phytoestrogens were all medium estrogenic. The endogenous androgen 5α-dihydrotestosterone, the mycotoxin Zea and Bisphenol AF (BPAF) were also in that category. The other three bisphenols (BPB, BPS, BPA) tested were categorized as weak estrogens. Progesterone, Ketoconazole, Atra and Reserp were classified as negative, which is indicated by a MI75 of zero.

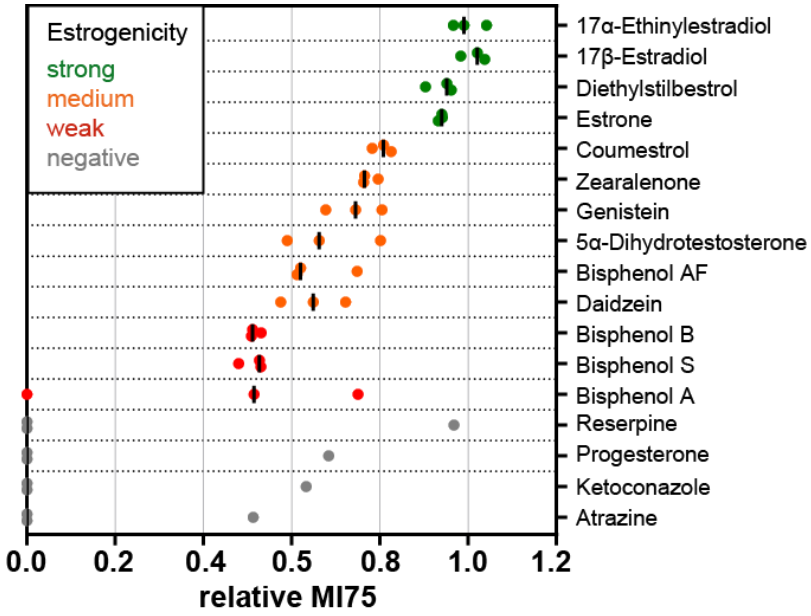

Figure 27: Relative MI75 values of the 17 tested substances.
MCF7/vBOS cells treated with 10 nM Fulvestrant and the listed 17 substances for 48 h. Cells stained for Hoechst 33342, CellTox Green, and CellTrace and analyzed with the image analysis software Harmony. The experiment was conducted in three biological replicates with three wells per treatment and nine images per well. The relative MI75 is defined as the logarithmic threshold concentration where the Morphology Index met 0.75 relative to the mean MI75 of 17α-Ethinylestradiol. The black line indicates the median of the three repeats (dot). The colors indicate the "estrogenicity" of the substance (green: strong; orange: medium; red: weak; grey: negative).

3.2.6. The predictive capacity of the E-Morph Assay

Two *in vitro* assay set-ups – receptor binding (OECD TG 493) and receptor transactivation (OECD TG 455) – were approved to be part of the OECD testing strategy for identification of substances with estrogenic potential (see Section 1.2.2) [77, 78]. Additionally, in the year 2015, the EPA as part of their ToxCast project published an ER model integrating the results of 18 *in vitro* assays into an ER agonist score [84]. To understand the predictive capacity of the E-Morph Assay, the relative MI75 values from the 17 tested substances were compared to the published reference data of the available test methods (Figure 28). For better comparison, the logarithmic EC, IC or PC values of the reference data were also normalized to the value of EE, respectively. Generally, the relative MI75 appeared to correlate very well with the published results. The four substances (Atra, Reserp, Ketoconazole and progesterone) identified as negative were also negative in the protein binding and transactivation assays. Atra, Reserp and Ketoconazole in the ToxCast model also had an ER agonist score of zero, while progesterone with an ER agonist score 0.05 was there categorized as very weakly estrogenic. The endogenous and pharmaceutical estrogens were again grouped together as the more potent estrogens though the exact order of estrogenicity differed between the assays. The classified weak and medium estrogenic substances were also less estrogenic in the published assays. Altogether, most of the tested substances localized on or very close to the dashed reference line indicating very similar relative estrogenicities when compared to the individual reference assays. Interestingly, in some cases e.g. 5α-dihydrotestosterone, the estrogenic potency appeared to also vary greatly between assays addressing the same endpoint.

In conclusion, it could be shown, that the E-Morph Assay yielded comparable results as compared to internationally accepted individual assays for the identification of estrogenic substances and even had a similar predictive capacity as compared to the ToxCast ER agonist score combining multiple assays.

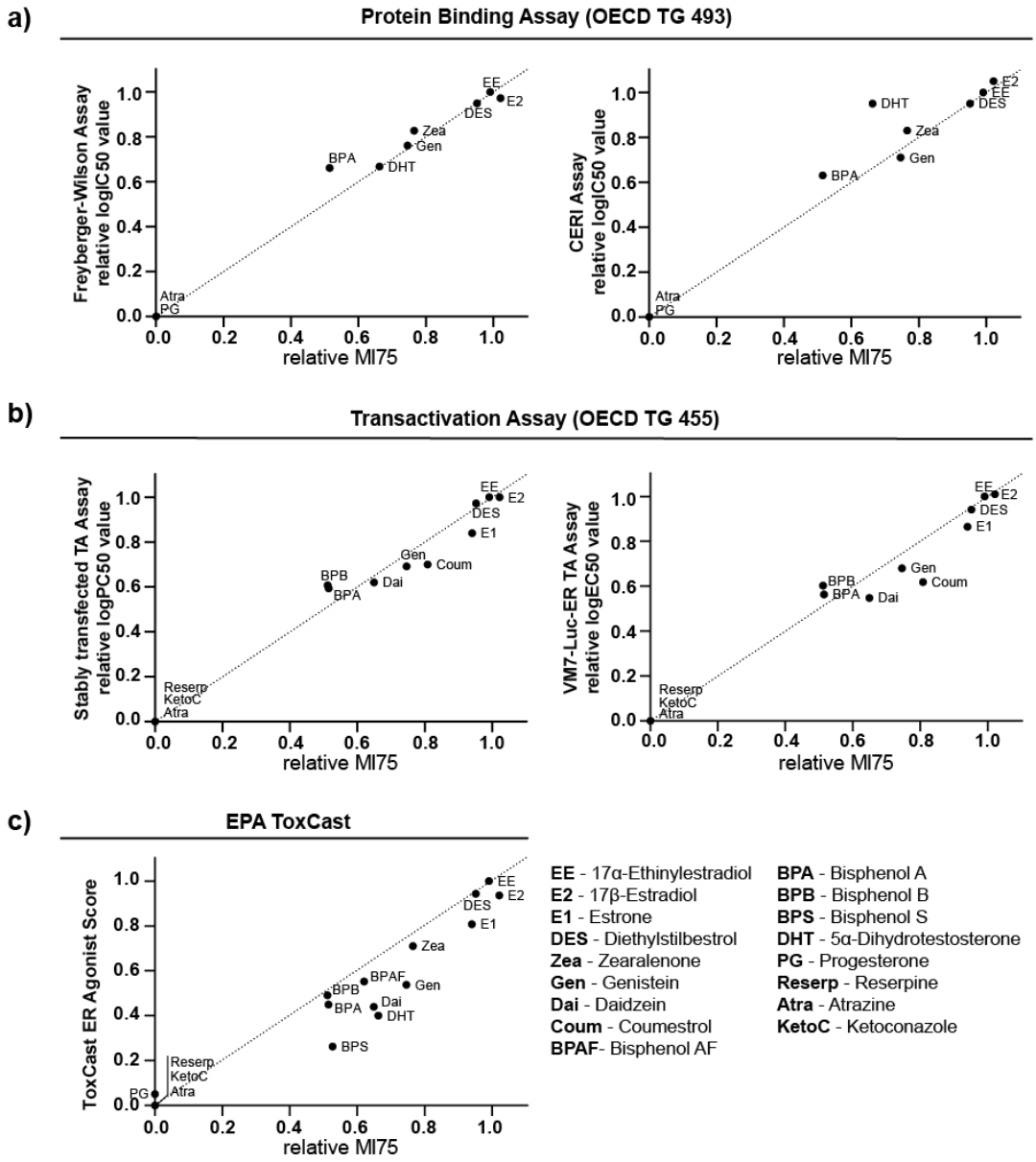

Figure 28: Correlation of the relative MI75 values of the tested substances to the published data of other assays.

a-c) MCF7/vBOS cells were treated with 10 nM Fulvestrant and the listed 17 substances for 48 h. Cells stained for Hoechst 33342, CellTox Green, and CellTrace and analyzed with the image analysis software Harmony. The experiment was conducted in three biological replicates with three wells per treatment and nine images per well. The relative MI75 is defined as the logarithmic threshold concentration where the Morphology Index (MI) met 0.75 relative to the mean MI75 of 17α-Ethinylestradiol (EE). The median values are shown. The contour line is indicated by the dotted line. a) The relative MI75 values set against the results of the two estrogen receptor protein binding assays – Freyberger-Wilson Assay and CERI Assay – normalized to EE [77]. b) The relative MI75 values set against the results of the two transactivation assays (TA) – stably transfected TA Assay and VM7-Luc-ER TA assay – normalized to EE [78]. c) The relative MI75 values set against the ToxCast estrogen receptor (ER) Agonist score [84].

4. Discussion

The important role of estrogen signaling during breast cancer development and progression has long been recognized [5, 21, 23]. Even though the exact mechanism is still under debate, several factors seem to contribute. Next to their effects on cell proliferation, estrogens have been discussed to influence E-Cad expression levels and cytoskeleton organization [33-35, 110]. Although several test methods for the identification and characterization of estrogenic environmental substances have been developed in recent years, most of them only cover the initial steps of estrogen signaling activation (e.g. binding and transcription activation) and only a single assay with a functional endpoint exists (E-SCREEN assay). This work introduces a novel HT-compatible test method, the E-Morph Assay, for the identification and characterization of estrogenic substances with AJ reorganization as a functional endpoint.

4.1. Adherens junction reorganization is estrogen receptor α mediated

Cells used in a test method for estrogenic substances need to be estrogen responsive and ideally well-characterized. Having retained ERα and E-Cad expression, the MCF7 cell line is an established model for luminal A breast cancer. The MCF7/vBOS cell line used in this work, which is a sub-clone of the parental MCF7/BOS cell line [88], is characterized by high ERα expression levels and strong estrogen responsiveness. The strong estrogen responsiveness could be verified in MCF7/vBOS cells by analyzing the gene expression of estrogen responsive genes after treatment with the estrogen E2, or the two antiestrogens Fulv and 4-OHT (Section 3.1, Figure 1). Although E2 treatment did not cause any changes on gene expression levels, treatment with either of the two antiestrogens significantly reduced the gene expression levels of the tested estrogen responsive genes. According to their characteristics as SERD and SERM respectively, the inhibition of estrogen responsive gene expression was stronger upon Fulv treatment than compared to 4-OHT. The lack of responsiveness towards E2 treatment was likely due to full saturation of the estrogen signaling capacity through residual E2 in the medium and sequestration of involved transcription factors. An induction of estrogen responsive gene expression beyond the level of the solvent control could only be achieved when the cells were cotreated with E2 and Fulv (Section 3.1.2, Figure 5). This effect may be explained by a reduced sequestration of the rate-limiting transcription factors required for ERα signaling activation when Fulv

treatment considerably depleted the available pool of ERα through its action as a SERD. Due the use of FCS with low hormone levels and reduction of FCS supplement under experimental conditions, the residual E2 levels in the cultivation medium (3.4-4.1 pM) are expected to be in the range of serum levels of postmenopausal women [111]. Additionally, the necessary Fulv concentration for the effective inhibition of estrogen responsive gene expression was similar to the steady-state plasma levels of patients undergoing Fulv-based endocrine therapy [112].

This work is mainly based on the observation that modulation of ERα signaling induces a striking AJ reorganization in MCF7/vBOS cells [87]. To ensure the applicability of AJ reorganization as an endpoint for the specific identification of estrogenic substances, the role of the different estrogen receptors ERα and GPER1 was studied in more detail (Section 3.1.2). Taken together, ERα could be verified as a key component involved in the modulation of AJ organization, while a significant role of GPER1 appears to be rather unlikely. Already the timing of AJ reorganization occurrence indicates a more prominent role of ERα as compared to GPER1. AJ reorganization took at least 28-30 h to develop (Section 3.2.2, Figure 22). While ERα directly mediates changes in gene expression and long-term effects, GPER1 is rather responsible for rapid non-genomic signal transduction [11]. Generally, treatment with different antiestrogens (ERα antagonists) induced AJ reorganization in a dose-dependent manner corresponding to their inhibitory effects on estrogen responsive gene expression (Section 3.1.1). Additionally, the known potency was also reflected in timing of the phenotype. Induction of AJ reorganization was much faster under Fulv treatment than under Tam. High concentrations of Fulv as well as other ERα antagonists are known to also activate GPER1 signaling [11, 16], however treatment with the GPER1 specific activator G1 did not have any effects on AJ reorganization (Section 3.1.2, Figure 6). Additionally, although E2 and Fulv both are thought to activate GPER1 signaling, titration of the estrogen E2 against a fixed concentration of the antiestrogen Fulv prevented AJ reorganization at concentrations in line with published binding affinities to the ERα (Section 3.1.2, Figure 5) [90]. Similarly, E1, which is reported to have no binding affinity towards GPER1 [11], could prevent AJ reorganization in the pilot screen (Section 3.2.5, Table 2). Specific inhibition of ERα signaling by siRNA-mediated ERα KD resulted in AJ reorganization, while GPER1 KD neither induced nor prevented AJ reorganization (Section 3.1.2, Figure 5, Figure 8). It needs to be considered however, that Western blot analysis and immunofluorescence staining could

only verify KD efficiency of ERα protein, while GPER1 KD efficiency could only be controlled at the mRNA level as no appropriate GPER1 antibody could be identified. Thus, it cannot be fully excluded that, due to low protein turnover and high protein stability, GPER1 protein levels may have remained sufficiently high to retain their functionality. The role of GPER1 was further investigated using the small molecule inhibitors G15 and G36 (Section 3.1.2, Figure 6, Figure 7). G15 could prevent Fulv-mediated but not ERα KD-mediated AJ reorganization, while G36 did not have any effect. Although G15 and G36 show similar antagonistic effects towards GPER1, it was reported that G15 in contrast to G36 can also bind to ERα and act as partial agonist of ERα-mediated transcription [94]. As G15 did only prevent Fulv-mediated but not ERα KD-mediated AJ reorganization, competitive displacement of Fulv through G15 at the ERα level appeared to be a plausible explanation. However, titration of G15 against a fixed concentration of Fulv did not significantly rescue Fulv-induced inhibition of estrogen responsive gene expression levels (Section 3.1.2, Figure 6). Additionally, increasing concentrations of Fulv against a fixed concentration of G15 could only partially rescue AJ reorganization (Section 3.1.2, Figure 7). Although competitive displacement of Fulv through G15 at the ERα level might in part explain the G15-mediated prevention of Fulv-induced AJ reorganization, other yet unknown mechanisms of Fulv and G15 action are likely involved and require further investigation. Cotreatment studies of G1, G15 and Fulv might help to further elucidate the action of G15.

Altogether, the data supports a causal relationship of ERα signaling inhibition and AJ reorganization. Regardless of the inconclusive results concerning G15 action, a significant involvement of GPER1 seems unlikely and AJ reorganization is primarily mediated through the ERα signaling pathway.

4.2. Adherens junction reorganization is a functionally relevant endpoint

In contrast to other endpoints such as receptor binding (OECD TG 493) or receptor transactivation (OECD TG 455), AJ reorganization is a more functionally relevant endpoint with regard to cancer development and progression.

Tumor progression, invasion and metastasis are in part dependent on the adhesiveness of the cancer cells [32]. Cell adhesion is primarily mediated by intercellular formation of Cadherin dimers between adjacent cells. Changes of E-Cad

expression levels are thought to be a hallmark in cancer progression [32]. However, recent research shows that expression levels alone are not necessarily indicative of prognosis and adhesion [31, 113]. While interaction between two individual E-Cad proteins of adjacent cells is rather weak, it is strengthened by lateral E-Cad clustering [27, 28]. The E-Cad ectodomains engage into *trans* (with neighboring cells) as well as *cis* (with E-Cad proteins of the same cell) interactions and both interactions are required for effective adhesion. Additionally, the actin cytoskeleton and lipid environment contribute the organization of E-Cad proteins into tightly packed nanoclusters as well as microclusters [28]. AJ reorganization seems to correlate with increased cell-cell adhesion through E-Cad microclusters. Upon AJ reorganization, E-Cad distribution converged from a continuous/regular to a discontinuous/irregular distribution. Additionally, while no change on *CDH1* mRNA levels were observed, AJ reorganization correlated with higher E-Cad protein levels likely through decreased protein turnover (Section 3.1.1, Figure 3). It was shown that the pool of E-Cad accessible to Trypsin cleavage was reduced upon AJ reorganization (Section 3.1.3, Figure 9). Trypsin is a serine protease endogenously found in the digestive system but is also standardly used to dissociate cells in cell culture. Whereas the amount of full-length E-Cad decreased upon Trypsin digestion in the solvent control, its levels remained unchanged in Fulv-treated cells displaying AJ reorganization. Accordingly, the additional low molecular weight bands emerging from the Trypsin digestion were also less pronounced in Fulv-treated cells even though total protein levels were elevated. As engagement of E-Cad in nano- or microclusters decreases the accessibility to proteases like Trypsin, it can be concluded, that next to AJ reorganization and increased E-Cad protein levels also the amount of E-Cad engaged in clusters is elevated. Similarly, Fulv-treated cells with induced AJ reorganization showed an increased resilience against calcium deprivation (Section 3.1.3, Figure 9). Incubation with the calcium chelating agent EGTA causes rounding of cells as E-Cad *trans* interactions are highly calcium dependent. Following, the amount intercellular E-Cad homodimers are reduced upon EGTA addition. The cell-cell contacts are lost, and the cells display a rounded morphology. As all non-covalent bonds exist in equilibrium and E-Cad at the membrane is subject to protein turnover, the time needed for full cell-cell contact detachment and rounding is depending on E-Cad clustering, protein turnover, and total amount of E-Cad intercellular dimers. Cell rounding occurred much faster in solvent control cells than compared to cells treated with Fulv. While more than 20 % of the

cells already exhibited rounded cell morphology after 40 min of incubation in the solvent control, nearly all Fulv-treated cells had still intact cell contacts. Even at the end of the measured time period of 120 min only about 20 % of the Fulv-treated cells showed rounded cell morphology whereas the fraction of rounded cells was twice as high in the solvent control. Thus, in line with the other results, also the quantitative calcium resilience assay indicates increased E-Cad clustering, decreased protein turnover and higher total amount of E-Cad intercellular dimers upon AJ reorganization.

Overall, the data conclusively links E-Cad microcluster formation by AJ reorganization with increased levels of bound E-Cad at the membrane – both of which are indicative of increased cell adhesion [28, 95]. Highlighting the functional relevance of AJ reorganization as endpoint for the identification of estrogenic substances, these findings are also important in the context of breast cancer therapy. Inhibition of estrogen signaling through ERα antagonists or aromatase inhibitors is an essential part in therapy of ERα-positive breast cancer [21]. Published results addressing the influence of ERα signaling on *CDH1* expression have been rather contradictory [33-35] and E-Cad levels alone have been shown to not be fully predictive of cancer progression [31, 113]. Increased adhesion through ERα-mediated AJ reorganization might represent another possible beneficial effect of endocrine therapy.

4.3. Signaling pathways involved in adherens junction reorganization

In addition to strengthening the functional relevance of AJ reorganization as endpoint for estrogenic substances, an understanding of the involved signaling pathways is important for the identification of potential false positive predictions from a screening assay. Figure 29 summarizes the key findings from this work about the relevant singling pathways involved in AJ reorganization including ERα, AREG, and EGFR signaling.

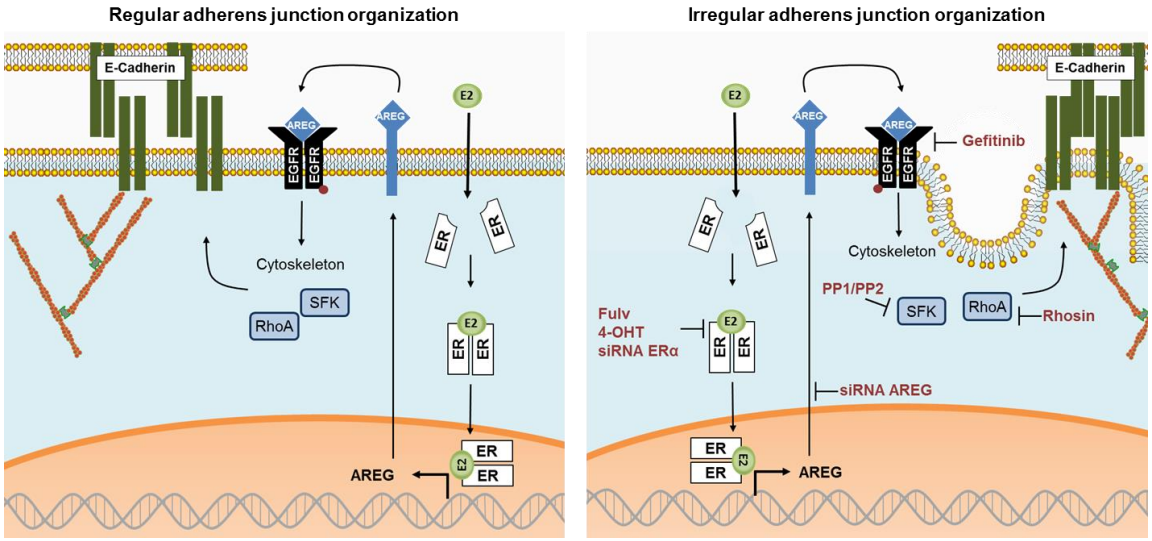

Figure 29: Working model for estrogen receptor α induced adherens junction reorganization. Activation of estrogen receptor α (ERα) signaling upon 17β-estradiol (E2) binding induces Amphiregulin (AREG) expression. At the membrane, AREG is processed and secreted. As an autocrine or paracrine growth factor, AREG activates the epidermal growth factor receptor (EGFR) signaling pathway. Through src family of kinases (SFK), RhoA or other regulators of the cytoskeleton regular adherens junction (AJ) organization is formed. Disruption of this signaling pathway causes irregular AJ organization/AJ reorganization. Disruption can happen through ERα signaling inhibition (antiestrogens (Fulvestrant (Fulv), 4-hydroxytamoxifen (4-OHT)); siRNA ERα knock down (KD)), AREG KD, inhibition of the EGFR (Gefitinib) or the modulation of cytoskeleton (PP1/PP2 or Rhosin). Red dot indicates phosphorylation.

AREG is part of the EGF family of growth factors and known to activate EGFR signaling in a juxta- and paracrine manner. In contrast to other EGFR ligands, expression of *AREG* is strongly estrogen-dependent and regulated by ERα activity. Ciarloni *et al* found that E2 treatment of ovariectomized mice specifically induced *Areg* expression but not of the other EGF ligands, while no *Areg* induction was observed in ERα KD mice [97]. Additionally, EREs were identified around the *AREG* promotor region *in vitro* and *in vivo* [1, 114]. Cell culture experiments with another MCF7 sub-clone showed a modulation of *AREG* expression depending on ERα signaling activity [98]. Additionally, it was reported that the xenoestrogen BPAF induced cell proliferation through ERα-mediated *AREG* expression and EGFR activation highlighting the relevance of AREG in EDC research [115]. In MCF7/vBOS cells, *AREG* was found to be one of the first genes to be significantly downregulated upon Fulv treatment with a two-fold inhibition after 4 h and a hundred-fold inhibition of expression levels after 48 h (Section 3.1.3, Figure 10). Similarly, the ERα KD resulted in a reduction of AREG mRNA and protein levels. In addition, it could be shown that Fulv-induced downregulation of AREG could be prevented by the addition of an

equimolar concentration of E2, and its expression levels could even been induced at higher E2 concentrations similar to other estrogen responsive genes (Section 4.1).

ERα-dependent *AREG* expression and EGFR signaling are crucial for the correct development and organization of the mammary duct as demonstrated in KD studies in mice. KD of ERα, AREG or EGFR impaired pubertal outgrowth of the ductal epithelium and ductal malformation upon ERα KD could be prevented by exogenous AREG administration [1, 97]. While AREG and EGFR are essential in the development of the mammary duct, both are also implicated in breast cancer development and progression [37, 44, 96]. Overexpression of AREG and EGFR in breast cancer is correlated with larger tumor size and cancer progression [37, 44]. AREG is discussed to be responsible for EGFR-mediated cell proliferation and invasion [44]. In MCF7/vBOS cells, the ERα-AREG-EGFR signaling axis was also found to be involved in the development of AJ reorganization (Section 3.1.3, Figure 10, Figure 11). Low AREG expression levels coincided with AJ reorganization and prevention of AREG downregulation also prevented the formation of AJ reorganization. Moreover, siRNA-mediated KD of either ERα or AREG induced AJ reorganization, while hAREG-GFP overexpression was able to restore endogenous AREG expression levels and prevent Fulv-mediated AJ reorganization. It was previously reported that next to ERα signaling, AREG expression can also be induced through an EGFR-dependent positive feedback loop [43, 44]. A rescue of endogenous AREG expression through hAREG-GFP overexpression thus indicates functional activity of the ectopically expressed AREG protein and an activation of the EGFR signaling pathway. In line with these findings, the small molecule EGFR inhibitors Gefitinib, PD153035, and BIBX1382 induced AJ reorganization as well (Section 3.1.3, Figure 11).

Notably, treatment with the EGFR inhibitors also caused a downregulation of ERα target gene expression levels including *AREG* (Section 3.1.3, Figure 11). As all three structurally different inhibitors had similar inhibitory effects on estrogen responsive gene expression, these changes are rather unlikely to be caused by off-target effects on the ERα. This bidirectional crosstalk between the ERα and the EGFR signaling pathway has also been reported in several publications [9, 11, 13]. While ERα mediates the expression of growth factors like AREG, EGFR signaling can influence ERα phosphorylation and thus activity [116]. Britton *et al* showed a direct relationship between AREG-dependent EGFR/MAPK signaling pathway activation and ERα phosphorylation at Ser 118 in Tam-resistant MCF7 cells. While the presence of AREG

induces Ser 118 phosphorylation, addition of the EGFR inhibitor Gefitinib results in reduced phosphorylation [114]. Similarly, Migliaccio *et al* reported a modulation of ERα phosphorylation at several sites by EGFR signaling and SFK activation [101, 116]. Upon phosphorylation, ERα associates with SFK and forms a complex, which induces ligand-independent estrogen responsive gene expression. Interestingly, this complex also in turn influences EGFR phosphorylation and activity [116]. Notably, while all the three small molecule EGFR inhibitors caused a general downregulation of estrogen responsive gene expression in MCF7/vBOS cells, a modulation of AREG levels (KD or overexpression), and thereby EGFR activity, itself did not influence ERα activity (Section 3.1.3, Figure 10) suggesting the involvement of additional growth factors.

Notably, an about two-fold upregulation of EGFR total protein levels could also be consistently observed upon AJ reorganization in MCF7/vBOS cells across all treatment conditions (Fulv/4-OHT treatment or ERα/AREG KD), which was however not reflected at the *EGFR* mRNA level (Section 3.1.3, Figure 11). The mechanism underlying this observation needs to be addressed by further studies. As AJ reorganization was a result of AREG depletion and EGFR signaling inhibition, the increased EGFR protein levels might be the result of a post-transcriptional compensatory mechanism. Additionally, E-Cad and EGFR are able to directly interact with each other at the cell membrane [26]. E-Cad expression and EGFR signaling activity are inversely correlated and EGFR signaling inhibition induces E-Cad upregulation and adhesion [117]. In MCF7/vBOS cells, AJ reorganization coincides with increased E-Cad clustering and protein levels. Thus, increased EGFR protein levels could also be caused by reduced turn over and membrane fluidity due to entrapment in E-Cad clusters. As interaction of E-Cad negatively influences EGFR signalling activity, E-Cad clustering might further strengthen EGFR inhibition and AJ reorganization. While an involvement of AREG in AJ reorganization could be clearly shown, further research is needed to fully elucidate the underlying mechanism and the role of the EGFR in the formation of AJ reorganization.

To conclude, while endpoints such as ERα transactivation or binding only address specific parts of the entire ERα signaling pathway in a rather artificial environment, the ERα-dependent AJ reorganization addressed by the E-Morph Assay represents an endpoint with a clear functional relevance. Moreover, as ERα-mediated AJ reorganization directly correlated with increased E-Cad clustering and involved the AREG-EGFR signaling pathway, the E-Morph Assay also addresses an endpoint with a

potential clinical relevance with regard to cancer progression and invasion, which remains to be investigated in more detail.

4.4. Adherens junction reorganization as an endpoint in a high-throughput compatible test method for estrogenic substances – the E-Morph Assay

Based on the collected data showing that AJ reorganization is mainly ERα dependent in MCF7/vBOS cells, AJ reorganization was used as an endpoint for developing a HT-compatible test method, referred to as the E-Morph Assay. In this assay, AJ reorganization can be used for both the identification of ERα agonists as well as antagonists depending on the set-up. ERα antagonists are identified directly by their capacity to induce AJ reorganization and ERα agonists are indirectly identified by their capacity to prevent Fulv-induced AJ reorganization. As most of the EAS act rather as ERα agonists than antagonists, it was decided to first establish the agonist set-up that is described in this thesis (Figure 30). In the E-Morph Assay, seeded cells are cotreated with a fixed concentration of Fulv and increasing concentrations of the test substance. Following, the cells are stained and then imaged using an automated high-content microscope. Finally, a machine learning-based image analysis pipeline allows the analysis of AJ organizations and thereby a characterization of the estrogenicity of a test substance.

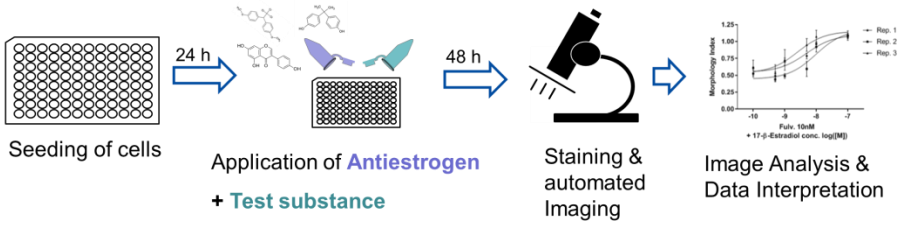

Figure 30: Schematic view of the E-Morph Assay.
MCF7/vBOS cells were seeded into a 96-well plate. The following day, 10 nM Fulv and different concentrations of the test substance were applied to the cells. Medium was exchanged the next day. After 48 h of incubation, the cells were stained with CellTrace, Hoechst 33342, and CellTox Green. Image acquisition was done with Opera Phenix High Content microscope. Image analysis was conducted with a machine learning based image analysis pipeline build within the integrated image analysis software Harmony.

The development process included several adaptation and optimization steps to achieve high efficiency and robustness of the assay. The cell staining was switched from E-Cad immunofluorescent stain to an indirect cytoplasmic staining (Section 3.2.1, Figure 19). Even though, this way, direct quantification and visualization of

AJ organization was not possible, cytoplasmic staining was found to be much faster and additionally had a better signal separation. During image analysis using the integrated Harmony software, cell segmentation is a multistep process including identification of nuclei as seeding points for the following detection of cell outlines based on a cytoplasmic staining. Direct membrane identification based on E-Cad staining is not a built-in option and more prone to mistakes during segmentation resulting in error prone classifications and decreased signal separation. The time point analysis confirmed 48 h to be the ideal incubation period as an incubation period shorter than 48 h was shown to be unfavorable with regard to signal separation due to incomplete AJ reorganization, while an incubation period beyond 48 h did not significantly improve classification (Section 3.2.2, Figure 22). Still, it is possible to test more than 12 substances a week in this set-up with still manual treatment and staining. Further optimization and automation of these steps will increase the throughput.

A key confounder of results in *in vitro* testing is cytotoxicity of the test substance. Often times, cytotoxicity is measured separately or only the cell count is included in an assay set-up. In the E-Morph Assay, addition of the CellTox Green dye during staining and minor adaptations of the image analysis pipeline enabled the easy integration of CellTox Green mean intensity and number of cells as two independent cytotoxicity endpoints (Section 3.2.3, Figure 23). Testing of three different substances with known cytotoxic properties underlined the performance of both endpoints in predicting cytotoxicity. Further optimization of the staining and imaging procedure might even increase the predicative capacity of CellTox Green. CellTox Green stains all dead or dying cells with impaired membrane integrity. As the staining procedure includes several washing steps, large amounts of dead cells are washed off. While it increased the sensitivity of the cell count as endpoint, it limited to the detection of dying but still attached cells. Addition of CellTox Green to and imaging of the cells prior to the general cell staining process might increase sensitivity, but would mean further steps. The CellTiter Blue assay is often used as a cytotoxicity marker [118]. Although being generally indicative for cytotoxicity, it was shown to not be an ideal endpoint in the E-Morph Assay as it was sensitive to ERα-dependent changes in the metabolic state of cells and also required additional sample preparation procedures.

To conclude, it was possible to develop a test method for the identification of estrogenic substances. Optimized staining procedures and image analysis enable the simultaneous read-out of three endpoints – estrogenicity as well as the two cytotoxicity

endpoints number of cells and membrane integrity. Future work will go towards the integration of the E-Morph Assay in a full automatic HT system.

4.5. Characterization of the limitations and applicability of the E-Morph Assay

The biologic and mechanistic relevance of AJ reorganization as an endpoint for a test method to identify and characterize estrogenic substances has already been described in detail in the previous paragraphs (Section 4.1 to 4.3). In addition, the applicability domain of a test method describing its applicability and limitations to certain groups of chemicals or reactivity mechanisms needs to be clearly characterized.

Certain limitations arise from the general *in vitro* assay set-up. Generally, for appropriate cell treatment, the substance needs to be soluble in the used medium. As only one cell line is used in an artificial 2D set-up, representation of toxicokinetics is very limited. In addition, barrier functions are also not reflected in this assay. However, the amount of Fulv used is physiologically relevant and in the future, physiologically based pharmacokinetic modelling models might allow the definition of bioavailable concentrations that might at least partially compensate for limitations of in vitro assays in respect to absorption, distribution, metabolism, and excretion. Similarly, breast cells do not have the same metabolic capacity as for example liver cells [119]. Substances that need specific metabolic activation might not be active in the E-Morph Assay. Likewise, substances which are normally rapidly metabolized to inactive compounds might appear as highly active.

As illustrated in the working model (Section 4.3, Figure 29), multiple signaling pathways are involved in AJ reorganization including ERα and AREG-EGFR, but also SFK and RhoA. The role of AREG and the EGFR signaling pathway for AJ reorganization has been discussed in detail in the previous Section 4.3. From these data one can conclude that test substances inducing AREG expression or activating EGFR in an ERα-independent manner may prevent Fulv-induced AJ reorganization and would consequently be detected as false positives in the E-Morph Assay. Similarly, EGFR inhibitors could possibly strengthen AJ reorganization independent of their estrogen action and be detected as false negatives. Analysis of estrogen responsive gene expression might help support the final decision. With regard to the applicability domain of the E-Morph Assay, the role of SFK as a downstream pathway of EGFR signaling needs to be considered. Although, an involvement of the two SFK c-src and

Fyn could be excluded, as neither the c-src-specific small molecule inhibitor kb-src4 nor Fyn KD influenced AJ organization, the small molecule SFK inhibitors PP1 and PP2 were able to efficiently induce AJ reorganization. PP1 and PP2 are standardly used as specific SFK inhibitors. Still, it is important to consider, that even though PP1 and PP2 are known to inhibit the activity of several SFK, publications by Bain *et al* show that they also act off-target on other kinases such as C-terminal src kinase (CSK) or cyclin G-associated kinase (GAK) [120, 121]. As already mentioned previously, SFK are known to be involved in the bidirectional crosstalk of ERα signaling and EGFR activity and influence ERα transcriptional activity [116]. While upon Fyn KD the expression level of AREG remained unchanged, PP1 and PP2 caused a downregulation of AREG expression. Interestingly, the expression levels of the other estrogen responsive genes remained unchanged (*TFF1*) or were even induced (*PGR*) indicating indirect modulation of the ERα potentially through changing its phosphorylation status. Additionally, cotreatment with E2 or G15 could also partially prevent PP2-induced AJ reorganization in a similar fashion as observed for Fulv-induced AJ reorganization, altogether indicating a crosstalk with ERα signaling.

Although this data points towards the involvement of SFKs or other PP1/2-inhibited kinases, the underlying mechanism by which PP1 and PP2 induce AJ reorganization remains to be clarified. To further elucidate a potential crosstalk with ERα, a thorough analysis of its phosphorylation status would be required. Independently, test substances influencing SFK may not be correctly identified concerning their estrogenicity.

Potential influences of the Rho GTPases Rac1, Cdc42, and RhoA/C on AJ reorganization have been investigated as well. Rho GTPases are major players in the regulation of actin cytoskeleton organization as well as AJ formation and maintenance [27]. In addition, Rho GTPase activity itself can be influenced by EGFR and SFK signaling [41]. A significant role in AJ reorganization of rac1 and cdc42 could be excluded as neither inhibition of Rac1 nor cdc42 through small molecule inhibitors had any effect. The role of RhoA however is still less clear. RhoA activation either through a RhoA activator or overexpression of constitutively active RhoA prevented AJ reorganization induced by Fulv or PP2. In contrast, inhibition of RhoA using the RhoGEF12/LARG-specific RhoA inhibitor Y16 [107] or overexpression of constitutively inactive RhoA had no effect. However, Rhosin, a direct small molecule RhoA inhibitor [106], did induce AJ reorganization but also inhibited the gene

expression of estrogen responsive genes, *AREG* as well as *RHOA* and *RHOC*. While modulation of ERα activity through the differential expression levels *RHOA* and *RHOC* has been discussed before [122], KD of RhoA or RhoC did not cause any obvious changes in *AREG* expression or AJ reorganization. Thus, an off-target effect of Rhosin on ERα cannot be excluded. Generally, although RHOC is induced upon Fulv treatment, no connection between AJ reorganization and RhoA or RhoC expression levels could be found at this point, as also overexpression of RhoA or RhoC did not influence AJ reorganization in any way.

Although further research is needed to fully characterize the role of RhoA in AJ reorganization, the data so far suggests a more permissive rather than instructive role of RhoA in AJ reorganization. RhoA is a major hub in cytoskeleton regulation and the prevention of AJ reorganization might just be the result of general changes in cytoskeleton organization. Nevertheless, these data indicate that test substances modulating the architecture of the actin cytoskeleton, e.g. by activating RhoA, may be detected as false positives in the E-Morph Assay, therefore limiting its applicability domain.

4.6. Characterization of the predictive capacity of the E-Morph Assay

In addition to the applicability domain, the predictive capacity of a test method is a key determinant describing its performance as compared to e.g. reference test methods that are accepted by regulatory agencies. A test set of six substances of known estrogenic potential was used to define a prediction model for the E-Morph Assay. After passing the initial quality control step permitting only plates with sufficient signal separation for further analysis, substances with an MI value above 0.75 at any non-toxic concentration in two out of three runs were defined as estrogenic/positive. The prediction model was then used to assess the estrogenic potential of an additional set of eleven reference substances that were also in part used in the validation of receptor binding (OECD TG 493) or receptor transactivation (OECD TG 455) assays, both internationally accepted. The relative MI75 (interpolated concentration at which the 0.75 threshold was crossed) of all 17 tested substances correlated well with relative logarithmic EC50 values from both assays (receptor binding (OECD TG 493) or receptor transactivation (OECD TG 455)) and further confirmed the ERα-dependency of the selected endpoint. Even Gen, known to also inhibit EGFR [75] thus a possible false-negative, was able to prevent AJ reorganization at reasonable concentrations. The

relative MI75 values correlated slightly better with the relative logarithmic IC50 of the Freyberger-Wilson Assay than compared to the CERI Assay with the relative value of 5α-dihydrotestosterone being the main difference. While the CERI assay uses the ERα binding domain produced in *Escherichia coli*, the Freyberger-Wilson Assay utilizes the full-length ERα protein made by insect cells [77]. In addition to protein length, also the expression system might influence the binding affinity as *Escherichia coli* and insect cells are known to have different capacities in protein folding and posttranslational modifications. Interestingly, the relative MI75 values correlated better with the stably transfected TA assay using ERα-HeLa cells than compared to the MCF7 based VM7-Luc-ER TA assay [78]. MCF7 cells are known for their clonal heterogeneity and their responsiveness to estrogens can vary greatly [88, 123]. The relative MI75 values also correlate well with EPA ToxCast ER agonist score. The ToxCast score is, in contrast to the other values, not a relative value derived from an effect concentration but a cumulative score derived from the results of 18 different assays. The good correlation highlights the good predictive capacity of the test method.

5. Conclusion and Outlook

This thesis describes the development of a novel test *in vitro* method – the E-Morph Assay – that allows the identification and characterization of estrogenic substances. In contrast to most existing *in vitro* assays, the E-Morph Assay has a functional endpoint, i.e. AJ reorganization, encompassing complex cellular mechanisms. Similar to cell proliferation as the endpoint in the E-SCREEN assay, AJ reorganization is also clinically relevant with regard to cancer progression. AJ reorganization was shown to be mediated by the ERα/AREG/EGFR signaling pathways and correlated with the clustering of E-Cad at the cell membrane and increased cell adhesion.

According to the A concept, multiple assays can be combined to cover the MIE and KEs leading towards an adverse effect [80]. While *in vitro* assays for the first two KE of ERα signaling activation (receptor binding and transcription activation [80]) exist, there is a need for new *in vitro* assays with functional endpoints which cover more complex KE. The E-SCREEN with proliferation as endpoint was so far the only functional assay. On its own, the E-Morph Assay cannot replace *in vivo* assays. However, it can contribute towards covering more complex KE in an ERα signaling AOP. Initial testing of 17 substances showed a good predictive capacity for

identification and characterization of estrogenic substances. Additionally, because of the direct relevance of AJ reorganization in the context of breast cancer, the E-Morph assay might be useful in the development of new drugs against breast cancer.

Further investigation is needed towards elucidating the underlying molecular mechanism downstream of ERα/EGFR and the functional relevance of AJ reorganization. Immuno-histological analysis of breast cancer section of antiestrogen-treated patients should be analyzed to underline the clinical relevance of this finding and the new potential beneficial effects of endocrine therapy. Testing of more substances with known and unknown estrogenic potential will be required to further define the predictive capacity and applicability domain of the E-Morph Assay. Internal and external validation studies to define the transferability and reliability of the E-Morph Assay would a prerequisite for the regulatory acceptance at international level, e.g. within the framework of an IATA.

6. Materials

6.1. Equipment

Table 3: List of equipment and machines used.

Equipment	Manufacturer
Apotome.2	Zeiss
Axio Observer.Z1	Zeiss
CKX41 inverted microscope	Olympus life science
Countess II FL Automated Cell Counter	Invitrogen
EcoVac vacuum pump	schuett-biotec
Fusion Solo 6S	Vilber
GENios	Tecan
Mastercycler nexus gradient	Eppendorf
Mini-Protean 3 cell	Bio-Rad
Nanodrop 2000 spectrophotometer	ThermoFisher Scientific
Opera Phenix High Content screening system	Perkin Elmer
QuantStudio 7 Flex	Applied Biosystems
THERMOstar	BMG Labtech
Thermostat 5320	Eppendorf
Trans-Blot SD Semi-Dry transfer cell	Bio-Rad
Zeiss LSM 880 AiryScan Confocal Microscope	Zeiss
ZOE Fluorescent Cell Imager	Bio-Rad

6.2. Cell culture

Cell culture reagents

Table 4: List of all the used cell culture reagents.

Name	Manufacturer	Order number
BioFreeze	Biochrom/Merk	F 2270
CellTiter-Blue Cell Viability Assay	Promega	G8080
DMEM 1 g/l Glucose phenol red free	Gibco	11880-028
DMEM 1 g/l Glucose with Glutamine	Biochrom/Merk	FG0415
Dulbecco’s Phosphate-Buffered Saline (PBS)	PAN biotech	P04-36500
EGTA	Roth	3054.1
Fetal bovine serum	Biochrom/Merk	S0613
FuGENE HD Transfection Reagent	Promega	E2311
Glutamax (100x)	Gibco	35050-38
HiPerFect Transfection Reagent	Qiagen	301705
Opti-MEM	Gibco	51985034
Penicillin/Streptomycin	Biochrom/Merk	A2212
Trypsin/EDTA-Solution (0.05 %/ 0.02 %)	Biochrom/Merk	L2143

Table 5: Cell culture media compositions

Name	Composition
Complete medium	DMEM 1 g/l Glucose with Glutamine 10 % FBS 1 % Penicillin/Streptomycin
Minimal medium	DMEM 1 g/l Glucose phenol red free 5 % FBS 1 % Penicillin/Streptomycin 1 % Glutamax

Cell lines

For this thesis, the MCF7/vBOS derived from the original MCF7 cell line [88] specifically selected for their estrogen responsiveness and MCF7/E-CadGFP cell line [124] were used.

6.3. Staining reagents

Cell labeling reagents

Table 6: List of all the cell labeling reagents used.

Name	Company	Order number
4‘,6-Diamidibo-2-phenylindole (DAPI)	Sigma	D9542
CellTox Green Dye, 1,000x	Promega	G8731
CellTrace Far Red Cell Proliferation Kit	Life Technologies	C34564
Hoechst 33342, Trihydrochloride, Trihydrate – 10 mg/mL Solution	ThermoFisher Scientific	H3570
LysoTracker Deep Red	Life Technologies	L12492

Antibodies

Table 7: List of the primary antibodies used.

Name	Manufacturer	Order number
Monoclonal Mouse Anti-E-Cadherin (G1)	Santa Cruz	sc-8426
Monoclonal Mouse Anti-EGFR (A10)	Santa Cruz	sc-373746
Monoclonal Mouse Anti-ERα (F10)	Santa Cruz	sc-8002
Monoclonal Mouse IgG2a, k Anti-E-Cadherin (C36)	BD Transduction Laboratories	BD 610 182
Polyclonal Rabbit Anti-Amphiregulin	Proteintech	16036-1-AP
Polyclonal Rabbit Anti-E-Cadherin (H-108)	Santa Cruz	sc-7870
Polyclonal Rabbit Anti-ERα (HC20)	Santa Cruz	sc-543

Table 8: List of the secondary antibodies used.

Name	Manufacturer	Order number
Donkey anti-Mouse IgG (H+L) Highly Cross-Adsorbed Secondary Antibody, Alexa Fluor 488	ThermoFisher Scientific	A-21202
Donkey anti-Mouse IgG (H+L) Highly Cross-Adsorbed Secondary Antibody, Alexa Fluor 555	ThermoFisher Scientific	A-31570
Donkey anti-Mouse IgG (H+L) Highly Cross-Adsorbed Secondary Antibody, Alexa Fluor 647	ThermoFisher Scientific	A-31571
Donkey anti-Rabbit IgG (H+L) Highly Cross-Adsorbed Secondary Antibody, Alexa Fluor 488	ThermoFisher Scientific	A-21206
Donkey anti-Rabbit IgG (H+L) Highly Cross-Adsorbed Secondary Antibody, Alexa Fluor 555	ThermoFisher Scientific	A-31572
Donkey anti-Rabbit IgG (H+L) Highly Cross-Adsorbed Secondary Antibody, Alexa Fluor 647	ThermoFisher Scientific	A-31573
Goat-anti-mouse- IgG-Horse-radish peroxidase	Santa Cruz	sc-2031
Goat-anti-rabbit- IgG-Horse-radish peroxidase	Santa Cruz	sc-2004

6.4. DNA and RNA constructs

Plasmid

Table 9: List of the plasmids used in this thesis

Protein	Vector-Backbone	Supplier	Cat. No
pcDNA3-EGFP-RhoA-Q63L	pcDNA 3-EGFP	Addgene	12968
pcDNA3-EGFP-RhoA-T19N	pcDNA 3-EGFP	Addgene	12967
pcDNA3-EGFP-RhoA-WT	pcDNA3-EGFP	Addgene	12965
pCMV6-AC-GFP-hAREG-GFP	pCMV6-AC-GFP	OriGene	RG203150
pCMV6-AC-GFP-RhoC-GFP	pCMV6-AC-GFP	OriGene	RG217556

siRNA

Table 10: List of the different siRNAs used in this thesis. All siRNAs were purchased by Qiagen as FlexiTube GeneSolution (product number 1027416).

Gene	Order number	siRNAs
AREG	GS374	SI03049683; SI00299936; SI00299852; SI00299845
ESR1	GS2099	SI02781401; SI03114979; SI03065615; SI00002527
FYN	GS2534	SI02659545; SI02654729; SI00605451; SI03095218
GPER1	GS2852	SI02776907; SI02654267; SI02654211; SI04434213
RHOA	GS387	SI02776907; SI02654267; SI02654211; SI04434213
RHOC	GS389	SI02776907; SI02654267; SI02654211; SI04434213
Negative Control siRNA	1027415	SI03650325

Oligonucleotides

Table 11: List of primers for the quantitative polymerase chain reaction including their sequence and melting temperature T_M. All primers were purchase by Eurofins.

Gene		Sequence (5'→3')	T_M
YWHAZ	forw	ACT TTT GGT ACA TTG TGG CTT CAA	58.3
	rev	CCG CCA GGA CAA ACC AGT AT	58.8
CDH1	forw	AGG AGC CAG ACA CAT TTA TGG AA	58.9
	rev	GCT GTG TAC GTG CTG TTC TTC AC	62.4
PGR	forw	TCAACTACCTGAGGCCGGAT	58.5
	rev	GCTCCCACAGGTAAGGACAC	56.3
GPER1	forw	AGCGGACAAAGGATCACTCAG	58.3
	rev	GGTGGGTCTTCCTCAGAAGG	57.7
ESR1	forw	CCACCAACCAGTGCACCATT	60.7
	rev	GGTCTTTTCGTATCCCACCTTTC	58.6
EGFR	forw	GGCAGGAGTCATGGGAGAA	58.8
	rev	GCGATGGACGGGATCTTAG	58.8
AREG	forw	TGGATTGGACCTCAATGACA	56.7
	rev	TAGCCAGGTATTTGTGGTTCG	65.4
TFF1	forw	CATCGACGTCCCTCCAGAAGAG	62.1
	rev	CTCTGGGACTAATCACCGTGCTG	61.7

Gene		Sequence (5‘→3‘)	T_M
EGR3	forw	GGTGACCATGAGCAGTTTGC	58.4
	rev	ACCGATGTCCATTACATTCTCTGT	57.5
PDZK1	forw	CTCCAGCTCCTACTCCCACT	55.2
	rev	ACCGCCCTTCTGTACCTCTT	56.7
RHOC	forw	AGCGGAAGCCCCACCAT	57.6
	rev	CAGTGTCCGGGTAGGAGAGA	61.4
RHOA	forw	AGCCAAGATGAAGCAGGAGC	58.6
	rev	TTCCCACGTCTAGCTTGCAG	58.1

6.5. Kits

Table 12: List of the different kits used.

Name	Manufacturer	Order number
DNase	Qiagen	79254
High Capacity cDNA reverse transcription kit	Applied Biosystems	4368814
Pierce BCA protein assay kit	ThermoFisher Scientific	23225
RNeasy Mini kit	Qiagen	74106

6.6. General material

Table 13: List of chemicals with known or suspected endocrine effects.

Name	CAS Number	Function	Supplier	Order number
(Z)-4-Hydroxytamoxifen	68047-06-3	ERα Antagonist	Tocris	3412
17α-Ethinylestradiol	57-63-6	ERα Agonist	Sigma	E4876
17β-Estradiol	50-28-2	ERα Agonist	Sigma	E8875
5α-Dihydrotestosterone	521-18-6	Androgen	Sigma	A8380
Atrazine	1912-24-9	Herbicide	Sigma	90935
Bisphenol A	80-05-7	Phenol	Sigma	239658
Bisphenol AF	1478-61-1	Phenol	Sigma	90477
Bisphenol B	77-40-7	Phenol	Sigma	50877
Bisphenol S	80-09-1	Phenol	Sigma	43034
Coumestrol	479-13-0	Isoflavone	Sigma	27885
Daidzein	486-66-8	Isoflavone	Sigma	D7802
Diethylstilbestrol	56-53-1	ERα Agonist	Sigma	D4628
Estrone	53-16-7	ERα Agonist	Sigma	E9750
Fulvestrant	129453-61-8	ERα Antagonist	Sigma	I4409
Fulvestrant	129453-61-8	ERα Antagonist	Tocris	1047
G1	881639-98-1	GPER1 Agonist	Tocris	3577
G15	1161002-05-6	GPER1 Antagonist	Tocris	3678
G36	1392487-51-2	GPER1 Antagonist	Tocris	4759
Genistein	446-72-0	Isoflavone	Sigma	G6649
Ketoconazole	65277-42-1	Antifungal	Sigma	K1003

Name	CAS Number	Function	Supplier	Order number
Progesterone	57-83-0	Hormone	Sigma	P0130
Reserpine	50-55-5	Drug	Sigma	R0875
Zearalenone	17924-92-4	Mycotoxin	Sigma	Z2125
ZK164015	177583-70-9	ERα Antagonist	Tocris	2183

Table 14: List of inhibitors or activators of specific cellular pathways.

Name	CAS number	Function	Supplier	Order number
BIBX 1382 dihydrochloride	1216920-18-1	EGFR inhibitor	Tocris	2416
Gefitinib/Iressa	184475-35-2	EGFR inhibitor	Tocris	3000
kb-src4	1380088-03-8	c-Src inhibitor	Tocris	4660
PD153035	183322-45-4	EGFR inhibitor	Tocris	1037
PP1	172889-26-8	SFK inhibitor	Tocris	1397
PP2	172889-27-9	SFK inhibitor	Tocris	1407
PP3	5334-30-5	EGFR inhibitor	Tocris	2794
Rho Activator II (CN03)	-	RhoA activator	Cytoskeleton	CN03-A
Rhosin	1281870-42-5	RhoA inhibitor	Tocris	5003
Y16	429653-73-6	RhoA inhibitor	Sigma	SML0873

Table 15: List of any additional material used.

Name	Manufacturer	Order number
30 % Acrylamide:Bisacrylamide 37.5:1	Bio-Rad	161-0158
37 % Formaldehyde	neoLab Migge	443.010.000
4x Laemmli Puffer	Bio-Rad	1610747
5-Fluorouracil	Sigma	F6627
Acetic acid 100 %	Roth	6755.1
Ammonium persulfate (APS)	Roth	9592.3
Bovine Serum Albumin (BSA)	Sigma	A4503
Bromophenol blue	Roth	A512.1
cOmplete Protease Inhibitor Cocktail	Sigma	4693124001
Dulbecco's phosphate buffered saline (PBS)	Sigma	D5652
Ethylenediaminetetraacetic acid (EDTA)	Roth	X986.1
Glycine	Sigma	G8898
Hydrogen chloride	Roth	4625.1
Igepal CA630	Sigma	I8896
Methanol	Merk	1.060.092.511
Non Fat dry milk	Roth	T145.3
PageRuler Plus prestained Protein ladder	ThermoFisher Scientific	26619
PhosSTOP Phosphatase Inhibitor Cocktail	Sigma	4906845001

Name	Manufacturer	Order number
Pierce SuperSignal West Femto	ThermoFisher Scientific	34095
Pierce Western Blotting Substrate	ThermoFisher Scientific	32109
PlusOne Coomassie Tablets, PhastGel Blue R-350	GE Healthcare life science	17-0518-01
Ponceau S	Roth	5938.1
Power UP SYBR Green PCR Master Mix	ThermoFisher Scientific	15310939
Sodium azide	Sigma	S8302
Sodium chloride	Roth	HNOO.3
Sodium deoxycholate	Roth	3484.1
Sodium dodecyl sulfate (SDS)	Bio-Rad	161-0301
Tetramethylenediamine (TEMED)	SERVA	35930
Tris	Roth	5429.2
Triton X-100	Sigma	T8787
Tween-20	Roth	9127.1
VectaShield	VectorLabs	H-1000
β-Mercaptoethanol	Sigma	M7154

6.7. Buffers and solutions

Table 16: List of the different buffers and solution used.

Name	Chemicals	Concentration/ volume
Standard Lysis buffer	Tris	20 mM
	NaCl	138 mM
	Glycerol	5 % (w/v)
	EDTA	4 mM
	Triton X-100	1 % (v/v)
Boehringer Lysis buffer	Tris/HCl pH 7.4	50 mM
	NaCl	150 mM
	Na-deoxycholate	0.1 % (w/v)
	SDS	0.1 % (w/v)
	Igepal CA630	1 % (v/v)
	EDTA, pH 8.0	5 mM
	EGTA	5 mM
10x polyacrylamide gel electrophoresis (PAGE) buffer pH 8.3	Tris	625 mM
	Glycine	4802.5 mM
1x SDS Running buffer 1000 ml	10x PAGE buffer	100 ml
	10 % SDS	10 ml
	add H_2O	
1x Transfer buffer 250 ml	10x PAGE buffer	25 ml
	Methanol	50 ml
	add H_2O	

Name	Chemicals	Concentration/ volume
10 % polyacrylamide separation gel 15 ml	Acrylamide Mix (30 %) 1.5 M Tris/HCl pH 8.8 10 % SDS H_2O 10 % APS TEMED	5 ml 3.8 ml 150 µl 5.9 ml 150 µl 6 µl
5 % polyacrylamide stacking gel 5 ml	Acrylamide Mix (30 %) 0.5 M Tris/HCl pH 8.8 10 % SDS H_2O 0.5 % Bromophenol blue 10 % APS TEMED	830 µl 0.63 ml 50 µl 3.4 ml 20 µl 50 µl 5 µl
10x Tris-buffered Saline (TBS)	Tris NaCl	0.2 M 1.5 M
TBS-T 1,000 ml	10x TBS Tween 20 add H_2O	100 ml 1 ml
0.1 % Ponceau S in 5 % Acetic acid 100 ml	Ponceau S 100 % Acetic acid add H_2O	0.1 g 5 ml
Coomassie Stock solution	1 tablet/80 ml H_2O add 120 ml Methanol	
Coomassie working solution 100 ml	Stock solution Methanol add H_2O	50 ml 25 ml
Distaining solution 100 ml	100 % Acetic acid Ethanol add H_2O	10 ml 50 ml

7. Methods

7.1. Cell culture

Maintenance

The MCF7/vBOS as well as the MCF7/E-CadGFP cells were kept in full medium (see Table 5) and splitted into a new flask every three to four days in a dilution ratio between one to five and one to ten. After eight to ten passages, the cells were discarded, and a new batch of cells was thawed. The cell stock was kept frozen in BioFreeze in liquid nitrogen.

Seeding and treatment

If not noted differently, the cells were seeded in minimal medium in a concentration to reach confluence the next day. Treatment with the test substance or a combination of substances was started the following day after the cells had settled. Medium was changed daily. After a treatment period of two to three days, the cells were prepared according to the analysis method (see Sections 7.2 to 7.4).

Quantitative calcium switch resilience assay

The cells were seeded in a 96-well glass bottom view plate (Perkin Elmer 6005430) and exposed to 10 nM Fulv or the solvent control as described. After 48 h, the cells were stained with CellTrace and Hoechst 33342 as defined in Section 7.2, no CellTox Green was added. After washing, minimal medium containing 8 mM EGTA was added to the cells. The cells were imaged as a time course experiment (images every 10 minutes for two hours) with the Opera Phenix HC microscope. Finally, the images were analyzed with the integrated Harmony software as described in Section 7.5.

Effect kinetic with MCF7/E-CadGFP cells

The effect kinetic experiment was conducted in a similar fashion as the quantitative calcium switch resilience assay. The MCF7-E-CadGFP cells were seeded in a 96-well glass bottom view plate (Perkin Elmer 6005430) and exposed to 10 nM Fulv and the solvent control as described. After 24 h, the cells were stained with Hoechst 33342 as defined in Section 7.2 and put into the Opera Phenix HC microscope at 37°C for imaging. Images were taken every 2 h for 24 h. At last, the images were analyzed with the integrated Harmony software as described in Section 7.5.

Trypsin Resistance Assay

For the Trypsin Resistance Assay, MCF7/vBOS cells were seeded into a 6-well plate and treated with 10 nM Fulv as described. After two days of treatment, the cells were washed with PBS and 300 µl Trypsin/EDTA solution was added. The cells were incubated for 4 min at 37 °C. Following, the supernatant was removed, and the proteins were extracted as described in Section 7.4.

Transfection of siRNA and plasmids

Depending on the analysis method, the cells were either seeded into a 12-well plate for RNA extraction (Section 7.3) or immunohistochemistry (Section 7.2) or into a 6-well plate for protein extraction (Section 7.4). Transfection was either directly after seeding or the following day. If the transfection was done the following day, the cells were seeded to reach a 70-80% confluence on the day of transfection.

siRNA transfection was done with the HiPerFect Transfection Reagent of Qiagen. For a 12-well plate, 10 nM siRNA and 9 µl of HiPerFect Transfection Reagent were used. For a 6-well plate, the reagent volumes were tripled, respectively.

Plasmid transfection was done with the transfection reagent FuGene by Promega. Reagent and plasmid were used in a ratio of 3:1 – 3µl of reagent for 1 µg plasmid.

The RNA or the plasmid was mixed with Opti-MEM and the transfection reagent was added. After 5-10 min incubation period, the mixture was added dropwise to the cells. The medium was exchanged the following day.

7.2. Cell imaging methods

Immunohistochemistry

For immunohistochemistry, the cells were seeded in 12-well plates and transfected and/ or treated with substances as described in Section 7.1. At the day of sample preparation, the cells were rinsed with PBS two times and fixed for 15 min with 3.7 % formaldehyde in PBS. Permeabilization was done for 30 min with a 0.2 % solution of Triton X 100 in PBS. Following, the cells were blocked for an hour with 5 % FBS. Incubation of the primary antibodies was done for either 90 min at room temperature or overnight at 4° C. DAPI and conjugated Phalloidin were added to the solution of the secondary antibodies. If not noted differently, all antibodies were diluted 1:100 in 1.5 % BSA in PBS. Between the different incubation steps, the cells were

washed with PBS three times for 5 mins. Finally, the cells were mounted on a slide using 3 µl of VectaShield. Imaging was done either with Axio Observer.Z1 including the Apotome.2 module, the Zeiss LSM 880 AiryScan Confocal Microscope or the Opera Phenix HC system. Images at the Zeiss LSM 880 AiryScan Confocal Microscope were collected by Sebastian Dunst.

CellTrace, Hoechst 33342 and CellTox for the test method

The cells were seeded in a 96 glass bottom view plate (Perkin Elmer 6005430) a concentration of 80,000 cells/well/200µl and treated for 48 hours as described in Section 7.1. For staining, the medium was removed and PBS containing 1:1,000 diluted CellTrace and 1:500 diluted 10 mg/ml Hoechst 33342 was added. The cells were incubated for 20 mins at 37° C. Following, the cells were rinsed three times with minimal medium. For substance testing, minimal medium containing 1:10,000 diluted CellTox Green were added. The cells were then imaged at the Opera Phenix HC system.

CellTiter Blue Cell Viability assay

For cytotoxicity endpoint comparison, the toxic effect of the substances was additionally analyzed with CellTiter Blue Cell Viability assay. After imaging of the plate, the medium containing CellTox Green was removed and 200 µl fresh reduced medium containing 1:10 diluted CellTiter Blue reagent was added. The cells were incubated for 2 h at 37 °C. Subsequently, 100 µl of the supernatant were transferred into black 96-well microtiter plate and the fluorescence was measured at 560 (excitation)/ 590 (emission) using a microplate reader.

7.3. RNA biologic methods

RNA extraction

The cells were seeded and treated in 12-well plate as described in Section 7.1. The RNA extraction was conducted with the RNeasy kit by Qiagen following the manufactures instructions. In short, the cells were rinsed with PBS two times before 350 µl RLT buffer were added. The solution was transferred into a 1.5 ml tube and mixed with an equal amount of 70 % ethanol before being relocated on the column. Between the two washing steps with RW1 buffer, the column was treated with a DNase digestion. The column was washed two times with RLT buffer before the RNA was eluted in 30 µl water. The RNA concentration was measured via the Nanodrop 2000 spectrophotometer.

Reverse transcription polymerase chain reaction (RT-PCR)

The RT-PCR was standardly conducted right after the RNA extraction with the RT-PCR kit by Applied Biosystems following the manufactures instructions. Depending on the RNA yield, 0.5 µg or 1 µg RNA were used. The RT-PCR samples were diluted in a ratio 1:10 or 1:20 for the following quantitative real time polymerase chain reaction (qPCR).

Quantitative real time polymerase chain reaction (qPCR)

Subsequent to the RNA extraction and RT-PCR, the samples were analyzed with qPCR. For one qPCR reaction, 1 µl of 1:10 or 1:20 diluted cDNA sample was mixed with 5 µl of SYBR Green PCR master mix. Additionally, 0.25 µl of forward and reverse primer (10 µM stock solutions) were diluted in 5.5 µl RNase free water. Both mixtures were added together to a final volume of 11 µl. The PCR run method was conducted as described in Table 17.

The results of the qPCR were analyzed via the ΔΔ C_T methods. The C_T value is the PCR cycle value, where the fluorescent signal of the dye passes a defined threshold in the linear area of the curve. Following, the C_T value of the gene of interest is normalized to the housekeeper gene, in this case YWHAZ [125], by subtraction (ΔC_T value). Subsequently, sample ΔC_T value is subtracted of the control sample ($\Delta\Delta C_T$ value). Fold change values are defined as $2^{\Delta\Delta CT}$.

Table 17: PCR run method for qPCR analysis including melt curve analysis.

Stage	Duration	Temperature [°C]
Holding stage	2 min	50
	10 min	90
Cycling stage (40 cycles)	15 s	95
	1 min	60
Melt curve stage	15 s	95
	1 min	60 (continuous to 95)
	30 s	95
	15 s	60

7.4. Protein biologic methods

Protein extraction

The cells were seeded in a 6-well plate and treated for 48 h as described in Section 7.1. Following, the cells were put on ice and rinsed two times with PBS. The PBS was removed and 150 µl of lysis buffer (standard or Boehringer) was added. The cells were scraped off and collected in a precooled 1.5 ml tube. The solution was placed on ice and incubated for 25-30 mins. Following, the cell debris was spun down for 10 min at full speed. The supernatant was transferred to a new tube for further analysis. The pellet was discarded.

Bicinchoninic acid assay

For protein determination, the bicinchoninic acid (BCA) assay was employed. It builds on the principle that copper ions (2+) interact with the protein backbone in a basic solution and are reduced. The reduced ions complex with BCA and cause a protein concentration dependent color shift.

In this study, the Pierce BCA protein assay kit was used following the manufacturer's instructions. In short, 25 µl of 1:5 diluted protein samples were mixed with 200 µl BCA reagent (solution A and solution B in a ratio 50:1) and incubated for 30 min at 37 °C. Following, the optical density was measured at a wavelength of 590 nm. For total protein concentration determination, a standard series of defined BSA concentrations (0 µg/ml, 25 µg/ml, 125 µg/ml, 250 µg/ml, 500 µg/ml, 750 µg/ml, 1,000 µg/ml, 1,500 µg/ml, 2,000 µg/ml) was included in every run.

Sodium dodecyl sulfate polyacrylamide gel electrophoresis (SDS-PAGE)

Before Western blotting, the proteins were separated via SDS-PAGE. In preparation, 4x Laemmli sample loading buffer containing β-mercaptoethanol was added to the lysed protein samples and they were heated to 95 °C for 3 min. If not noted differently, 25 µg of protein was loaded on the gel. The SDS-gel consisted of a 5 % stacking gel and 10 % separation gel. The electrophoresis was run for 30 min on a constant voltage of 80 V and 60 min at 120 V.

Western Blot and protein detection

After protein separation via SDS-PAGE, the proteins were transferred on a membrane following the Western blot method. The two blotting techniques tank-blot and semi-dry were used. The principle is the same for both. The gel is placed on the membrane with filter paper on either side soaked in blotting buffer. Following, an

electric field was applied in a way that caused the negatively charged proteins to transfer on to the membrane. For tank blot, only one filter paper was needed as the whole sandwich of gel, membrane and filter paper is placed vertically in a tank filled with blotting buffer and ice packs for further cooling. In semi-dry Western blotting, three pieces of filter paper on each side were used. There, the sandwich was placed horizontally between two plate electrodes. The tank blot was run for 120 min at constant 400 mA, while the semi-dry blot was run at a constant voltage of 25 V for 90 mins.

To check for a successful transfer, the membrane was rinsed with TBS and then stained for 1 min with 0.1 % Ponceau. The membrane was washed with TBS until the background was sufficiently removed. The Ponceau stain was recorded and then removed by subsequent washing with TBS. Following, the membrane was blocked with 5 % milk powder in TBS-T for 30-60 min. Afterwards, 1:1,000 or 1:2,000 dilution of the primary antibody in blocking solution was added to the membrane and incubated at 4 °C over night. The next day, the membrane was washed three times for 5 min with TBS-T and the blocking solution containing a horse radish peroxidase coupled secondary antibody in dilution of 1:2,000 was added. The membrane was incubated at room temperature for 2-5 h. The incubation period was followed by another washing step (3x5 min with TBS-T) and protein detection using the SuperSignal West Femto Chemiluminescent kit. Luminol Enhancer solution was mixed in equal volumes with the peroxide solution and spread on the membrane. After an incubation period of 5 min, the luminescence caused by the peroxidase can be detected using a gel documentation system. To saturate the peroxidase bound through the antibody to the membrane, the membrane was incubated 0.1 % sodium azide for 20 min.

Coomassie staining of the membrane

After complete immunodetection, a whole protein stain was done with Coomassie blue. The membrane was incubated with the Coomassie staining solution for 1 min. Next, the membrane was destained to reduce the background by incubating it in the destaining solution overnight. When the membrane was sufficiently destained, it was washed with water and left to dry. The dried membrane was recorded.

7.5. Bioinformatics

7.5.1. Analysis of Western blot data

The Western blot image analysis was done using the software ImageJ [126]. The signal intensity was visualized in form of a histogram. The background was subtracted and the area under the curve was quantified. The resulting intensity values were then normalized on the Coomassie total protein stain and the corresponding control sample.

7.5.2. Quantitative image analysis for adherens junction reorganization

Quantitative image analysis was performed using a pipeline that built either on the integrated Harmony software or on a combination of CellProfiler and CellProfiler Analyst (CP/CPA analysis) [91, 92]. If not noted differently, all images collected at the Opera Phenix HC system were analyzed as maximum projection of a stack at least 10 planes with the Harmony software and all images collected at Zeiss LSM 880 AiryScan Confocal Microscope as a single image with a CP/CPA analysis pipeline.

All image analysis pipelines can be divided into the same principle three steps – segmentation, extraction of cellular parameters, and a parameter-based classification of cells into two classes – regular AJ organization and irregular AJ reorganization.

Image analysis Opera Phenix High Content data

The segmentation of the nucleus and cytoplasm in the Harmony based pipeline were done with the Find Nuclei module (Method C) and Find Cytoplasm module (Method A), respectively. Following, cells at the edges were excluded (Select Population module). Cellular parameters were extracted using the STAR method (threshold compactness and profile) integrated into the Calculate Morphology Properties module. The parameter-based classification of the cells was done with the Linear Classifier method of the Select Population module. Supervised training was done on a subset of cells, followed by parameter-based automatic classification of all cells within the entire image dataset.

For the MCF7/E-CadGFP time course experiment, each replicate was analyzed separately. Cytoplasm segmentation was done on the grounds of the stably transfected E-Cad-GFP signal. For the supervised training, 50 cells were selected for each of the two classes. For the comparison of the different cell staining methods, 60 cells with regular AJ organization and 60 with irregular AJ organization were selected from each repetition (a total of 180 cells per class) for supervised training. For the validation of the

test method, 40 cells per group per plate were used (a total of 360 cells per class). For the substance testing, additional 50 cells per class were added to the validation set. Lastly, CellTox Green was quantified in the nucleus region using the Calculate Intensity module. CellTox Green positive cells were determined with the Filter by Property method of the Select population module. The thresholds were set manually to the value of negative control with three times its standard deviation for each experiment.

For comparison of the two image analysis software, a CP/CPA analysis pipeline was also build for images collected with Opera Phenix HC system. Two consecutive CP pipelines are needed. The first pipeline groups the exported raw images per well, field, and channel and conducts a maximum projection. Following, the projected images are loaded into the second image analysis pipeline. There, the nuclei were identified as the primary objects (nuclei) from the Hoechst 33342 channel by global thresholding using Otsu's method. Starting from the nuclei, the cells (secondary objects) were defined with Watershed-Gradient method following the signal distribution of the CellTrace channel. Lastly, morphological parameters of the cells were measured with MeasureTexture module and the MeasureGranularity and written into a database file.

The database file was imported into the Classifier module of the CPA software for supervised training with a subset of cells, and subsequent parameter-based automatic classification of all cells within the entire image dataset. Supervised training was conducted based on the cell morphology of the CellTrace channel with two classes – regular AJ organization and irregular AJ reorganization – with 60 cells sorted in each class respectively. The cytotoxicity endpoint CellTox Green was not included in the CP/CPA analysis.

Image analysis of immunofluorescent images

Quantitative image analysis of the immunofluorescent images stained for E-Cad was performed with a similarly build CP/CPA analysis pipeline. In the segmentation process, primary objects (nuclei) were also identified from DAPI staining by global thresholding using Otsu's method. Additionally, the size of the nuclei was measured and nuclei with an area smaller than 1,000 px were filtered out. The correct segmentation of the nuclei was checked and if need be edited manually. Next, the secondary objects (cell) were defined using the Watershed-Gradient method with the primary objects serving as seeding points. Following, secondary objects that were touching the border or too large (> 8,000 px) (clumped nuclei) were excluded. The cell membrane was defined as the area three pixel inward of the border of the cell. The

module MeasureTexture was used to extract cellular parameters of the cell membrane area and the data was stored in a database file.

The database file was again imported into the Classifier module of the CPA software for supervised training. Supervised training based on cell membrane features (E-Cad channel) was conducted with two classes representing regular AJ and irregular AJ (50 cells per class).

Quantitative image analysis of calcium switch resilience assay

The principle image analysis for the quantitative calcium switch resilience assay was as described for the Harmony Software before. The cells were segmented into nucleus and cell. Following, morphologic parameters were calculated for the cell. In addition to the STAR method profile, the parameters for radial and axial cell symmetry were also included. Again, supervised training was done on a subset of cells followed by parameter-based automatic classification of all cells within the entire image dataset. The cells were classified into two classes – "rounded" and "not-rounded" cells. 120 cells per class were used, respectively. Not-rounded cells were selected from each treatment at the first time point, rounded cells after 120 min treatment. Each replicate was analyzed independently.

Statistical Analysis

Generally, calculations were done either with Microsoft Excel or GraphPad Prism 8. Statistical analysis and data visualization were done in GraphPad Prism 8.

Calculation of the MI75

The MI75 was calculated using the two concentrations (conc) were the MI score (MI) is just below (b) and just above (a) the MI score of 0.75. As approximation, a linear relationship was assumed allowing the use of the following equation:

$$\mathrm{MI75} = \log_{10}\left(conc_b + \frac{(0.75 - MI_b) * (conc_a - conc_b)}{(MI_a - MI_b)}\right)$$

8. References

1. McBryan, J., et al., *Amphiregulin: role in mammary gland development and breast cancer.* J Mammary Gland Biol Neoplasia, 2008. **13**(2): p. 159-69.
2. Korol, D.L. and S.L. Pisani, *Estrogens and cognition: Friends or foes?: An evaluation of the opposing effects of estrogens on learning and memory.* Horm Behav, 2015. **74**: p. 105-15.
3. Pike, C.J., et al., *Protective actions of sex steroid hormones in Alzheimer's disease.* Front Neuroendocrinol, 2009. **30**(2): p. 239-58.
4. Khosla, S., M.J. Oursler, and D.G. Monroe, *Estrogen and the skeleton.* Trends Endocrinol Metab, 2012. **23**(11): p. 576-81.
5. Nelson, L.R. and S.E. Bulun, *Estrogen production and action.* J Am Acad Dermatol, 2001. **45**(3 Suppl): p. S116-24.
6. Hammond, G.L., *Plasma steroid-binding proteins: primary gatekeepers of steroid hormone action.* J Endocrinol, 2016. **230**(1): p. R13-25.
7. Jensen, E.V., *On the mechanism of estrogen action.* Perspect Biol Med, 1962. **6**: p. 47-59.
8. Heldring, N., et al., *Estrogen receptors: how do they signal and what are their targets.* Physiological reviews, 2007. **87**(3): p. 905-931.
9. Hall, J.M., J.F. Couse, and K.S. Korach, *The multifaceted mechanisms of estradiol and estrogen receptor signaling.* J Biol Chem, 2001. **276**(40): p. 36869-72.
10. Planey, S.L., R. Kumar, and J.A. Arnott, *Estrogen receptors (ERalpha versus ERbeta): friends or foes in human biology?* J Recept Signal Transduct Res, 2014. **34**(1): p. 1-5.
11. Prossnitz, E.R. and J.B. Arterburn, *International Union of Basic and Clinical Pharmacology. XCVII. G Protein-Coupled Estrogen Receptor and Its Pharmacologic Modulators.* Pharmacol Rev, 2015. **67**(3): p. 505-40.
12. Marino, M., P. Galluzzo, and P. Ascenzi, *Estrogen signaling multiple pathways to impact gene transcription.* Curr Genomics, 2006. **7**(8): p. 497-508.
13. Hammes, S.R. and E.R. Levin, *Extranuclear steroid receptors: nature and actions.* Endocr Rev, 2007. **28**(7): p. 726-41.
14. Su, X., et al., *ER-alpha36: a novel biomarker and potential therapeutic target in breast cancer.* Onco Targets Ther, 2014. **7**: p. 1525-33.
15. Olde, B. and L.M. Leeb-Lundberg, *GPR30/GPER1: searching for a role in estrogen physiology.* Trends Endocrinol Metab, 2009. **20**(8): p. 409-16.
16. Thomas, P., et al., *Identity of an estrogen membrane receptor coupled to a G protein in human breast cancer cells.* Endocrinology, 2005. **146**(2): p. 624-32.
17. Clemons, M. and P. Goss, *Estrogen and the risk of breast cancer.* N Engl J Med, 2001. **344**(4): p. 276-85.
18. International Agency for Research on Cancer, *World cancer report 2014.* World Health Organization, 2014.
19. International Agency for Research on Cancer, *World cancer report 2020.* World Health Organization, 2020.
20. Kaatsch, P., et al., *Krebs in Deutschland für 2013/2014.* Berlin: Robert Koch-Institut und die Gesellschaft der epidemiologischen Krebsregister in Deutschland, 2017.
21. Harbeck, N., et al., *Breast cancer.* Nat Rev Dis Primers, 2019. **5**(1): p. 66.
22. Robertson, J.F., et al., *A good drug made better: the fulvestrant dose-response story.* Clin Breast Cancer, 2014. **14**(6): p. 381-9.
23. Beatson, G.T., *On the Treatment of Inoperable Cases of Carcinoma of the Mamma: Suggestions for a New Method of Treatment, with Illustrative Cases.*

Trans Med Chir Soc Edinb, 1896. **15**: p. 153-179.
24. Canas-Marques, R. and S.J. Schnitt, *E-cadherin immunohistochemistry in breast pathology: uses and pitfalls.* Histopathology, 2016. **68**(1): p. 57-69.
25. Bhatt, T., et al., *Signaling and mechanical roles of E-cadherin.* Cell Commun Adhes, 2013. **20**(6): p. 189-99.
26. Klezovitch, O. and V. Vasioukhin, *Cadherin signaling: keeping cells in touch.* F1000Res, 2015. **4**(F1000 Faculty Rev): p. 550.
27. Baum, B. and M. Georgiou, *Dynamics of adherens junctions in epithelial establishment, maintenance, and remodeling.* J Cell Biol, 2011. **192**(6): p. 907-17.
28. Yap, A.S., G.A. Gomez, and R.G. Parton, *Adherens Junctions Revisualized: Organizing Cadherins as Nanoassemblies.* Dev Cell, 2015. **35**(1): p. 12-20.
29. Buckley, C.D., et al., *Cell adhesion. The minimal cadherin-catenin complex binds to actin filaments under force.* Science, 2014. **346**(6209): p. 1254211.
30. Halbleib, J.M. and W.J. Nelson, *Cadherins in development: cell adhesion, sorting, and tissue morphogenesis.* Genes Dev, 2006. **20**(23): p. 3199-214.
31. Padmanaban, V., et al., *E-cadherin is required for metastasis in multiple models of breast cancer.* Nature, 2019. **573**(7774): p. 439-444.
32. Ashaie, M.A. and E.H. Chowdhury, *Cadherins: The Superfamily Critically Involved in Breast Cancer.* Curr Pharm Des, 2016. **22**(5): p. 616-38.
33. Cardamone, M.D., et al., *ERalpha as ligand-independent activator of CDH-1 regulates determination and maintenance of epithelial morphology in breast cancer cells.* Proc Natl Acad Sci U S A, 2009. **106**(18): p. 7420-5.
34. Oesterreich, S., et al., *Estrogen-mediated down-regulation of E-cadherin in breast cancer cells.* Cancer Res, 2003. **63**(17): p. 5203-8.
35. Fujita, N., et al., *MTA3, a Mi-2/NuRD complex subunit, regulates an invasive growth pathway in breast cancer.* Cell, 2003. **113**(2): p. 207-19.
36. Kowalczyk, A.P. and B.A. Nanes, *Adherens junction turnover: regulating adhesion through cadherin endocytosis, degradation, and recycling.* Subcell Biochem, 2012. **60**: p. 197-222.
37. Masuda, H., et al., *Role of epidermal growth factor receptor in breast cancer.* Breast Cancer Res Treat, 2012. **136**(2): p. 331-45.
38. Jeong, Y., et al., *EGFR is a Therapeutic Target in Hormone Receptor-Positive Breast Cancer.* Cell Physiol Biochem, 2019. **53**(5): p. 805-819.
39. Osborne, C.K., et al., *Crosstalk between estrogen receptor and growth factor receptor pathways as a cause for endocrine therapy resistance in breast cancer.* Clin Cancer Res, 2005. **11**(2 Pt 2): p. 865s-70s.
40. Normanno, N., et al., *Epidermal growth factor receptor (EGFR) signaling in cancer.* Gene, 2006. **366**(1): p. 2-16.
41. Huveneers, S. and E.H. Danen, *Adhesion signaling - crosstalk between integrins, Src and Rho.* J Cell Sci, 2009. **122**(Pt 8): p. 1059-69.
42. Finn, R., *Targeting Src in breast cancer.* Annals of oncology, 2008. **19**(8): p. 1379-1386.
43. Berasain, C. and M.A. Avila, *Amphiregulin.* Semin Cell Dev Biol, 2014. **28**: p. 31-41.
44. Busser, B., et al., *The multiple roles of amphiregulin in human cancer.* Biochim Biophys Acta, 2011. **1816**(2): p. 119-31.
45. Tata, J.R., *One hundred years of hormones.* EMBO Rep, 2005. **6**(6): p. 490-6.
46. Dodds, E.C., et al., *Oestrogenic activity of certain synthetic compounds.* Nature, 1938. **141**(3562): p. 247.
47. Dodds, E.C. and W. Lawson, *Synthetic strogenic agents without the phenanthrene nucleus.* Nature, 1936. **137**(3476): p. 996.

48. Pincus, G., et al., *Fertility control with oral medication.* Am J Obstet Gynecol, 1958. **75**(6): p. 1333-46.
49. World Health Organization, *IPCS global assessment of the state-of-the-science of endocrine disruptors.* WHO/PCS/EDC/02.2, 2002: p. 35-50.
50. Bergman, Å., et al., *State of the science of endocrine disrupting chemicals 2012*. 2013: World Health Organization.
51. Sonne, C., et al., *Xenoendocrine pollutants may reduce size of sexual organs in East Greenland polar bears (Ursus maritimus).* Environ Sci Technol, 2006. **40**(18): p. 5668-74.
52. Schug, T.T., et al., *Minireview: Endocrine Disruptors: Past Lessons and Future Directions.* Mol Endocrinol, 2016. **30**(8): p. 833-47.
53. Kabir, E.R., M.S. Rahman, and I. Rahman, *A review on endocrine disruptors and their possible impacts on human health.* Environ Toxicol Pharmacol, 2015. **40**(1): p. 241-58.
54. Smith, O.W., *Diethylstilbestrol in the prevention and treatment of complications of pregnancy.* Am J Obstet Gynecol, 1948. **56**(5): p. 821-34.
55. Dieckmann, W.J., et al., *Does the administration of diethylstilbestrol during pregnancy have therapeutic value?* Am J Obstet Gynecol, 1953. **66**(5): p. 1062-81.
56. Hilakivi-Clarke, L., *Maternal exposure to diethylstilbestrol during pregnancy and increased breast cancer risk in daughters.* Breast Cancer Res, 2014. **16**(2): p. 208.
57. Herbst, A.L., H. Ulfelder, and D.C. Poskanzer, *Adenocarcinoma of the vagina. Association of maternal stilbestrol therapy with tumor appearance in young women.* N Engl J Med, 1971. **284**(15): p. 878-81.
58. Hoover, R.N., et al., *Adverse health outcomes in women exposed in utero to diethylstilbestrol.* N Engl J Med, 2011. **365**(14): p. 1304-14.
59. Veurink, M., M. Koster, and L.T. Berg, *The history of DES, lessons to be learned.* Pharm World Sci, 2005. **27**(3): p. 139-43.
60. Michalowicz, J., *Bisphenol A--sources, toxicity and biotransformation.* Environ Toxicol Pharmacol, 2014. **37**(2): p. 738-58.
61. Vandenberg, L.N., et al., *Human exposure to bisphenol A (BPA).* Reprod Toxicol, 2007. **24**(2): p. 139-77.
62. Calafat, A.M., et al., *Urinary concentrations of bisphenol A and 4-nonylphenol in a human reference population.* Environ Health Perspect, 2005. **113**(4): p. 391-5.
63. Wetherill, Y.B., et al., *In vitro molecular mechanisms of bisphenol A action.* Reprod Toxicol, 2007. **24**(2): p. 178-98.
64. Zhang, X., et al., *Bisphenol A disrupts steroidogenesis in human H295R cells.* Toxicol Sci, 2011. **121**(2): p. 320-7.
65. Rochester, J.R., *Bisphenol A and human health: a review of the literature.* Reprod Toxicol, 2013. **42**: p. 132-55.
66. EFSA Panel on Food Contact Materials, E., Flavourings and Processing Aids,, *Scientific Opinion on the risks to public health related to the presence of bisphenol A (BPA) in foodstuffs.* EFSA Journal 2015, 2015. **13**(1): p. 3978.
67. Rochester, J.R. and A.L. Bolden, *Bisphenol S and F: A Systematic Review and Comparison of the Hormonal Activity of Bisphenol A Substitutes.* Environ Health Perspect, 2015. **123**(7): p. 643-50.
68. Serra, H., et al., *Evidence for Bisphenol B Endocrine Properties: Scientific and Regulatory Perspectives.* Environ Health Perspect, 2019. **127**(10): p. 106001.
69. Massart, F. and G. Saggese, *Oestrogenic mycotoxin exposures and precocious pubertal development.* Int J Androl, 2010. **33**(2): p. 369-76.
70. Rogowska, A., et al., *Zearalenone and its metabolites: Effect on human health,*

metabolism and neutralisation methods. Toxicon, 2019. **162**: p. 46-56.
71. Codex Committee on Food Additives and Contaminants, J.F.W.E.C.o.F.A., *Position Paper on Zearalenone*. Publication CCFAC 2000. **00/19.**(Codex Alimentarius Commission Rome, Italy).
72. Metzler, M., E. Pfeiffer, and A. Hildebrand, *Zearalenone and its metabolites as endocrine disrupting chemicals.* World Mycotoxin Journal, 2010. **3**(4): p. 385-401.
73. Rietjens, I., J. Louisse, and K. Beekmann, *The potential health effects of dietary phytoestrogens.* Br J Pharmacol, 2017. **174**(11): p. 1263-1280.
74. Patisaul, H.B., *Endocrine disruption by dietary phyto-oestrogens: impact on dimorphic sexual systems and behaviours.* Proc Nutr Soc, 2017. **76**(2): p. 130-144.
75. Dixon, R.A. and D. Ferreira, *Genistein.* Phytochemistry, 2002. **60**(3): p. 205-11.
76. Organisation for Economic Co-operation and Development, *Revised Guidance Document 150 on Standardised Test Guidelines for Evaluating Chemicals for Endocrine Disruption*. 2018.
77. Organisation for Economic Co-operation and Development, *Test No. 493: Performance-Based Test Guideline for Human Recombinant Estrogen Receptor (hrER) In Vitro Assays to Detect Chemicals with ER Binding Affinity*. 2015.
78. Organisation for Economic Co-operation and Development, *Test No. 455: Performance-Based Test Guideline for Stably Transfected Transactivation In Vitro Assays to Detect Estrogen Receptor Agonists and Antagonists*. 2016.
79. European Chemical Agency and European Food Safety Authority with the technical support of the Joint Research Centre, *Guidance for the identification of endocrine disruptors in the context of Regulations (EU) No 528/2012 and (EC) No 1107/2009.* EFSA Journal, 2018. **16**(6): p. e05311.
80. Browne, P., et al., *Application of Adverse Outcome Pathways to U.S. EPA's Endocrine Disruptor Screening Program.* Environ Health Perspect, 2017. **125**(9): p. 096001.
81. Hecker, M. and H. Hollert, *Endocrine disruptor screening: regulatory perspectives and needs.* Environmental Sciences Europe, 2011. **23**(1): p. 1-14.
82. Tralau, T., et al., *Regulatory toxicology in the twenty-first century: challenges, perspectives and possible solutions.* Arch Toxicol, 2015. **89**(6): p. 823-50.
83. Organisation for Economic Co-operation and Development, *Revised Guidance Document on Developing and Assessing Adverse Outcome Pathways*. Series on Testing and Assessment No. 184. 2017.
84. Browne, P., et al., *Screening chemicals for estrogen receptor bioactivity using a computational model.* Environmental science & technology, 2015. **49**(14): p. 8804-8814.
85. Soto, A.M., et al., *The E-SCREEN assay as a tool to identify estrogens: an update on estrogenic environmental pollutants.* Environ Health Perspect, 1995. **103 Suppl 7**: p. 113-22.
86. Organisation for Economic Co-operation and Development, *Case Study on the Use of an Integrated Approach to Testing and Assessment for Identifying Estrogen Receptor Active Chemicals*. Series on Testing and Assessment No. 309. 2019.
87. Bischoff, P., Kornhuber, M., et al., *Inhibition of ERalpha signaling clusters adherens junction in breast cancer cells through AREG/EGFR and increases cell stability and stiffness.* under review, 2020.
88. Soto, A.M. and C. Sonnenschein, *The role of estrogens on the proliferation of human breast tumor cells (MCF-7).* J Steroid Biochem, 1985. **23**(1): p. 87-94.
89. Wakeling, A.E., *Similarities and distinctions in the mode of action of different*

classes of antioestrogens. Endocr Relat Cancer, 2000. **7**(1): p. 17-28.
90. Wakeling, A.E., M. Dukes, and J. Bowler, *A potent specific pure antiestrogen with clinical potential.* Cancer Res, 1991. **51**(15): p. 3867-73.
91. Carpenter, A.E., et al., *CellProfiler: image analysis software for identifying and quantifying cell phenotypes.* Genome Biol, 2006. **7**(10): p. R100.
92. Jones, T.R., et al., *CellProfiler Analyst: data exploration and analysis software for complex image-based screens.* BMC Bioinformatics, 2008. **9**: p. 482.
93. Dennis, M.K., et al., *In vivo effects of a GPR30 antagonist.* Nature Chemical Biology, 2009. **5**: p. 421.
94. Dennis, M.K., et al., *Identification of a GPER/GPR30 antagonist with improved estrogen receptor counterselectivity.* J Steroid Biochem Mol Biol, 2011. **127**(3-5): p. 358-66.
95. Shewan, A.M., et al., *Myosin 2 is a key Rho kinase target necessary for the local concentration of E-cadherin at cell-cell contacts.* Mol Biol Cell, 2005. **16**(10): p. 4531-42.
96. Peterson, E.A., et al., *Amphiregulin Is a Critical Downstream Effector of Estrogen Signaling in ERalpha-Positive Breast Cancer.* Cancer Res, 2015. **75**(22): p. 4830-8.
97. Ciarloni, L., S. Mallepell, and C. Brisken, *Amphiregulin is an essential mediator of estrogen receptor alpha function in mammary gland development.* Proc Natl Acad Sci U S A, 2007. **104**(13): p. 5455-60.
98. Martinez-Lacaci, I., et al., *Estrogen and phorbol esters regulate amphiregulin expression by two separate mechanisms in human breast cancer cell lines.* Endocrinology, 1995. **136**(9): p. 3983-92.
99. Bromann, P.A., H. Korkaya, and S.A. Courtneidge, *The interplay between Src family kinases and receptor tyrosine kinases.* Oncogene, 2004. **23**(48): p. 7957-68.
100. Biscardi, J.S., et al., *Tyrosine kinase signalling in breast cancer: Epidermal growth factor receptor and c-Src interactions in breast cancer.* Breast Cancer Research, 2000. **2**(3): p. 203.
101. Migliaccio, A., et al., *Steroid receptor regulation of epidermal growth factor signaling through Src in breast and prostate cancer cells: steroid antagonist action.* Cancer Res, 2005. **65**(22): p. 10585-93.
102. Traxler, P., et al., *Use of a pharmacophore model for the design of EGF-R tyrosine kinase inhibitors: 4-(phenylamino)pyrazolo[3,4-d]pyrimidines.* J Med Chem, 1997. **40**(22): p. 3601-16.
103. Brandvold, K.R., et al., *Development of a highly selective c-Src kinase inhibitor.* ACS Chem Biol, 2012. **7**(8): p. 1393-8.
104. Hanke, J.H., et al., *Discovery of a novel, potent, and Src family-selective tyrosine kinase inhibitor. Study of Lck- and FynT-dependent T cell activation.* J Biol Chem, 1996. **271**(2): p. 695-701.
105. Flatau, G., et al., *Toxin-induced activation of the G protein p21 Rho by deamidation of glutamine.* Nature, 1997. **387**(6634): p. 729-33.
106. Shang, X., et al., *Rational design of small molecule inhibitors targeting RhoA subfamily Rho GTPases.* Chem Biol, 2012. **19**(6): p. 699-710.
107. Shang, X., et al., *Small-molecule inhibitors targeting G-protein-coupled Rho guanine nucleotide exchange factors.* Proc Natl Acad Sci U S A, 2013. **110**(8): p. 3155-60.
108. Iversen, P.W., et al., *HTS assay validation*, in *Assay Guidance Manual [Internet]*. 2012, Eli Lilly & Company and the National Center for Advancing Translational Sciences.
109. Klinge, C.M., *Estrogenic control of mitochondrial function and biogenesis.* J Cell

Biochem, 2008. **105**(6): p. 1342-51.
110. DePasquale, J.A., W.A. Samsonoff, and J.F. Gierthy, *17-beta-Estradiol induced alterations of cell-matrix and intercellular adhesions in a human mammary carcinoma cell line.* J Cell Sci, 1994. **107 (Pt 5)**: p. 1241-54.
111. Rothman, M.S., et al., *Reexamination of testosterone, dihydrotestosterone, estradiol and estrone levels across the menstrual cycle and in postmenopausal women measured by liquid chromatography-tandem mass spectrometry.* Steroids, 2011. **76**(1-2): p. 177-82.
112. McCormack, P. and F. Sapunar, *Pharmacokinetic profile of the fulvestrant loading dose regimen in postmenopausal women with hormone receptor-positive advanced breast cancer.* Clin Breast Cancer, 2008. **8**(4): p. 347-51.
113. Omidvar, R., et al., *Atomic force microscope-based single cell force spectroscopy of breast cancer cell lines: an approach for evaluating cellular invasion.* J Biomech, 2014. **47**(13): p. 3373-9.
114. Britton, D.J., et al., *Bidirectional cross talk between ERalpha and EGFR signalling pathways regulates tamoxifen-resistant growth.* Breast Cancer Res Treat, 2006. **96**(2): p. 131-46.
115. Zhao, Q., et al., *Bisphenol AF promotes estrogen receptor-positive breast cancer cell proliferation through amphiregulin-mediated crosstalk with receptor tyrosine kinase signaling.* PLoS One, 2019. **14**(5): p. e0216469.
116. Migliaccio, A., et al., *Cross talk between epidermal growth factor (EGF) receptor and extra nuclear steroid receptors in cell lines.* Mol Cell Endocrinol, 2010. **327**(1-2): p. 19-24.
117. Azadi, S., et al., *Epidermal growth factor receptor targeting alters gene expression and restores the adhesion function of cancerous cells as measured by single cell force spectroscopy.* Mol Cell Biochem, 2016. **423**(1-2): p. 129-139.
118. Riss, T.L., et al., *Cell Viability Assays*, in *Assay Guidance Manual*, G.S. Sittampalam, et al., Editors. 2004, Eli Lilly & Company and the National Center for Advancing Translational Sciences: Bethesda (MD).
119. Lehmann, L. and J. Wagner, *Gene expression of 17beta-estradiol-metabolizing isozymes: comparison of normal human mammary gland to normal human liver and to cultured human breast adenocarcinoma cells.* Adv Exp Med Biol, 2008. **617**: p. 617-24.
120. Bain, J., et al., *The specificities of protein kinase inhibitors: an update.* Biochem J, 2003. **371**(Pt 1): p. 199-204.
121. Bain, J., et al., *The selectivity of protein kinase inhibitors: a further update.* Biochem J, 2007. **408**(3): p. 297-315.
122. Malissein, E., et al., *RhoA and RhoC differentially modulate estrogen receptor alpha recruitment, transcriptional activities, and expression in breast cancer cells (MCF-7).* J Cancer Res Clin Oncol, 2013. **139**(12): p. 2079-88.
123. Osborne, C.K., K. Hobbs, and J.M. Trent, *Biological differences among MCF-7 human breast cancer cell lines from different laboratories.* Breast Cancer Res Treat, 1987. **9**(2): p. 111-21.
124. de Beco, S., et al., *Endocytosis is required for E-cadherin redistribution at mature adherens junctions.* Proceedings of the National Academy of Sciences, 2009. **106**(17): p. 7010-7015.
125. Chua, S.L., et al., *UBC and YWHAZ as suitable reference genes for accurate normalisation of gene expression using MCF7, HCT116 and HepG2 cell lines.* Cytotechnology, 2011. **63**(6): p. 645-54.
126. Schindelin, J., et al., *Fiji: an open-source platform for biological-image analysis.* Nat Methods, 2012. **9**(7): p. 676-82.

9. List of Figures and Tables

List of Figures

Figure 1: Schematic view of the genomic and non-genomic estrogen signaling pathways. 5
Figure 2: Antiestrogens are able to modulate estrogen responsive gene expression. 22
Figure 3: Antiestrogen treatment does not cause an increase in E-Cadherin expression but adherens junction reorganization. 23
Figure 4: Quantification of adherens junction reorganization. 25
Figure 5: Adherens junction reorganization is prevented by estrogen addition and induced by ERα siRNA knock down. 28
Figure 6: GPER1 antagonists influence adherens junction organization in contrast to GPER1 agonists. 30
Figure 7: G15 can prevent Fulvestrant-induced adherens junction reorganization but not ERα knock down induced. 32
Figure 8: GPER1 KD does not influence adherens junction organization. 33
Figure 9: Adherens junction reorganization results in increased cell-cell contact stability. 35
Figure 10: Adherens junction reorganization is depended on Amphiregulin expression. 39
Figure 11: The EGFR protein level is increased in cells with adherens junction reorganization. 42
Figure 12: Src family kinase inhibitors PP1 and PP2, but not knock down of Fyn, induced adherens junction reorganization. 45
Figure 13: G15 and E2 can partially prevent PP2-induced adherens junction reorganization. 46
Figure 14: RhoA activator CN03 can rescue normal adherens junction organization after Fulvestrant or PP2 treatment. 48
Figure 15: Inhibition of RhoA through Rhosin induces adherens junction reorganization. 50
Figure 16: Overexpression of constitutive active RhoA prevents adherens junction reorganization 52
Figure 17: RhoC expression did not influence adherens junction reorganization. 53

Figure 18: Inhibition of Rac1 or Cdc42 does neither induce nor prevent adherens junction reorganization. 54
Figure 19: CellTrace cytoplasmic staining is sufficient for differentiation between regular and irregular adherens junction organization. 57
Figure 20: The different staining methods show all similar dose-response curves. 59
Figure 21: Quantification of CellTrace stained cells can also be conducted with a CellProfiler/ CellProfiler Analyst analysis pipeline. 60
Figure 22: Treatment of the cells for 48 h is the ideal time point. 62
Figure 23: Number of cells and CellTox Green are appropriate markers for cytotoxicity. 65
Figure 24: Testing of three substances with different estrogenic potential. 67
Figure 25: Testing of three substances with different estrogenic potential. 68
Figure 26: Schematic view of the acceptance criteria and the prediction model for the testing of potentially estrogenic substances in this test set-up. 69
Figure 27: Relative MI75 values of the 17 tested substances. 72
Figure 28: Correlation of the relative MI75 values of the tested substances to the published data of other assays. 74
Figure 29: Working model for estrogen receptor α induced adherens junction reorganization. 80
Figure 30: Schematic view of the E-Morph Assay. 83

List of Tables

Table 1: Classification and MI75 of the six tested substances. 70
Table 2: Classification and MI75 of the eleven additionally tested substances. 71
Table 3: List of equipment and machines used. 90
Table 4: List of all the used cell culture reagents. 90
Table 5: Cell culture media compositions 91
Table 6: List of all the cell labeling reagents used. 91
Table 7: List of the primary antibodies used. 91
Table 8: List of the secondary antibodies used. 92
Table 9: List of the plasmids used in this thesis 92
Table 10: List of the different siRNAs used in this thesis. All siRNAs were purchased by Qiagen as FlexiTube GeneSolution (product number 1027416). 93
Table 11: List of primers for the quantitative polymerase chain reaction including their sequence and melting temperature T_M. All primers were purchase by Eurofins. 93

Table 12: List of the different kits used. 94
Table 13: List of chemicals with known or suspected endocrine effects. 94
Table 14: List of inhibitors or activators of specific cellular pathways. 95
Table 15: List of any additional material used. 95
Table 16: List of the different buffers and solution used. 96
Table 17: PCR run method for qPCR analysis including melt curve analysis. 101

10. List of Abbreviations

4-OHT	4-Hydroxytamoxifen
AF	Activation function
AJ	Adherens junctions
AOP	Adverse outcome pathway
AP-1	Activating protein-1
APS	Ammonium persulfate
AREG	Amphiregulin
Atra	Atrazine
BCA	Bicinchoninic acid
BPA	Bisphenol A
BPAF	Bisphenol AF
BPB	Bisphenol B
BPS	Bisphenol S
BSA	Bovine serum albumin
cDNA	Complementary deoxyribonucleic acid
CERI	Chemical Evaluation and Research Institute
Coum	Coumestrol
CP	CellProfiler
CPA	CellProfiler Analyst
CSK	C-terminal src kinase
DAPI	4‘,6-Diamidibo-2-phenylindole
Dai	Daidzein
DES	Diethylstilbestrol
DMEM	Dulbecco's Modified Eagle's Medium
DNA	Deoxyribonucleic acid
E1	Estrone
E2	17β-Estradiol
EAS	Endocrine active substances
EATS	Estrogenic, androgenic, thyroidal and steroidogenic
EC	Extracellular
E-Cad	E-Cadherin
EDC	Endocrine disrupting chemicals
EDSP	Endocrine Disruptor Screening Program
EDSTAC	Endocrine Disruptor Screening and Testing Advisory Committee
EDTA	Ethylenediaminetetraacetic acid
EE	17α-Ethinylestradiol
EFSA	European Food Safety Authority
EGFR	Epidermal growth factor receptor
EGTA	Ethylene glycol-bis(β-aminoethyl ether)-N,N,N′,N′-tetraacetic acid
EE	17α-Ethinylestradiol
EPA	Environmental Protection Agency
E-Morph	estrogen morphology
EMT	Epithelial-mesenchymal transition
EPA	Environmental Protection Agency
ER	Estrogen receptor
ERE	Estrogen responsive elements
ERK	Extracellular signal-regulated kinase
ERα	Estrogen receptor α
ERβ	Estrogen receptor β
FAK	Focal adhesion kinase
FSH	Follicle-stimulating hormone
Fulv	Fulvestrant
GD	Guidance document
GEF	Guanine nucleotide exchange factors
Gen	Genistein
GFP	Green fluorescent protein
GnRH	Gonadotropin-releasing hormone
GPER1	G-Protein coupled estrogen receptor 1
GSK	G-associated kinase
hAREG-GFP	GFP-tagged human AREG
HC	High Content
HER2	Human epidermal growth factor receptor
HPG	hypothalamic-pituitary-gonadal axis
HrER	Human Recombinant Estrogen Receptor
HT	High throughput
JECFA	Joint Committee by the Food and Agriculture Organization of the United Nations and WHO
KD	Knock down
KE	Key Events
LARG	Leukemia-associated Rho guanine nucleotide exchange factor
MAPK	Mitogen activating protein kinase
MCF7	Michigan Cancer Foundation - 7
mER	Membrane associated ER
MIE	Molecular Initiating Event
MI	Morphology Index
mRNA	Messenger ribonucleic acid
MTA3	Metastasis associated gene protein 3
norm.	Normalized
NST	invasive ductal carcinoma no special type

OECD	Organization for Economic Cooperation and Development	**SW**	Signal window
PAGE	Polyacrylamide gel electrophoresis	**TA**	Transactivation
PBS	Phosphate buffered saline	**Tam**	Tamoxifen
PGR	Progesterone receptor	**TBS**	Tris-buffered saline
PI3K	Phospatidyl-inositol-3-kinase	**TBS-T**	Tris-buffered saline Tween20
qPCR	Quantitative real time polymerase chain reaction	**TEMED**	N,N,N',N'-Tetramethyl ethylenediamine
REACH	Registration, Evaluation, Authorization and Restriction of Chemicals	**US**	United States
SFK	Src-family kinases	**WHO**	World Health Organization
SH2	Src homology 2	**WT**	Wild-type
siRNA	Silencing ribonucleic acid	**Z'**	Z' value
SP-1	Stimulating protein-1	**Zea**	Zearalenone
SRC-1	Steroid receptor co-activator-1	**ZK**	ZK164015
STTA	Stably Transfected Transactivation		

11. List of publications

EPO EP3517967A1 / WIPO WO2019145517 Screening method for estrogenic and anti-estrogenic activity - European Patent Office / World Intellectual Property Organization Schönfelder G.; Oelgeschläger M.; Bischoff P.; **Kornhuber M.**, Dunst S.; Vogl S.

Bischoff P.*, **Kornhuber M**.*, Dunst S., Zell J., Fauler B., Mielke T., Taubenberger A.V., Guck J., Oelgeschläger, M., Schönfelder, G., *Inhibition of ERalpha signaling clusters adherens junction in breast cancer cells through AREG/EGFR and increases cell stability and stiffness*, 2020, under review *equal contribution

M. Kornhuber, S. Dunst, M. Oelgeschläger, G. Schönfelder, *Adherens junction reorganization as a novel endpoint for the identification of estrogenic substances* Abstracts of the 83rd Annual Meeting of the German Society for Experimental and Clinical Pharmacology and Toxicology (DGPT) and the 19th Annual Meeting of the Association of the Clinical Pharmacology Germany (VKliPha) With contribution of the Arbeitsgemeinschaft für Angewandte Humanpharmakologie e. V. (AGAH) Naunyn-Schmiedeberg's Arch Pharmacol, 2017, 390 (Suppl 1): 1.

M. Kornhuber, S. Dunst, S. Klutzny, M. Oelgeschläger, G. Schönfelder, *A new functional assay to identify chemicals with estrogenic potential*, Abstracts of the 55th Congress of the European Societies of Toxicology (EUROTOX 2019) TOXICOLOGY SCIENCE PROVIDING SOLUTIONS, 2019, Toxicology Letters, Volume 314, Supplement